Investigation and Analysis of RCCI using NVO on a Converted Spark Ignition Engine

by

Robert V. Klikach

A thesis submitted in partial fulfillment of the requirements for the degree of

Master of Science

Department of Mechanical Engineering
University of Alberta

Abstract

Dual-fuel Reactivity Controlled Compression Ignition (RCCI) combustion is investigated as an efficient combustion mode on a modified 4-cylinder production Gasoline Direct Injection (GDI) engine. RCCI uses Low-Temperature Combustion (LTC) to provide high efficiency combustion while avoiding NOx and soot formation. High-reactivity liquid n-heptane is direct injected during compression while compressed natural gas is port injected during the intake stroke. The use of Negative Valve Overlap (NVO) with RCCI is investigated to recirculate exhaust gases to the next cycle. Two injection strategies for the n-heptane were investigated, a single pilot injection and a split injection strategy with a pilot injection and an injection in the NVO.

The sensitivity of the combustion timing and load to NVO duration, intake air temperature, fueling rates and n-heptane pilot injection timing were investigated. A feedback control scheme is proposed from these sensitivities. The single and split injection RCCI strategies both improve the engine's thermal and combustion efficiency and reduced NOx emissions compared to the engine running in SI mode with natural gas. The split injection strategy has longer burn duration, lower peak pressure rise rates, improved efficiency and reduced unburnt methane and carbon monoxide over then single injection case.

Acknowledgements

I would like to thank my supervisor Dr. Koch for his support and help during my graduate studies. His experience and knowledge has made him a great mentor and has helped me develop as an engineer and a person. A special thanks to Bernard Faulkner and to Khashayar Ebrahimi who have both aided me in completing my research. Bernie's experience as a technician has been invaluable asset in the engine lab. The experimental research would not have been possible without the direction and expertise of Khashy who helped me with experiments. I would like to thank the rest of my colleagues in our research group over my time as a graduate student. To David, Masoud, Giffin, Craig, Daniel and Armin, thanks for not only being excellent colleagues but good friends. Lastly I would like to thank my fiancée Joanne whose love, support and patience gave me the motivation I needed to pursue and complete my graduate studies.

Table of Contents

List of Tables

List of Figures

Nomenclature

Acronyms

aTDC	after Top Dead Center
BD	Burn Duration
bTDC	before Top Dead Center
CA10-90	Crank Angles for 10% to 90% mass burned
CA50	Crank Angle of 50% mass burned
CI	Compression Ignition
CO	Carbon Monoxide
CO_2	Carbon Dioxide
CR	Compression Ratio
DAQ	Data AcQuisition
EGR	Exhaust Gas Recirculation
EOC	End of Combustion
EPA	Environmental Protection Agency
EVC	Exhaust Valve Closing
EVO	Exhaust Valve Opening
GDI	Gasoline Direct Injection
HCCI	Homogeneous Charge Compression Ignition
HTHR	High Temperature Heat Release
HRR	Heat Release Rate

IAT	Intake Air Temperature
IMEP	Indicated Mean Effective Pressure
IVC	Intake Valve Closing
IVO	Intake Valve Opening
LHV	Low Heating Value
NO_x	Oxides of Nitrogen
NVO	Negative Valve Overlap
O_2	Oxygen
PRR	Pressure Rise Rate
PVO	Positive Valve Overlap
RPM	Revolutions Per Minute
SI	Spark Ignition
SOC	Start of Combustion
TDC	Top Dead Center
VVT	Variable Valve Timing

Symbols

λ	Airfuel Equivalence Ratio
η_{comb}	Combustion Efficiency
η_{th}	Thermal Efficiency
η_{vol}	Volumetric Efficiency
θ	Crankshaft Angle
θ_{CA50}	Angle of 50% Mass Burned
θ_{DI1}	NVO N-heptabe Injection Start Angle
θ_{DI2}	Pilot N-heptane Injection Start Angle
θ_{PI1}	Natural Gas Injection Start Angle
θ_{IG}	Spark Start Angle
ρ_a	Intake Air Density
ϕ_{NVO}	Negative Valve Overlap Phasing
E_{DI1}	Injected Fuel Energy of the N-Heptane NVO Injection
E_{DI2}	Injected Fuel Energy of the N-Heptane Pilot Injection
E_{PI1}	Injected Fuel Energy of the Natural Gas Injection
E_t	Total Injected Fuel Energy
HRR	Heat Release Rate
k	Specific Heat Ratio
m_a	Mass of Air
m_f	Mass of Fuel
m_{f_i}	Mass of Fuel injected on a single injection
n	Engine Speed in RPM
n_{inj}	Number of Injections
N_c	Number of cycles per second

P	Pressure
P_{inj}	Fuel Injection Pressure
PRR	Pressure Rise Rate
Q_{HR}	Heat Release
R	Ideal Gas Constant
S_X	Normalized Sensitivity to Parameter X
t	Time
t_{pw}	Fuel Injection Pulse Width Time
T	Temperature
T_{in}	Intake Air Temperature
T_{exh}	Exhaust Gas Temperature
V	Cylinder Volume
V_d	Displaced Volume
W_i	Indicated Work
X	Parameter

Chapter 1

Introduction

1.1 RCCI

Reactivity Controlled Compression Ignition (RCCI) is a form of Low-Temperature Combustion (LTC) that utilizes auto-ignition to initiate combustion. This combustion occurs quickly providing a concentrated heat release for improved efficiency. The low temperature of the combustion avoids NOx production while the lean regions of combustion avoid soot formation. Auto-ignition has no direct mechanism to initiate combustion like the spark in a Spark Ignition (SI) engine and the fuel injection in a Compression Ignition (CI) engine since the combustion is dictated by chemical kinetics [1]. The reactivitity of a fuel is a measure of how readily a fuel will ignite on its own due to high temperature and pressure conditions. A fuel with a high-reactivity is prone to auto-ignite easily while a low-reactivity fuel is able to withstand higher temperatures before self-igniting. RCCI is a dual-fuel combustion strategy that uses both a high and low-reactivity fuel. The combustion timing can be controlled by varying reactivity of the overall fuel mixture by changing the ratio between the two fuels.

1.2 Problem Statement

The objective of this research is to investigate the use of RCCI on 4 cylinder gasoline direct injection engine to provide a high efficiency and low emissions operating mode for production spark ignition. Different injection strategies are investigated based on their efficiency and cylinder out emissions.

1.3 Motivation

Vehicle emissions standards continue to be a growing concern of public and governmental interest. The United-States Environmental Protection Agency (EPA) is currently in phase 2 of their light duty vehicles emissions and fuel economy standards for model years 2017-2025 [2]. There is great interest in the automotive industry to pursue alternative combustion methods to reach these standards. LTC provides a method to increase engine efficiency thus increasing fuel economy and CO_2 emissions per mile. Using LTC also produces less NOx emissions compared to conventional SI engines.

1.4 Thesis Structure

The structure of this thesis is outlines in the thesis structure road map shown in Figure 1.1. Chapter 2 gives background into LTC combustion methods. Chapter 3 describes the setup of the General Motors LNF engine. The chapter also includes the experiments and modifications conducted to achieve RCCI combustion on this experimental setup. The combustion metrics and the combustion analysis methodology used in this research are explained in Chapter 4. Chapter 5 contains the four test cases conducted for this experiment. RCCI tests were conducted using only a pilot injection for the high-reactivity fuel in Case 1. RCCI test were then conducted

with NVO in Case 2. A split injection strategy was investigated in Case 3 still while using NVO. In Case 4 the emissions of split and the single injection strategy were compared with the engine operating in SI mode. The results are discussed and analyzed in detail in Chapter 6. The conclusions of this research and possible future work are presented in Chapter 7.

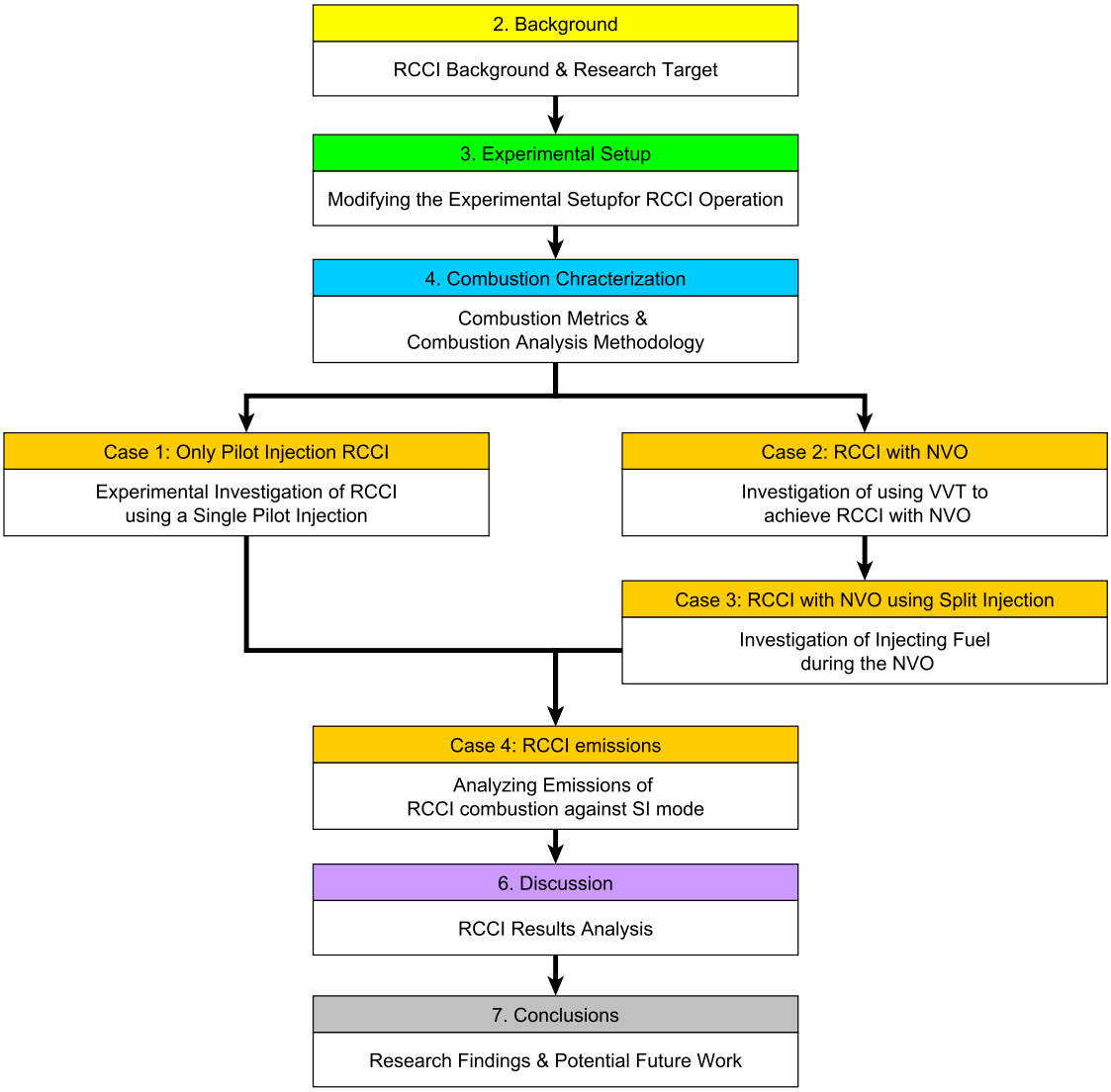

Figure 1.1: Thesis Structure Road Map

Chapter 2

Background

2.1 Low-Temperature Combustion

LTC is a collection of combustion strategies that utilize a low combustion temperature through fuel auto-ignition to take advantage of combustion chemistry that avoids the formation of harmful emissions [3]. Kamimoto's local equivalence ratio-temperature, ϕ-T, map [4] in Figure 2.1 shows the soot and NOx formation regions with respect to SI, DI and LTC combustion regimes. The formation of soot can be avoided by staying lean while NOx production can be avoided with low combustion temperatures.

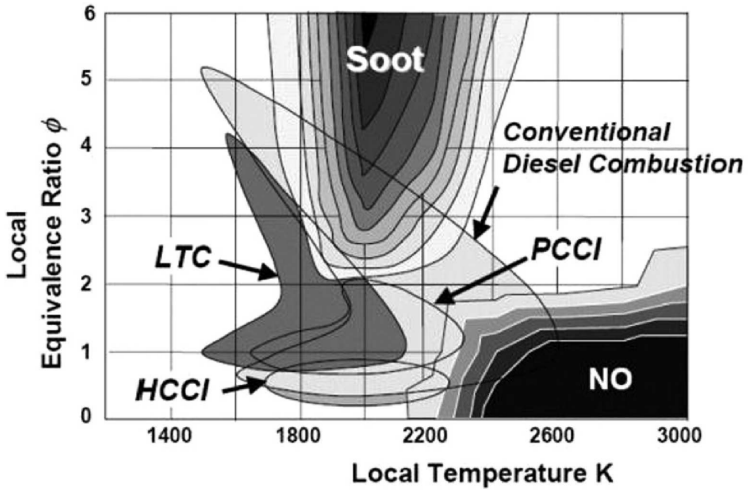

Figure 2.1: Kamimoto's ϕ-T map with Soot and NOx formation regions [4]

Homogeneous Charge Compression Ignition (HCCI) is a form of LTC which uses a single fuel that is fully premixed with air and globally lean. The air-fuel mixture auto-ignites quickly compared to SI combustion [5] thus gives higher efficiency by more closely imitating the constant volume pressure rise of the Otto cycle [6]. The combustion timing of HCCI is dictated by chemical kinetics [1] thus it is difficult to control since it does not rely on a spark or diffusion flame from a direct injection.

Dual-Fuel HCCI uses a blend of two fuels to control combustion phasing [7]. Dual-fuel HCCI fully premixes the two fuels and allows for fuels with low-reactivity like natural gas to be used at lower compression ratios by combining them with higher reactivity fuels. Premixed-Charged Compression Ignition (PCCI), also known as Partially Premixed Combustion (PPC), uses a single fuel injected early during compression to stratify the charge. PCCI has had problems avoiding the NOx-soot tradeoff that exists with diesel combustion without the use of heavy amounts of EGR [8, 9].

Mazda's SKYACTIV-X gasoline engine Spark Controlled Compression Ignition (SPCCI), to be released in 2019 model vehicles, uses HCCI like auto-ignition of gasoline fuel in addition to a flame propagating from a spark [10]. This method was developed using complex and accurate simulations of the combustion chemistry. This developed method allows for direct control over the ignition timing through the use of the spark while expanding the range in which combustion can occur compared to traditional HCCI.

2.2 RCCI

RCCI is a dual-fuel partially premixed auto-ignition strategy that controls the combustion timing by varying the ratio between a high-reactivity and a low-reactivity fuel. RCCI has yielded lower maximum Pressure Rise Rates (PRR) compared to HCCI and

PCC strategies [11]. The low-reactivity fuel is typically port-injected while the direct injectors spray the high-reactivity fuel directly into the engine cylinder. A high-reactivity fuel injection during the cylinder compression allows for a large amount of controllability over the ignition timing [11]. However when the direct injection is closer to TDC more NOx emissions are formed. Multiple direct injections can be used during the compression stroke to create stratification of the fuel reactivity [8]. Fuel stratification can cause lower PRR, higher gross indicated efficiencies and near-zero NOx production.

2.3 NVO and Fuel Reforming

Residual gas can be recycled in the engine cylinder to help raise the cylinder temperature at the Intake Valve Closing (IVC) using internal Exhaust Gas Recirculation (EGR) through the use of Negative Valve Overlap (NVO). Raising the cylinder temperature by mixing the intake with hot residual gas assists fuel auto-ignition with low compression ratio engines [12]. Direct injection of liquid fuel during the NVO recompression can decrease the temperature of the intake stroke due to the latent heat of evaporation of the injected fuel. The reduced temperature of the air mixture causes an increased delay in the igniton thus inhibiting NOx production [13]. Injecting fuel at the beginning of the NVO compresses the fuel and can cause endothermic fuel reforming [14]. Fuel reforming forms chemical species that promote auto-ignition during the NVO.

Chapter 3

Experimental Setup

3.1 LNF Engine

The engine used for this work is a 2.0L Gasoline Direct Injection Engine (GDI) General Motors Ecotec II LNF engine from a 2009 Chevrolet Cobalt as shown in Figure 3.1. The engine is equipped with dual camshaft Variable Valve Timing (VVT) phasers, a high pressure fuel rail direct injection systemand a twin scroll turbocharger. Relays allow for either the stock engine controller or an external customized controller to actuate the direct injectors and spark. NGI-2 injectors were added to the intake manifold to allow gaseous fuels like natural gas or liquid fuels to be port injected in addition to the direct injectors. More details about the engine setup are given in [15]. For this work the stock pistons were replaced with larger pistons to increase the engine's compression ratio.

3.1.1 Fueling System

Fuel tanks supply the direct injection fuel system using a Walbro GSL 391 inline fuel pump regulated to 60 psi using an Aeromotive 13129 EFI fuel pressure regulator. This fuel is then fed to the stock high pressure fuel system which is capable of operating to pressures up to 15 MPa. The direct injection fuel rail pressure was held at a

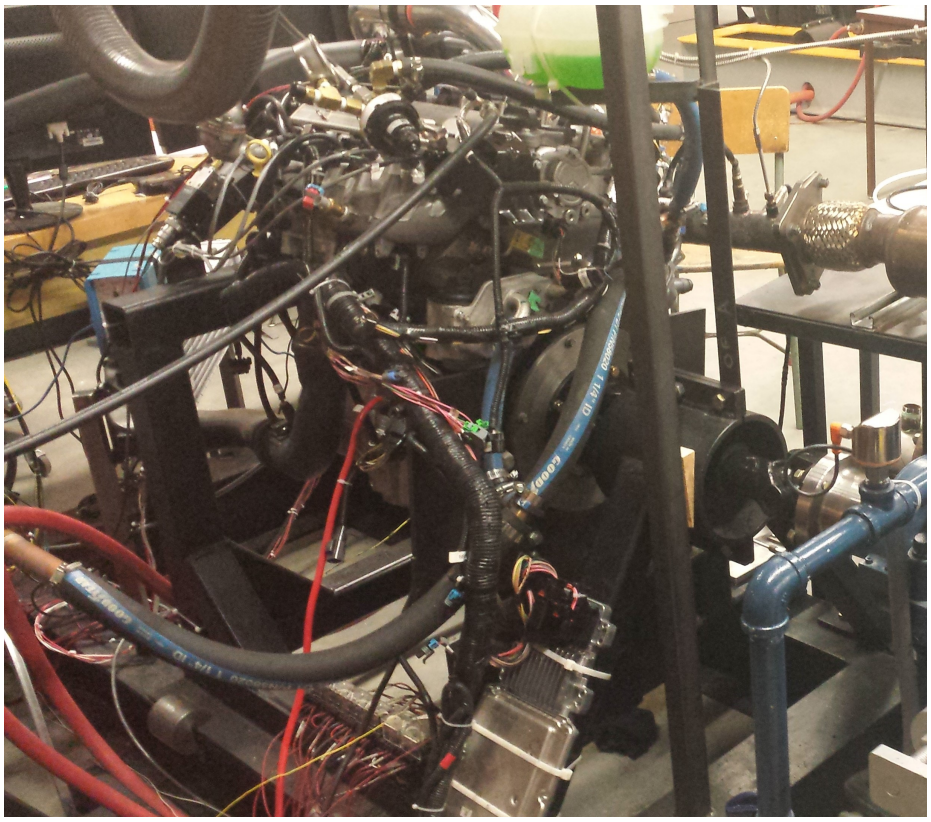

Figure 3.1: The 2.0L General Motors Ecotec II LNF Engine, modified with additional port injection, higher compression ratio and research control

constant pressure for the tests performed in this study. However, changing the fueling rate rapidly when going to a different load will cause the injection rail pressure to fluctuate [15]. In this study tests are conducted with a constant fuel pulse width to maintain accuracy in estimating fueling rates since the fuel rate is calibrated by pulse width at a given injection pressure. N-heptane fuel was used in the direct injection system.

The LNF engine was modified to also have port injected natural gas. The port injectors use an IMPCO Technologies HPR-3600 high pressure regulator to regulate the 138 bar (2000 psi) natural gas supply down to 7 bar (100 psi). The standard line natural gas composition is shown in Table 3.1 [16].

Fuel injection calibration tests were conducted to obtain the relation between

Table 3.1: Natural Gas Properties

CH_4 dry molar content	95.39%
C_2H_6 dry molar content	1.9%
N_2 dry molar content	1.93%
CO_2 dry molar content	0.78%
Molar mass (kg/kmol)	16.76
H/C ratio	3.92
LHV (kJ/kg)	44 818

injected fuel amount and the pulse width duration. A natural gas tank and the n-heptane fuel container were placed on a scale to measure the amount of fuel consumed over the measured test duration with a constant injection pulse width. The engine speed is kept constant thus the amount of injections for the entire test is known. The total fuel consumed per injection can be calculated as follows

$$m_{f_i} = \frac{\dot{m}_f}{n_{inj}} = \frac{m_{f,tot}}{n \cdot t_{tot} \cdot \frac{2}{60}}$$

where m_{f_i} is the mass of fuel injected per injection (mg), $\dot{m}_f$ is the mass flow rate of injected fuel (mg/s), n_{inj} is the number of injectors, $m_{f,tot}$ is the total fuel used from the fuel container during the test (mg), t_{tot} is the total time of the test (s) and n is the engine speed (RPM).

With operating points of various injection pulse widths a calibration equation for the fuel injected amount versus the pulse width duration of the injector is generated using a linear regression. The calibration for the natural gas port injectors is shown in Figure 3.2, while the n-heptane direct injectors at an injection pressure of 10 MPa (100 bar) is shown in Figure 3.3. The error for the injected fuel mass was calculated based of the measurement errors for the fuel container mass $m_{f,tot}$. The minimum n-heptane fuel injection pulse width is around 0.28 ms. With lower pulse widths the injector does not fully open and no fuel is injected.

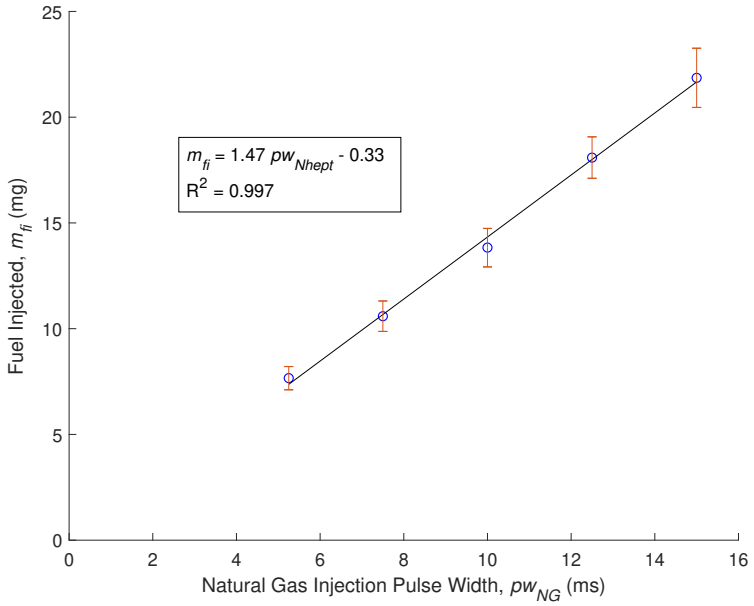

Figure 3.2: Natural gas port injector fuel calibration, P_{inj} 6 bar (100 psi)

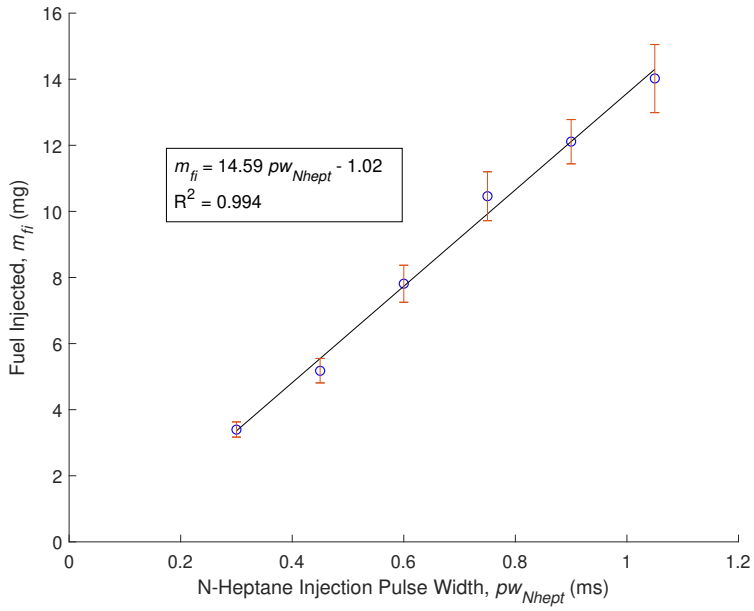

Figure 3.3: N-heptane direct injector fuel calibration, P_{inj} = 100 bar

3.1.2 Engine Control System

The General Motors stock Engine Control Unit (ECU) remains connected to the engine and controls and commands auxiliary systems throughout operation. The dSPACE MicroAutoBox II 1511/1512 (MAB) with RapidPro 1601 power electronics system (RP) controls the main operating parameters of the engine. Relays allow for the direct injectors and the spark to be controlled by either the stock ECU or the MAB shown in Figure 3.4. Switching to the stock ECU allows engine operation using the production controller with no modifications. For this study the relays were set for the MAB controller as the engine no longer uses the stock pistons and the direct injected fuel is n-heptane instead of gasoline.

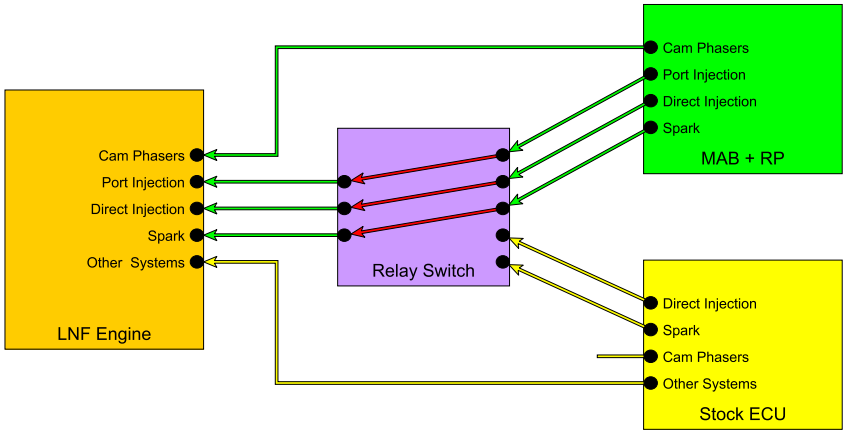

Figure 3.4: Engine Controller Relay Diagram

3.1.3 Intake Air Heating

The engine's intercooler located after the engine's turbocharger and before the intake manifold is replaced with an Omegalux AHF-14240 2000W 240V inline air heater shown in Figure 3.5. The heater is controlled using a Type W20HMT3 Variac Autotransformer with an adjustable output voltage from 0 - 240V. The heater may only be in operation while there is airflow through the heating element. Thus the heater

must only be turned on after the engine is started and must be turned off before the engine stops.

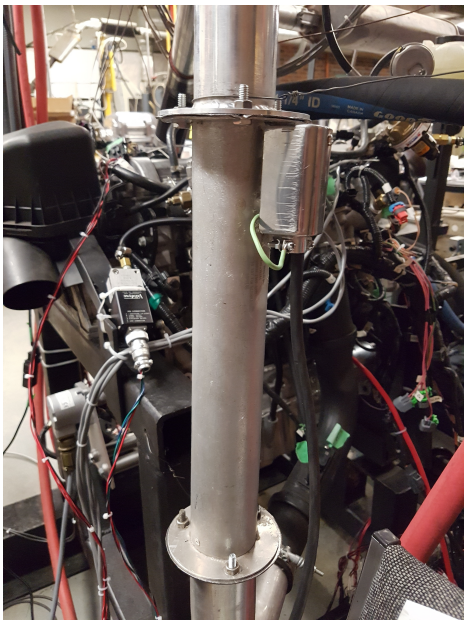

Figure 3.5: Omegalux AHF-14240 2000W 240V inline Air Heater

3.1.4 Cam Phasing

The LNF engine has independent cam phasers for the intake and exhaust camshafts. Both the exhaust and intake cams have a constant cam profile. The phasers are actuated hydraulically by an oil pump located at the driveshaft end of the exhaust camshaft. The exhaust camshaft is fully advanced at the parked position while the intake cam is fully retarded. The exhaust valve can be retarded up to 50 CAD while the intake cam can be advanced by 50 CAD. At the fully phased position both intake and exhaust valves are open causing Positive Valve Overlap (PVO) as shown in Figure 3.6. The phasing information for the cams is detailed in Table 3.2.

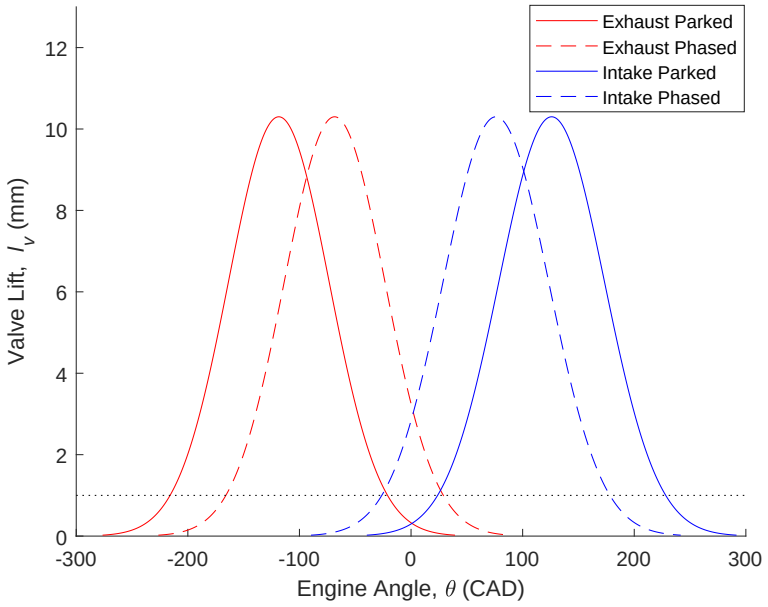

Figure 3.6: Original Valve Lift Profile Timings for the Parked and Phased positions

Negative Valve Overlap (NVO) can be used to help trap residual gases in the cylinder from the previous cycle in a process called internal Exhaust Gas Recirculation (EGR). In order to achieve NVO, the exhaust and intake cams must both be closed during the TDC between the exhaust and intake stroke of the engine thereby trapping exhaust gas for the next cycle. This was achieved by rotating the camshafts with respect to the timing chain to advance the exhaust camshaft and retard the intake camshaft. When the phasers are fully phased, there is no negative valve overlap, similar to the parked position of the stock configuration. Now the LNF engine needs to start up in this fully phased position, denoted as the "default position", since the engine can't start with the valves phased for NVO. Once the engine is up to speed the intake and exhaust phasing can be reduced thus advancing the exhaust cam and retarding the intake cam increasing the NVO as shown in Figure 3.7.

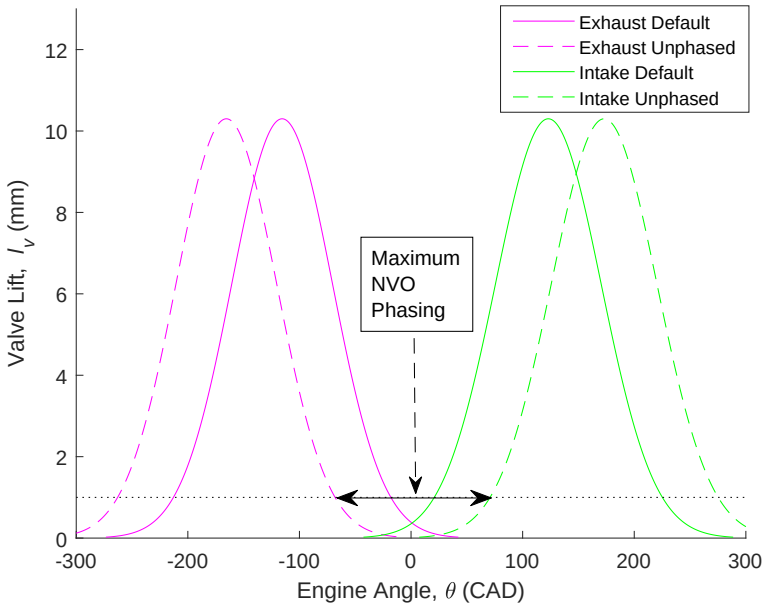

Figure 3.7: Modified Valve Lift Profile Timings for the Default and Unphased positions

Table 3.2: Cam Phasing Information for different Phaser Configurations

Cam Position	**Parked**	**Phashed**	**Default**	**Unphased**
Intake Centerline (CAD aTDC)	126	76	123	173
Intake Duration @ 1mm lift (CAD)	203.5	203.5	203.5	203.5
Exhaust Centerline (CAD aTDC)	-118.5	-68.5	-115.5	-165.5
Exhaust Duration @ 1mm lift (CAD)	194	194	194	194
NVO @ 1 mm lift (CAD)	46	-54	40	140
NVO Phasing Duration, ϕ_{NVO} (CAD)	6	-94	0	100

3.2 Sensors and Data Acquisition

The LNF Engine is connected to several sensors, controllers and computers in order to control the engine and dynamometer for the laboratory experiments. A signal diagram of the shown the measured signals in blue and the control signals in red arrows in Figure 3.8.

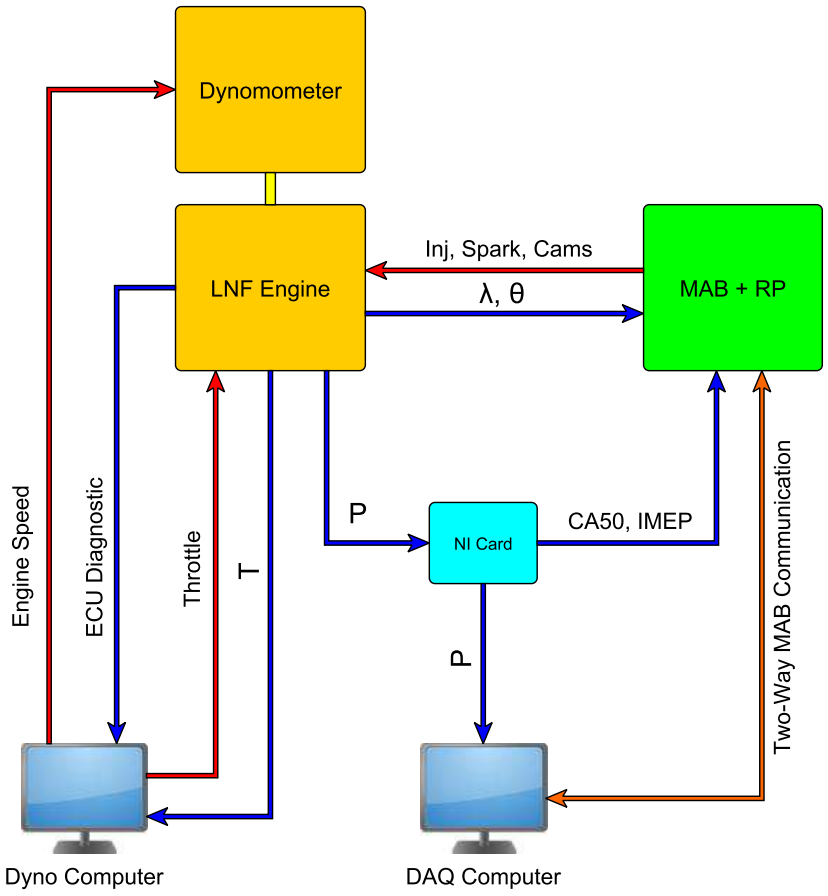

Figure 3.8: Signal Diagram for the LNF Engine Setup

3.2.1 Cylinder Pressure

Kistler 6125C11U20 pressure transducers mounted onto the engine head measure the in-cylinder pressure of the engine up to pressures of 300 bar. A Kistler Type 5064C charge amplifier boosts the pressure transducer signal to a 0-5 V signal. The NI-CARD records this voltage on a Data AQuisition (DAQ) computer. A BEI 3600 encoder (model XH25D-F1-SS-3600-ABZC-28V/VSM18) mounted to the engine's crankshaft triggers the recording of the cylinder pressure allowing for data to be recorded with a 0.1 CAD resolution.

3.2.2 Dyno Computer

The Dyne Systems 1014W eddy current dynamometer shown in Figure 3.9 is attached directly to the engine output crankshaft with a Machine Service MSI-41RE ISO-TEC vibration dampening rubber isolated driveshaft. A Labview interface shown in Figure 3.10 allows for control of the Dynamometer including the engine speed and the engine throttle actuator position. The Labview interface also displays and records thermocouple readings of the engine intake and exhaust gas temperatures.

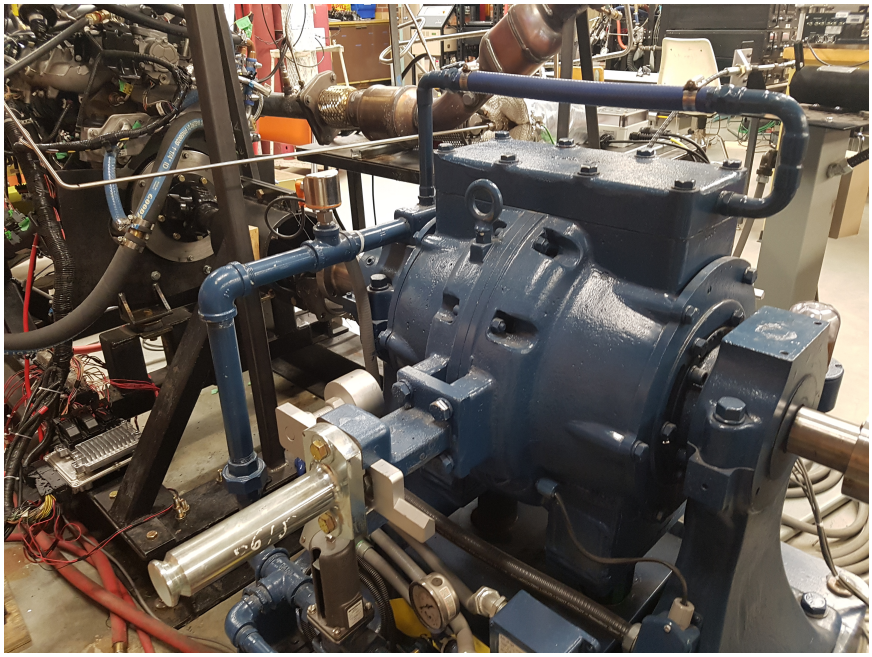

Figure 3.9: Dyne Systems 1014W eddy current Dynamometer

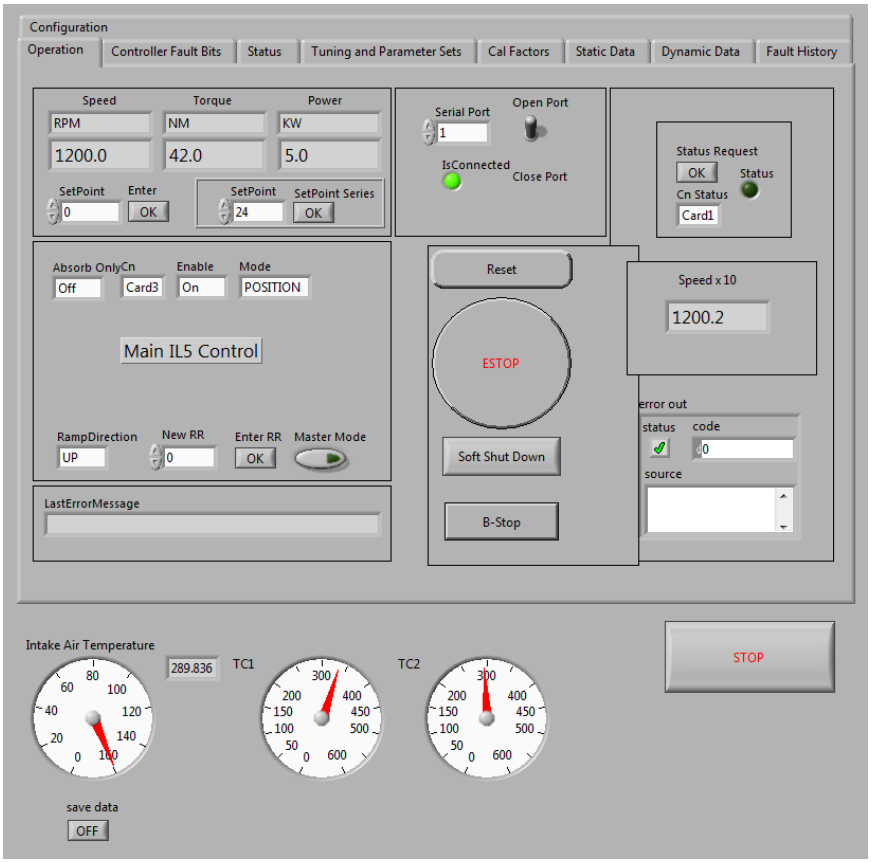

Figure 3.10: Labview Dynamometer control interface on the Dyno Computer

A HP Tuners VCM Scanner program shown in Figure 3.11 scans, charts and records the diagnostic data from the stock ECU in real time. This allows for monitoring of the engine's auxiliary systems during engine operation and testing.

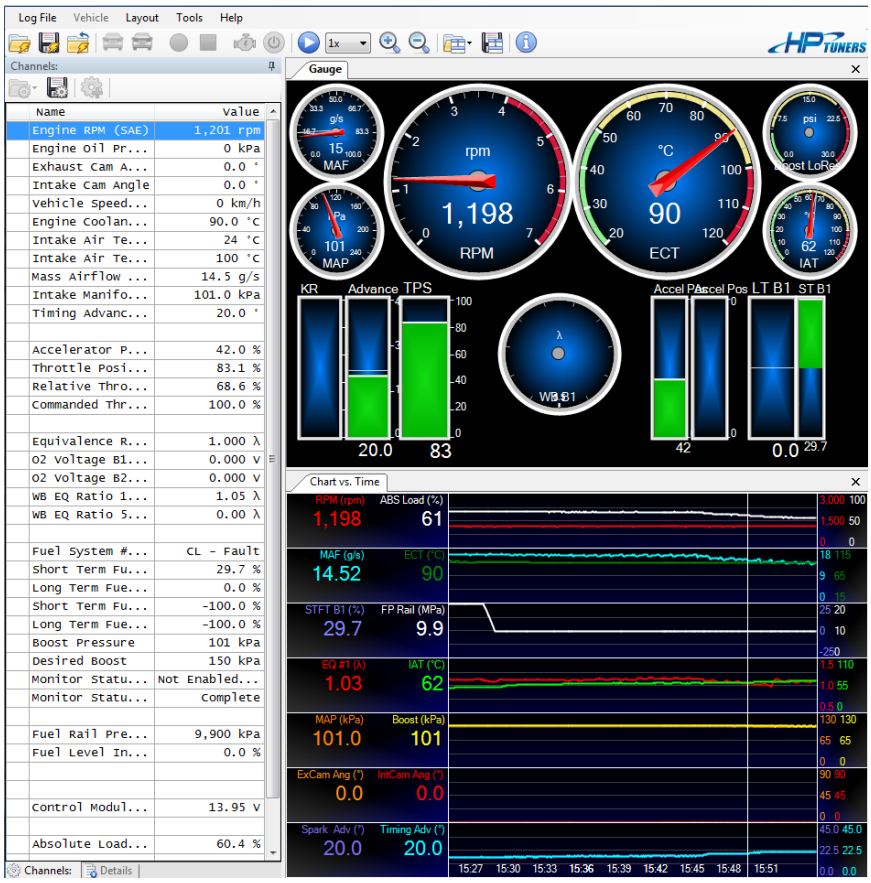

Figure 3.11: HP Tuners VCM Scanner live diagnostic tool on the Dyno Computer

3.2.3 DAQ Computer

The DAQ computer is mainly used to interface with the MAB controller during operation, to monitor the cylinder pressure trace and to update the MAB/RP controller configuration when the system is offline. The ControlDesk program shown in Figure 3.12 from dSpace allows for live interfacing with the MAB engine controller. Parameters from the MAB may be viewed, recorded or modified during operation. The injection and ignition timings/durations of the port and direct injectors, the ignition spark and cam phasing are manipulated from the ControlDesk interface.

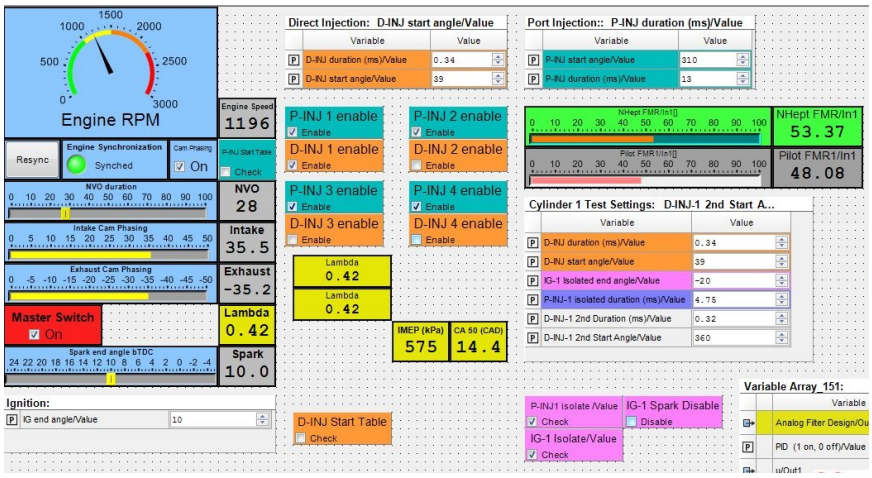

Figure 3.12: dSpace Control Desk interface on the DAQ Computer

Modifications to the MAB controller itself are conducted offline by modifying the dSpace Simulink control diagram shown in Figure 3.13 on the DAQ computer, generating code, then downloading it to the MAB.

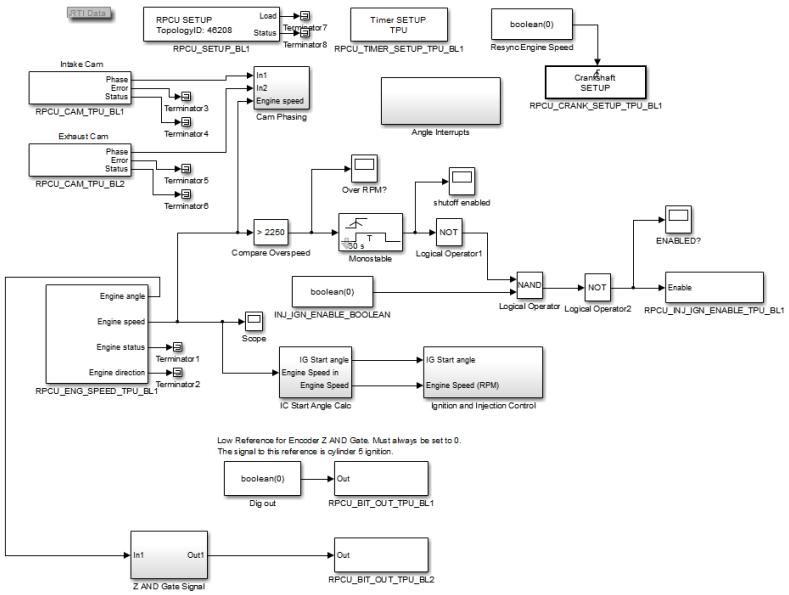

Figure 3.13: Simulink Controller block diagram for the MAB

The DAQ computer also displays the cylinder and manifold pressure traces from the NI-card on a live cycle-by-cycle basis and can also display cycle-by-cycle calcu-

lations of the combustion timing CA50, peak cylinder pressure location, engine load IMEP, maximum Pressure Rise Rate (PRR) and maximum Heat Release Rate (HRR) shown in Figure 3.14.

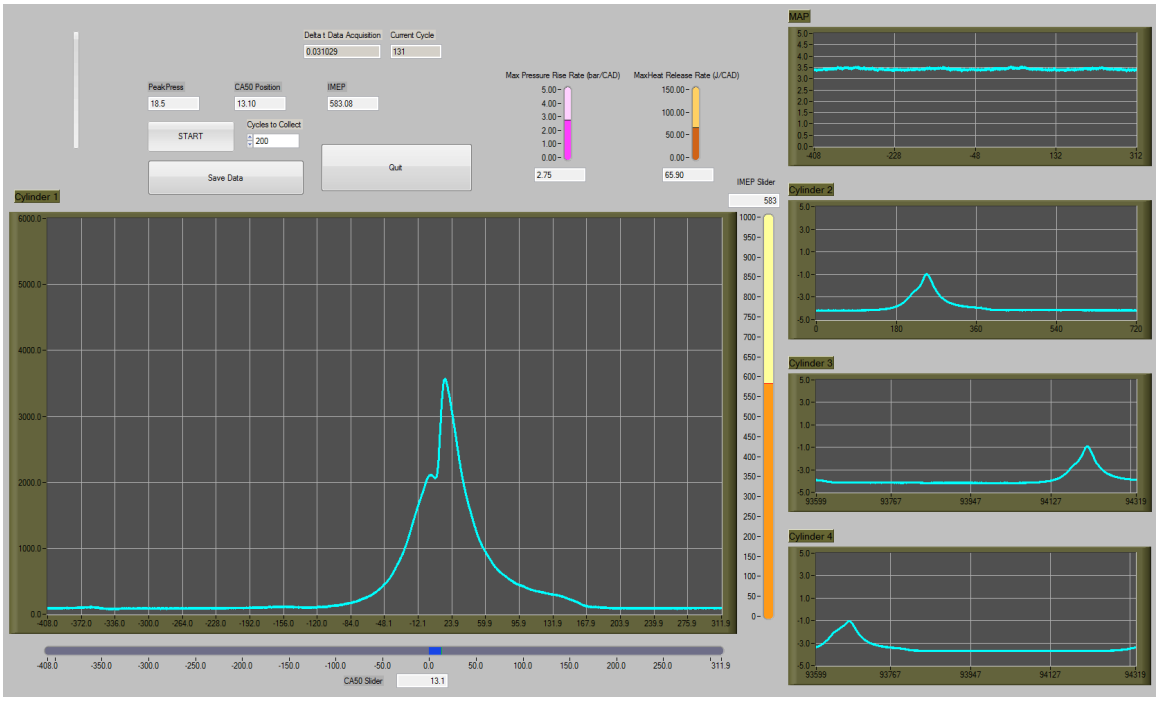

Figure 3.14: Live Labview Cylinder Pressure Trace plotting graphic

3.2.4 FTIR Real-Time Gas Analyser

The MultiGas 2030 FTIR Continuous Gas Analyzer shown in Figure 3.15 is a real-time multigas analyzer that is used to determine the exhaust gas composition from the LNF engine. The Fourier Transform Infrared (FTIR) spectrometer passes an infrared beam through a gas sample, obtains the interference pattern of the gas and identifies the gas composition based off of the absorption spectrum of the gas constituents [17].

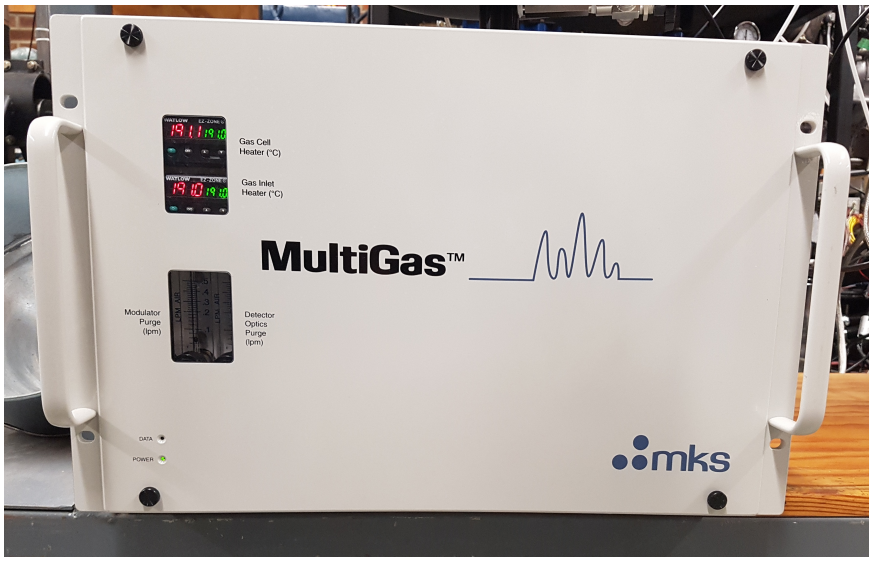

Figure 3.15: MultiGas 2030 FTIR Continuous Gas Analyzer

The gas composition data is collected at a 5 Hz frequency using the MKS Series 2000 MultiGas Analyzer software version 10.1 shown in 3.16. The gas composition is reconstructed based off of elements included in the "gas recipe" selected. For this study the 'CNG Low NMNEHC (below 500 ppmC) 5Hz R4' recipe is used. The gas composition can be seen live within the data collection software shown in Figure 3.17.

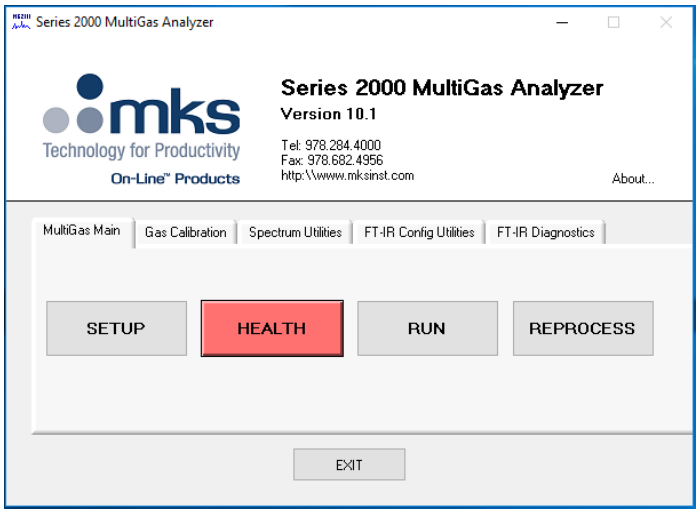

Figure 3.16: MKS Series 2000 MultiGas Analyzer software program for the FTIR

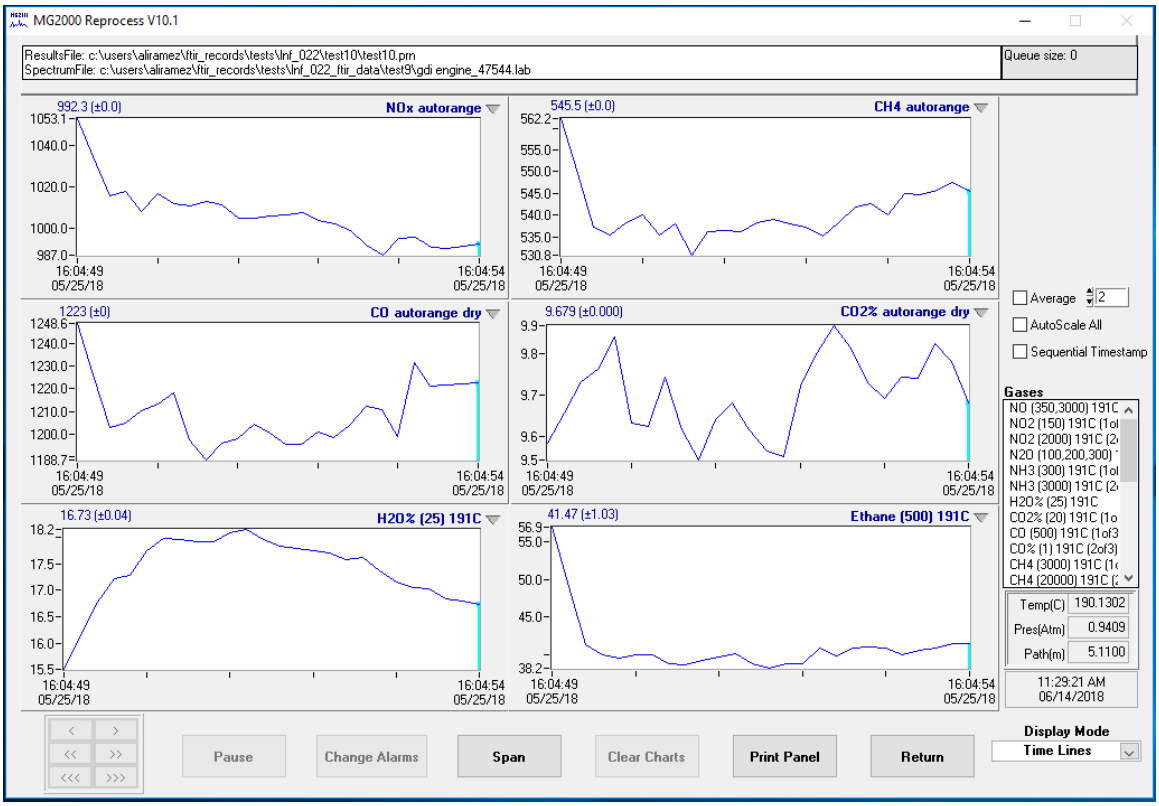

Figure 3.17: FTIR Emissions of NOx, CH_4, CO, CO_2 and H_2O over 5 seconds

For this study the emissions sampling port is located on the exhaust manifold next to the cylinder 1 exhaust before it mixes with the other cylinders. This allows for emissions for only one cylinder to be sampled. The sample then passes through two Flexotherm Mod-Flex Heated Filters (model number MFF-7.0-S-K-A-6-L5-C-X-S-L5-M) shown in Figure 3.18 connected with Flexotherm 5' Heated Sample Lines (model number P/N GT-E-6/4-AT-KL-191C-B-6S-60-48) heated to 191°C. From there the sample passes through the MKS heated pump and filter attached to the gas analyzer.

Figure 3.18: Flexotherm Mod-Flex Heated Filters

3.3 Engine Modifications for RCCI

Modifications to the LNF engine testing apparatus were necessary to achieve auto-ignition of high-reactivity fuels on the engine. Typically HCCI/RCCI tests are conducted on test-cell engines and high compression ratio converted diesel engines. This is due to the high in-cylinder temperature and pressure required to auto-ignite a pre-mixed fuel air mixture. HCCI tests have been conducted on gasoline spark ignition engines with the assistance of higher compression ratio pistons, intake air heating, internal Exhaust Gas Recirculation (EGR) and intake air boosting using external supercharging.

Modified pistons were custom made by Wiseco pistons to increase engine's compression ratio from 9.2:1 to 11.1:1. Tests were conducted on one engine cylinder to determine if the n-heptane, natural gas and air mixture could auto-ignite without the need for intake air heating or boosting. These test were conducted with a late

"safety spark" after TDC to ensure ignition of the fuel occurred for the case when the fuel failed to auto-ignite. This was to ensure that unburnt fuel was not being accumulated in the engine's exhaust system. Auto-ignition was not achieved in these tests, therefore it was determined that intake air boosting and/or heating would be required.

The engine's built-in turbocharger was not capable of providing sufficient boost at the lower engine speeds that HCCI/RCCI was tested. Combustion simulations in Appendix B using Cantera software [18] determined that with 100°C intake air auto-ignition could occur. Thus the engine's intercooler was removed and replaced with an Omegalux AHF-14240 2000W 240V inline air heater. With the heater auto-ignition was achieved however was quite sporadic. The direct injection pressure was increased allowing for later pilot injection timings and more consistent auto-ignition.

3.3.1 Installation of Wiseco Pistons to Raise Compression Ratio

The compression ratio of the engine can be determined as follows

$$CR = \frac{V_{max}}{V_{min}} \tag{3.1}$$

where CR is the engine's compression ratio, where V_{max} and V_{min} are the maximum and minimum in-cylinder volume respectively.

Larger compression ratios are typically required to achieve fuel auto-ignition for HCCI/RCCI. The compression ratio of the stock GDI engine is $CR = 9.2$ which is low compared to converted diesel engines who run HCCI/RCCI [11]. As such engine pistons were manufactured by Wiseco Performance Products in order to raise the compression ratio of the engine for this research. Details of the piston order are in Appendix A. The piston bowl shape of the stock General Motors piston was replaced with a domed piston top shown in Figure 3.19. The domed piston top is designed

to minimize the volume in the cylinder and thus maximize the compression ratio for this engine.

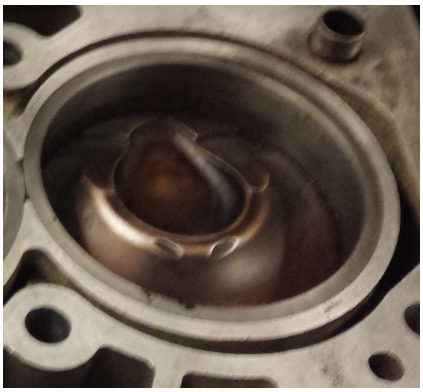

(a) Stock Piston Head Shape

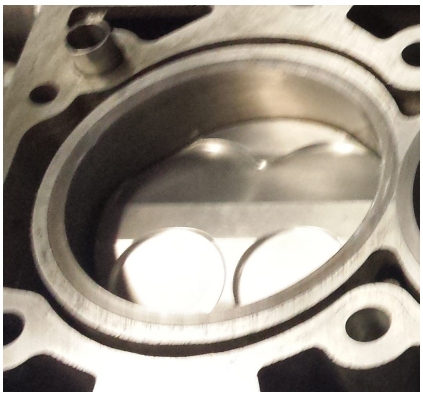

(b) Wiseco Piston Head Shape

Figure 3.19: Engine Piston Head Shapes

The increase in the piston volume for the Wiseco was measured by filling the chambers containing the Wiseco and the stock pistons with oil as shown in Figure 3.20. The volume of oil necessary to reach the rim of the cylinder chamber was recorded for both piston designs. The chamber with the Wiseco piston installed required 11.3 mL or cm^3 less oil. The difference between oil; required to reach the chamber rim corresponds to an increase of 11.3 cm^3 in cylinder head volume. With the unchanged displacement volume of 500 mL per cylinder, the larger Wiseco piston head and using Equation 3.1, the engine's compression ratio was determined to be 11.1 with the Wiseco Pistons.

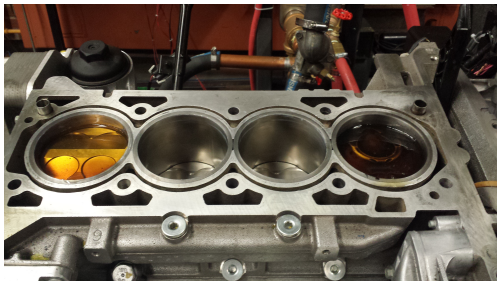

Figure 3.20: Oil Measurements on the LNF Engine head to determine the Volume Increase of the Wiseco Piston Design

3.3.2 Intake Air Heating

Tests were conducted with the Wiseco pistons to determine if auto-ignition could be achieved with the larger compression ratio. The operating conditions for this test can be found in Table 3.3. The test were conducted at 1000 RPM, lean operating conditions and with a safety spark at 5 CAD aTDC in order to avoid unburnt fuel being trapped in the engine exhaust. Figure 3.21 shows the pressure trace from one such test. From the pressure trace it can be observed that no heat release or ignition occurs after the n-heptane pilot injection. The ignition of the fuel occurs after the safety spark.

Engine Speed, n	1000 RPM
Lambda, λ	1.25, 1.18 and 1.11
Intake Air Pressure, P_{in}	55 kPa
Safety Spark Timing, θ_{IG}	-5 CAD bTDC
N-Heptane pilot timing	25 CAD bTDC
NG injection timing	360 CAD bTDC

Table 3.3: Preliminary N-Heptane Test Operating Conditions

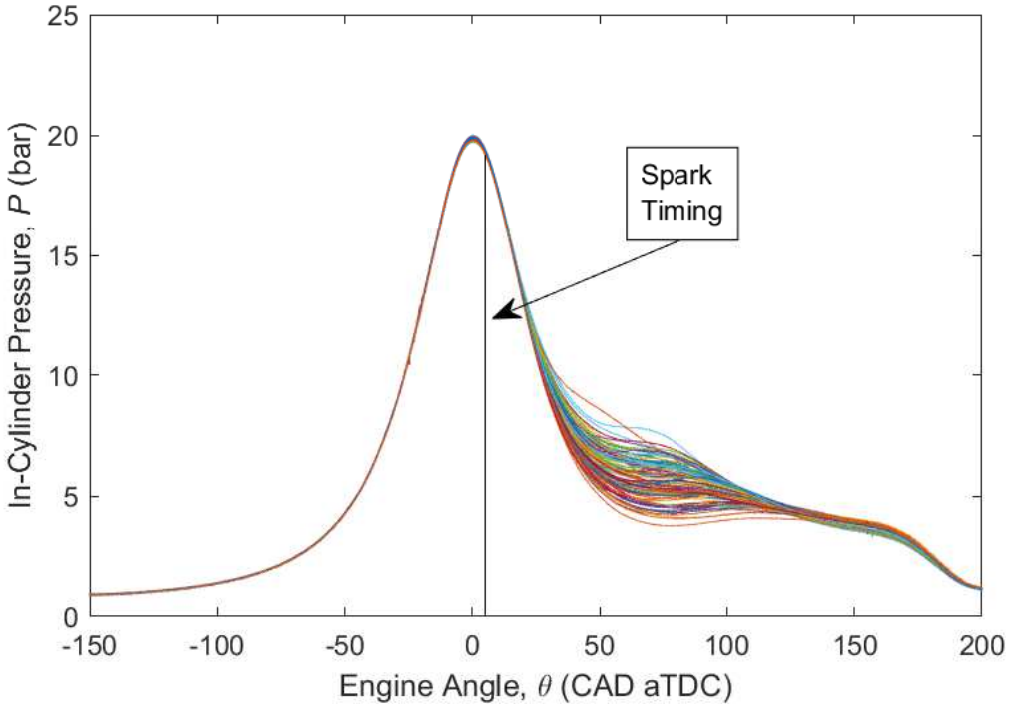

Figure 3.21: N-heptane Pilot Injection Test Pressure Trace for 100 Cycles
$\lambda = 1.11$, θ_{IG} = -5 CAD BTDC

Cantera simulations were used to determine what intake air temperature would be required to attain fuel auto-ignition of n-heptane. Details of the Cantera simulation can be found in Appendix B. These results indicate that the LNF engine with the Wiseco Pistons requires roughly intake air at roughly 100°C to achieve n-heptane auto-ignition.

Given that the tests were done at 31°C and intake pressure of 55kPa. We can estimate how much power is require to heat the intake air using Equation 3.2.

$$Q = m_a \, c_p \, \Delta T \tag{3.2}$$

With the mass of air used is given by the Equation 3.3.

$$\dot{m}_{air} = V_d \, \rho_a \, \frac{n}{2(60)} \tag{3.3}$$

The largest density of air desired occurs at ambient temperature and $T_{in} = 100°C$ would give the largest value for heat required. This occurs when the intake is not throttled when the pressure is near ambient. This gives an estimated 0.0310 kg/s of air required at an engine speed of 1000 RPM. Thus using Equation 3.3, the maximum required power to heat untrottled intake air to 100°C at 1000 RPM is 2.160 kW.

With the addition of the Omegalux AHF-14240 2000W 240V inline air heater enabled auto-ignition with n-heptane and natural gas mixtures on the LNF engine with a raised compression ratio using the Wiseco pistons.

3.3.3 Raised Injection Pressure

RCCI auto-ignition tests were conducted with a low 2 MPa n-heptane fuel-rail injection pressure with the Wiseco pistons and 100°C intake air temperature shown in Figure 3.22. The low injection pressure meant the n-heptane fuel had to be injected early at the end of the intake stoke at 200 CAD bTDC. The full operating parameters are detailed in Table 3.4. This early injection timing is required for the n-heptane to properly atomize and mix with the air and natural gas in the cylinder. This is because the fuel atomizes more readily when it is at a higher pressure than the cylinder pressure [19]. The higher injection pressure creates smaller droplets and increases the penetration depth of the injected fuel [20].

Table 3.4: RCCI Direct Injection Pressure Test Operating Conditions

D-Inj Pressure, P_{inj} (MPa)	2	10
Engine Speed, n (RPM)	1000	1000
IAT, T_{in} (°C)	100	100
D-Inj Timing, θ_{DInj} (CAD bTDC)	200	30
Air-Fuel Equivalence Ratio, λ (-)	1.09	1.20

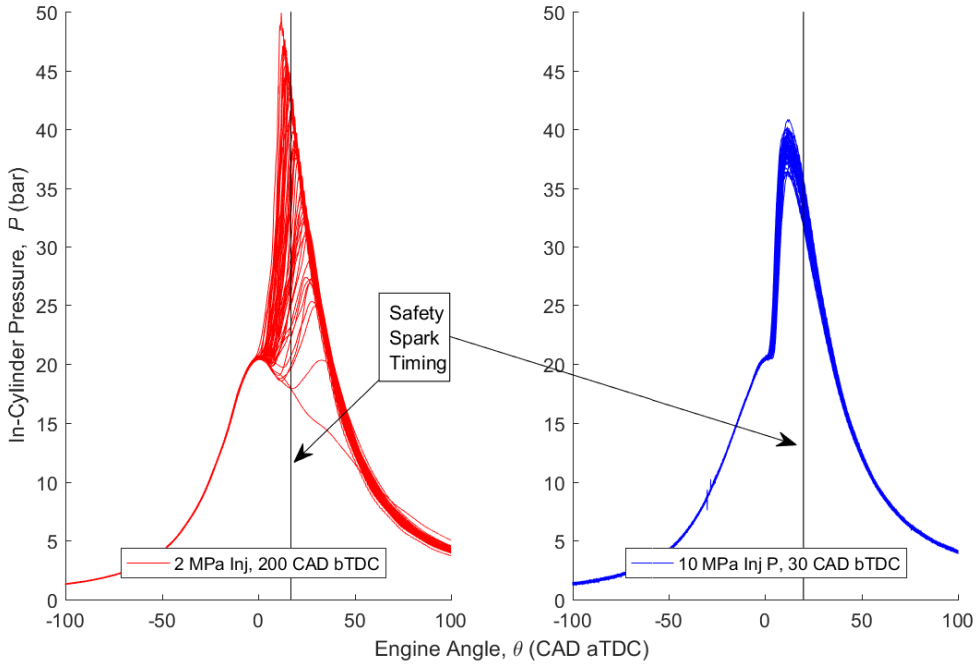

Figure 3.22: Comparison of In-Cylinder Pressure Traces for low, $P_{inj} = 2$ MPa, and high, $P_{inj} = 10$ MPa, n-heptane injection pressure strategies for 50 engine cycles

With the injection pressure raised to 10 MPa, the n-heptane will atomize and mixes quickly allowing for late pilot injection timings such as 30 CAD bTDC shown in Figure 3.22. The combustion timing for the two injection pressure auto-ignition points for 50 cycles are shown in Figure 3.23 and the mean and standard deviation are given in Table 3.5. The details of the heat release, CA10, CA50 and CA90 are given in the next chapter.

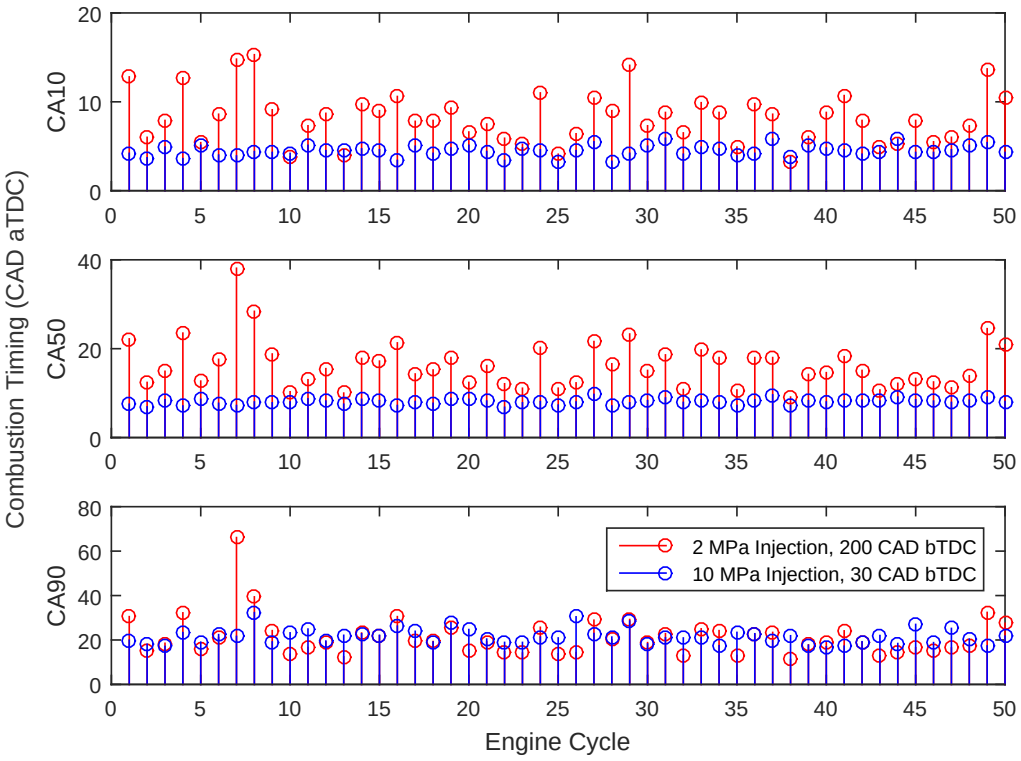

Figure 3.23: Comparision of the Combustion Stability of Low (2 MPa) and High (10 MPa) N-heptane Injection Pressure Strategies.

Table 3.5: Combustion Timing for low, P_{inj} = 2 MPa, and high, P_{inj} = 10 MPa, n-heptane injection pressure strategies

Combustion Completion (CAD aTDC)	2 MPa Injection, 200 CAD aTDC		10 MPa Injection, 30 CAD aTDC	
	Mean	Std Dev	Mean	Std Dev
CA10	8.3	2.9	4.5	0.6
CA50	16.4	5.4	8.1	0.6
CA90	21.0	9.0	21.6	3.5

The higher injection pressure strategy using a pilot n-heptane injection provides less combustion timing variance to the auto-ignition combustion. Since early auto-ignitions can cause engine knock and retarded ignitions can cause possible misfire, the higher injection pressure was used in this study.

Chapter 4

Combustion Characteristics

4.1 Combustion Metrics

The metrics in Table 4.1 were used to characterize combustion operating points from the cylinder pressure trace and will be described in detail.

Table 4.1: Combustion Metrics

Combustion Metric	Symbol	Units
Maximum Pressure Rise Rate	PRR_{max}	bar/CAD
Indicated Mean Effective Pressure	$IMEP$	bar
Heat Release Rate	HRR	J/CAD
Crank Angle of X% Mass Fraction Burned	$CA10$, $CA50$, $CA90$, etc	CAD
Indicated Thermal Efficiency	η_{th}	%
Combustion Efficiency	η_{comb}	%
Volumetric Efficiency	η_{vol}	%

Pressure rise rate, PRR, is a measure of how quickly the pressure increases during combustion. Thus PRR is simply the derivitaive of cylinder pressure with respect to the engine angle as:

$$PRR = \frac{\delta P}{\delta \theta} \tag{4.1}$$

where P is the cylinder pressure and θ is the engine angle (CAD).

Indicated Mean Effective Pressure (IMEP) is a measure of the engine's output power calculated [21] as:

$$IMEP = \frac{W_i}{V_d} \tag{4.2}$$

where V_d is the displacement volume of the engine and W_i is the indicated work which is calculated [21] as

$$W_i = \int P\, dV \tag{4.3}$$

where V is the cylinder volume.

The Heat Release Rate, HRR is calculated [21] as

$$HRR = \frac{dQ_{HR}}{d\theta} = \frac{1}{k-1} V \frac{dP}{d\theta} + \frac{k}{k-1} P \frac{dV}{d\theta} \tag{4.4}$$

where k, V, θ, and Q_{HR} are the specific heat ratio, in-cylinder volume, engine crank angle, and the heat released respectively.

The indicated thermal efficiency, η_{th} is calculated [21, 22] as

$$\eta_{th} = \frac{W_i}{E_t} \tag{4.5}$$

where E_t is the total injected fuel energy calculated using the fuel mass injected per cycle times the Lower Heating Value (LHV) of the two fuel (LHV_{NG} = 47.14 MJ/kg and LHV_{Nhept} = 44.57 MJ/kg, where the subscripts NG and $Nhept$ denote natural gas and n-heptane respectively. It is noted that the electrical work required to operate the intake air heater is not accounted for in this calculation of indicated thermal efficiency.

For this study the combustion efficiency, η_{comb}, is calculated the ratio between the

cumulative heat release and the energy of the fuel injected [22] as:

$$\eta_{comb} = \frac{\int_{SOC}^{EOC} Q_{HR}\, d\theta}{E_t} \tag{4.6}$$

where the heat release Q_{HR} is integrated from the Start Of Combustion SOC to the End Of Combustion EOC. This method can be used to compare the efficiency of combustion on an engine when the emissions data is not readily available.

The volumetric efficiency, η_{vol}, is calculated [21] as

$$\eta_{vol} = \frac{\dot{m}_a}{V_d\, \rho_a\, N_c} \tag{4.7}$$

where $\dot{m}_a$ is the intake air mass flow rate (kg/s), ρ_a is the intake air density (kg/m^3) and N_c is the engine speed (cycles per second).

4.2 Combustion Analysis Methodology

The combustion metrics used for this analysis, found in Table 4.1, are derived from the measured pressure trace. Figure 4.1 shows a schematic of an RCCI test with NVO between the EVC and IVO of the engine cycle.

4.2.1 Experimental Post-Processing for RCCI tests with NVO

Figure 4.2 shows the timings and nomenclature of the direct and port injection events.

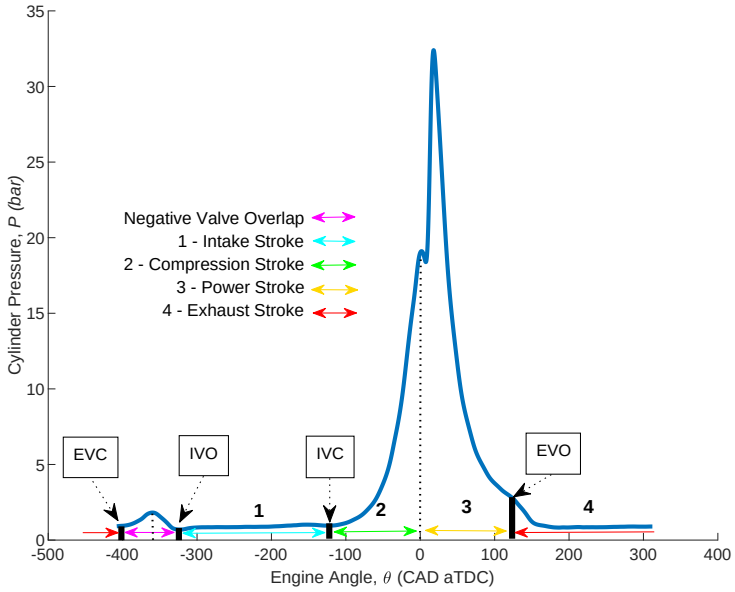

Figure 4.1: RCCI Engine Stroke Schematic showing Cylinder Pressure and valve timing for RCCI with NVO versus crank angle

The n-heptane injection during the NVO recompression of exhaust gasses is named DI1. The pilot n-heptane injection that occurs during the compression stroke before TDC of the power stroke is named DI2. This injection is denoted the pilot injection since it is used to initiate combustion of the premixed charge [11]. The single port fuel injection that occurs during the intake stroke after IVO is PI1. A safety spark is used during all auto-ignition tests to ensure that ignition of the fuel occurs every cycle even if the fuel mixture fails to auto-ignite and is set to 20 CAD aTDC for all auto-ignition tests unless stated otherwise.

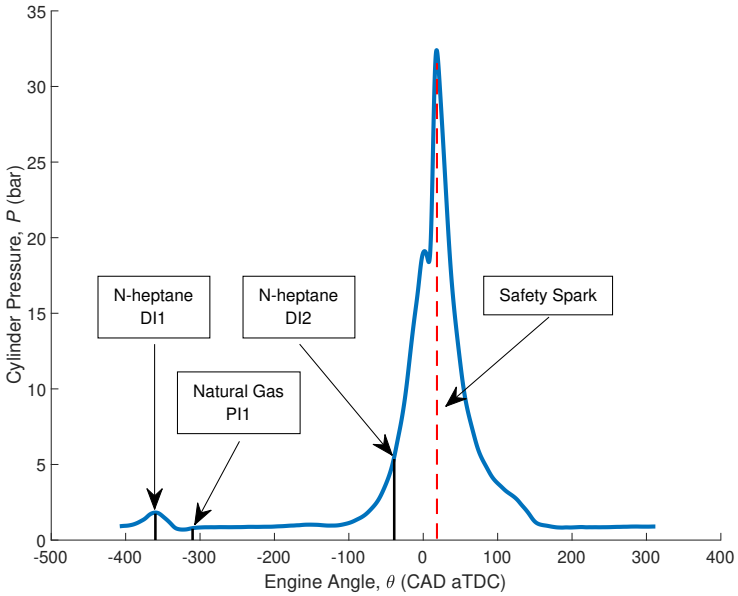

Figure 4.2: The Injection and Ignition Events for RCCI with NVO on the Cylinder Pressure Trace

The heat release from the auto-ignition can be characterized by finding the Heat Release Rate, HRR, from the pressure trace using Equation 4.4. An example of the HRR is shown in Figure 4.3. Many auto-ignited fuels undergo a two-stage heat release during HCCI/RCCI combustion [23]. The low-temperature heat release occurs just before 0° TDC at the end of the compression stroke while the high-temperature heat release occurs rapidly shortly after TDC at the start of the power stroke. The safety spark occurs at the tail end of the high-temperature heat release.

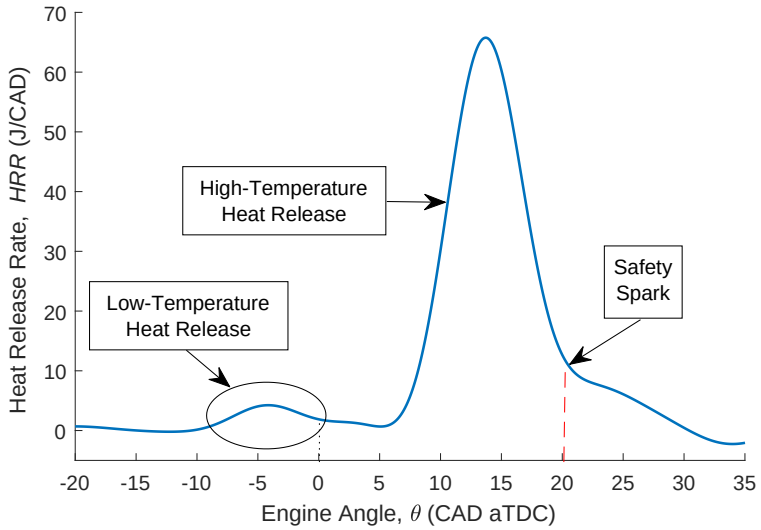

Figure 4.3: The Heat Release Rate of RCCI with NVO

The mass fraction of burned fuel can be determined by integrating HRR from IVC to EVO and finding the crank angle θ where that percentage of heat has been released. For example the CA50 occurred when $Q(\theta) = 0.5\,Q_{max}$. Figure 4.4 illustrates the relevant mass fractions used in this analysis. CA1 or CA3 is used to determine the timing of the Low-Temperature Heat Release (LTHR) depending on the total magnitude of the High-Temperature Heat Release (HTHR). CA10 is used to denoted the Start of Combustion (SOC) while CA90 is used to denote the End of Combustion (EOC). As such, the burn duration is defined as the duration in CAD from CA10-CA90 giving $\theta_{BD} = \theta_{CA90} - \theta_{CA10}$. The combustion timing of the HTHR is denoted by the CA50 given as θ_{CA50}.

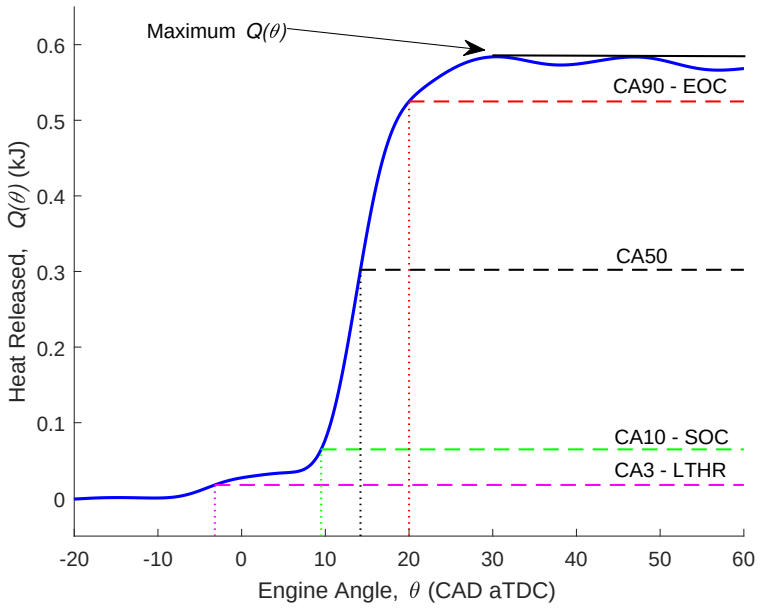

Figure 4.4: Cumulative Heat Release

4.3 Operating Limits for Knock and Misfire

Auto-ignition combustion is susceptible to engine knocking conditions since high-reactivity fuels are being used. If the combustion phasing is too advanced rapid pressure rises may occur causing early fuel detonation which may quickly damage the engine [6, 24]. A method for determining the acceptable pressure rise rate for SI engines operating with HCCI was developed using the ringing intensity as follows [25]:

$$RingingIntensity = \frac{1}{2k}\frac{\left(0.05\left(\frac{\delta P}{\delta t}\right)_{max}\right)^2}{P_{max}}\sqrt{k\,R\,T_{max}} \tag{4.8}$$

where R is the ideal gas constant. This method was used to determine acceptable PRR by Sandia National Laboratories [26] with a knock limit ringing intensity of 5 MW/m^2 with P_{in} = 1 bar, n = 1200 RPM of PRR$_{max}$ = 8 bar/CAD. Using similar conditions and a more conservative limit of 2 MW/m^2 we can estimate that low intensity knocking will occur at PRR$_{max}$ = 5 bar/CAD. For this experiment any

knocking is deemed unexceptable due to the possibility of runaway knock damaging the engine. A hard cap of $\mathbf{PRR}_{max}$ **= 3.5 bar/CAD** was imposed for all auto-ignition tests at n = 1200 RPM due to the high cyclic nature of the experimental setup [15].

Since auto-ignition is reliant on in-cylinder temperature conditions to ignite instead of a spark, the likelyhood of partial late ignitions or even misfire increases. Engine misfires send unburnt fuel into the exhaust which can damage modern catalytic converters [27]. For this research a safety spark is used after TDC to initiate combustion if the fuel mixture fails to auto-ignite. An increase in the frequency of very late combustion is an indicator for the fuel mixture failing to auto-ignite on time or at all. The combustion phasing is to be advanced when the variability of the combustion timing, CA50, increases due to these late ignitions started by the safety spark. These limits are determined by the engine operator observing the combustion live through the Labview interface shown previously in Figure 3.14.

Chapter 5

Research Results

5.1 Case 1: Only Pilot Injection RCCI

This section details the effects of the n-heptane pilot injection timing for RCCI combustion with only a single n-heptane injection. Natural gas is injected (PI1) and the n-heptane pilot (DI2) are as shown in Figure 4.2. The effects on the combustion timing, CA50, BD, HRR, and efficiencies are determined.

5.1.1 Test Operating Conditions

RCCI auto-ignition tests were conducted around an operating point with the n-heptane pilot injection DI2 timing as the only manipulated parameter. Two operating points are examined, one at 1000 RPM with lean combustion $\lambda = 1.19$ as shown in Table 5.1 denoted R1A, and another at 1200 RPM with combustion closer to stoichiometric with a $\lambda = 1.04$ as shown in Table 5.2 denoted R1B. The tests for operating point R1A was conducted before the timing chain of the LNF engine was adjusted (detailed in Section 3.1.4), so the NVO Phasing Duration, ϕ_{NVO}, is 6 CAD, the minimum for the original stock configuration.

Table 5.1: RCCI Engine Operating Conditions for R1A

NVO Phasing Duration, ϕ_{NVO} (CAD)	6
Engine Speed, n [RPM]	1000 ± 1
Cycles Collected	100
Intake Air Flow Rate, m_{air} [g/s]	13.2 ± 0.4
Intake Air Temperature, T_{in} [°C]	100 ± 5
Exhaust Gas Temperature, T_{exh} [°C]	340 ± 5
Air-Fuel Equivalence Ratio, λ	1.19 ± 0.02
N-Heptane Fuel Mass Ratio [%]	35.1
Injected Fuel Energy DI1, E_{DI1} [kJ]	-
Injection Start Angle DI1, θ_{DI1} [CAD bTDC]	-
Injected Fuel Energy DI2, E_{DI2} [kJ]	0.293
Injection Start Angle DI2, θ_{DI2} [CAD bTDC]	33
Injected Fuel Energy PI1, E_{PI1} [kJ]	0.574
Injection Start Angle PI1, θ_{PI1} [CAD bTDC]	360
Total Injected Fuel Energy, E_t [kJ]	0.866

Table 5.2: RCCI Engine Operating Conditions for R1B

NVO Phasing Duration, ϕ_{NVO} (CAD)	0
Engine Speed, n [RPM]	1200 ± 1
Cycles Collected	200
Intake Air Flow Rate, m_{air} [g/s]	15.7 ± 0.5
Intake Air Temperature, T_{in} [°C]	81.5 ± 0.3
Exhaust Gas Temperature, T_{exh} [°C]	350 ± 5
Air-Fuel Equivalence Ratio, λ	1.04 ± 0.01
N-Heptane Fuel Mass Ratio [%]	36.8
Injected Fuel Energy DI1, E_{DI1} [kJ]	-
Injection Start Angle DI1, θ_{DI1} [CAD bTDC]	-
Injected Fuel Energy DI2, E_{DI2} [kJ]	0.345
Injection Start Angle DI2, θ_{DI2} [CAD bTDC]	39
Injected Fuel Energy PI1, E_{PI1} [kJ]	0.625
Injection Start Angle PI1, θ_{PI1} [CAD bTDC]	310
Total Injected Fuel Energy, E_t [kJ]	0.970

The combustion metrics (Section 4.1) for each operating result were calculated following Section 4.2. The combustion metrics are summarized in Table 5.3 and Table 5.4 for R1A, and Table 5.5 and Table 5.6 for R1B. Each parameter was calculated as a mean with one standard deviation as the uncertainty calculated for 100 cycles

Table 5.3: Combustion Timing Operating Results for R1A varying Pilot Injection timing (θ_{DI2}), n=1000, λ=1.19

θ_{DI2} (CAD aTDC)	LTHR (CA1) (CAD aTDC)	CA10 (CAD aTDC)	CA50 (CAD aTDC)	CA90 (CAD aTDC)	BD (CAD)
-26	-0.0 ± 1.2	8.1 ± 0.9	13.8 ± 1.2	29.7 ± 3.5	21.7 ± 3.6
-27	-0.0 ± 1.6	7.0 ± 0.8	12.6 ± 1.1	27.7 ± 3.3	20.7 ± 3.3
-28	-1.6 ± 0.7	7.6 ± 0.8	13.3 ± 1.0	28.4 ± 3.4	20.9 ± 3.5
-29	-2.2 ± 0.7	6.8 ± 0.9	12.2 ± 0.9	26.1 ± 2.5	19.3 ± 2.6
-30	-1.8 ± 1.1	6.4 ± 0.7	11.6 ± 0.9	25.0 ± 2.4	18.6 ± 2.5
-31	-2.8 ± 0.8	6.6 ± 0.9	11.8 ± 1.0	24.4 ± 2.5	17.8 ± 2.6
-32	-3.7 ± 0.8	5.9 ± 0.8	10.9 ± 0.8	23.1 ± 2.3	17.2 ± 2.6
-33	-3.6 ± 1.0	5.1 ± 0.7	9.8 ± 0.8	21.1 ± 1.9	16.0 ± 2.1
-34	-4.5 ± 0.8	5.3 ± 0.8	10.1 ± 0.8	21.5 ± 2.3	16.1 ± 2.6
-35	-5.1 ± 0.7	5.4 ± 0.7	10.3 ± 0.8	20.9 ± 2.0	15.5 ± 2.2
-36	-5.4 ± 0.7	5.5 ± 0.8	10.3 ± 0.9	20.5 ± 1.8	15.0 ± 1.9
-37	-4.9 ± 1.1	5.3 ± 0.8	9.9 ± 0.8	18.7 ± 1.8	13.4 ± 1.9
-38	-5.5 ± 1.3	5.9 ± 0.9	10.8 ± 1.0	19.6 ± 1.9	13.7 ± 2.0
-39	-5.9 ± 1.2	6.6 ± 0.9	11.8 ± 1.2	20.6 ± 2.2	14.0 ± 2.0
-40	-6.3 ± 0.8	7.2 ± 1.1	12.8 ± 1.5	21.8 ± 2.6	14.6 ± 2.2

for R1A and 200 cycles for R1B.

5.1.2 Effect of the Pilot Injection on the Combustion Timing for R1A

For test R1A the timing of the n-heptane pilot injection DI2 was varied while all other parameters were kept constant. The pilot injection timings were examined from θ_{DI2} = 26 to 40 CAD bTDC at engine speed of 1000 RPM and λ = 1.19. A total of 100 cycles per operating point were collected and used to generate an ensemble average for the measured pressure trace in Figure 5.1. The HRR is then calculated from the pressure traces and shown in Figure 5.2. The LTHR characterized as CA1 for R1A, is shown in the pressure trace and the HRR.

Table 5.4: Combustion Metrics Operating Results for R1A varying Pilot Injection timing (θ_{DI2}), n=1000, λ=1.19

θ_{DI2} (CAD aTDC)	$\mathrm{PRR}_{\mathrm{max}}$ (bar/CAD)	$\mathrm{HRR}_{\mathrm{max}}$ (J/CAD)	IMEP (bar)	η_{th} (%)	η_{comb} (%)
-26	2.01 ± 0.33	72.3 ± 6.4	5.62 ± 0.12	32.5 ± 0.7	66.0 ± 3.5
-27	2.19 ± 0.33	69.0 ± 6.5	5.67 ± 0.11	32.7 ± 0.6	67.6 ± 3.3
-28	2.05 ± 0.28	70.3 ± 6.2	5.72 ± 0.11	33.0 ± 0.6	67.7 ± 3.5
-29	2.25 ± 0.29	70.8 ± 5.7	5.82 ± 0.10	33.6 ± 0.6	70.1 ± 2.9
-30	2.36 ± 0.30	68.7 ± 5.5	5.85 ± 0.09	33.8 ± 0.5	71.2 ± 2.7
-31	2.35 ± 0.38	70.5 ± 6.2	5.92 ± 0.09	34.2 ± 0.5	72.1 ± 2.7
-32	2.54 ± 0.35	69.5 ± 5.4	5.95 ± 0.08	34.4 ± 0.4	72.9 ± 2.3
-33	2.75 ± 0.37	66.2 ± 5.5	5.91 ± 0.07	34.1 ± 0.4	72.8 ± 1.8
-34	2.69 ± 0.38	65.0 ± 5.2	5.96 ± 0.08	34.4 ± 0.4	73.1 ± 2.3
-35	2.65 ± 0.34	67.1 ± 5.7	5.98 ± 0.07	34.5 ± 0.4	73.8 ± 2.0
-36	2.67 ± 0.32	66.0 ± 5.0	6.00 ± 0.06	34.6 ± 0.3	74.4 ± 1.8
-37	2.84 ± 0.34	66.5 ± 4.6	6.01 ± 0.06	34.7 ± 0.3	75.0 ± 1.4
-38	2.59 ± 0.35	67.5 ± 6.5	6.04 ± 0.05	34.8 ± 0.3	75.6 ± 1.8
-39	2.41 ± 0.41	69.3 ± 6.9	6.06 ± 0.06	35.0 ± 0.3	76.2 ± 1.9
-40	2.13 ± 0.44	72.1 ± 6.7	6.03 ± 0.06	34.8 ± 0.4	76.0 ± 2.1

Table 5.5: Combustion Timing Operating Results for R1B varying Pilot Injection timing (θ_{DI2}), n=1200, λ=1.04

θ_{DI2} (CAD aTDC)	LTHR (CA1) (CAD aTDC)	CA10 (CAD aTDC)	CA50 (CAD aTDC)	CA90 (CAD aTDC)	BD (CAD)
-36	-0.8 ± 0.7	13.1 ± 1.5	20.1 ± 2.2	32.9 ± 4.3	19.8 ± 3.9
-39	-2.8 ± 0.6	10.9 ± 1.1	16.7 ± 1.5	26.5 ± 2.6	15.6 ± 2.4
-40	-2.9 ± 0.6	11.5 ± 1.2	17.6 ± 1.6	27.2 ± 2.7	15.8 ± 2.3
-41	-3.4 ± 0.6	11.0 ± 1.1	16.8 ± 1.4	25.7 ± 2.3	14.7 ± 2.0
-43	-3.8 ± 0.6	11.4 ± 1.3	17.7 ± 1.7	26.5 ± 2.8	15.1 ± 2.3

Table 5.6: Combustion Metrics Operating Results for R1B varying Pilot Injection timing (θ_{DI2}), n=1200, λ=1.04

θ_{DI2} (CAD aTDC)	$\mathrm{PRR}_{\mathrm{max}}$ (bar/CAD)	$\mathrm{HRR}_{\mathrm{max}}$ (J/CAD)	IMEP (bar)	η_{th} (%)	η_{comb} (%)
-36	1.39 ± 0.39	88.5 ± 6.1	6.46 ± 0.23	33.3 ± 1.2	66.6 ± 5.4
-39	2.11 ± 0.46	95.8 ± 7.2	6.77 ± 0.17	34.9 ± 0.9	74.0 ± 3.9
-40	1.95 ± 0.44	92.9 ± 7.6	6.79 ± 0.17	35.0 ± 0.9	74.2 ± 4.0
-41	2.16 ± 0.44	95.4 ± 7.0	6.87 ± 0.16	35.4 ± 0.8	76.2 ± 3.8
-43	1.96 ± 0.46	93.1 ± 7.8	6.93 ± 0.14	35.7 ± 0.7	76.8 ± 3.7

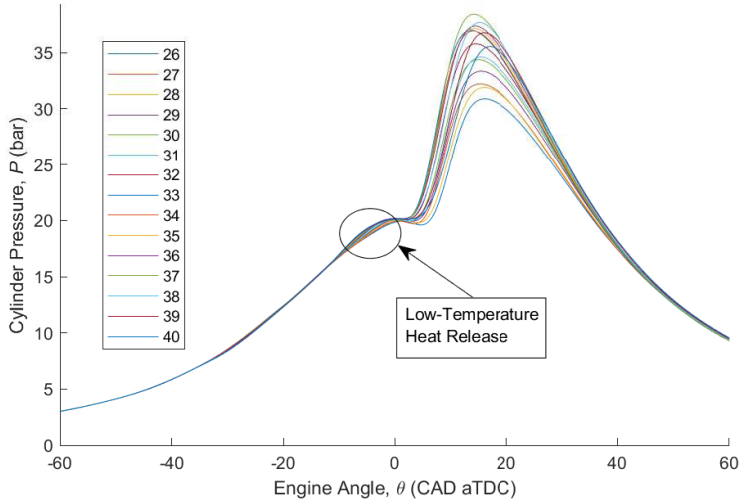

Figure 5.1: Cylinder Pressure varying Pilot Injection Timing θ_{DI2} (CAD bTDC) for R1A, n=1000, λ=1.19

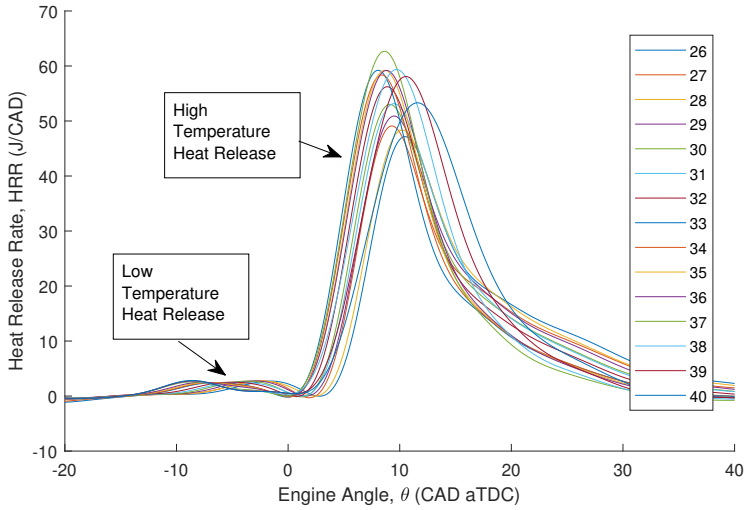

Figure 5.2: Heat Release Rate varying Pilot Injection Timing θ_{DI2} (CAD bTDC) for R1A, n=1000, λ=1.19

The timing of the LTHR (CA1), CA50, the SOC (CA10) and EOC (CA90) are plotted versus pilot injection timing θ_{DI2} in Figure 5.3. The LTHR is linearly correlated with the pilot injection timing. Delaying the θ_{DI2} by 2 CAD delays the LTHR by roughly 1 CAD. This suggests that the LTHR does not occur after a specific fixed

amount of time after the fuel injection but is also affected by the compression pressure after injection.

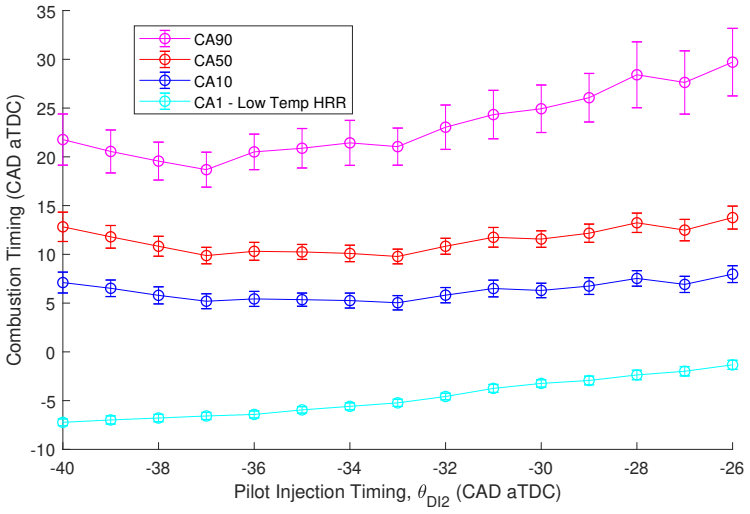

Figure 5.3: Combustion Timing versus Pilot Injection Timing θ_{DI2} (CAD bTDC) for R1A, n=1000, λ=1.19

The CA50 appears to follow a slight "U" shaped pattern with an optimally advanced CA50 with θ_{DI2} between -35 to -33 CAD aTDC. Advancing or retarding the θ_{DI2} from there delays the SOC and the CA50 and thus reduces the power output (IMEP) shown in Table 5.4. The EOC (CA90) follows a similar trend however is delayed even more with delayed θ_{DI2}. This later EOC could be attributed to less well mixed fuel mixtures causing less reactive natural gas fuel pockets to be ignited late due to the flame propagation instead of auto-ignition.

5.1.3 Effect of the Pilot Injection on the Heat Release for R1A

The burn duration, BD (CA90-CA10) is the shortest at 13.4 CAD with a θ_{DI2} of -37 CAD aTDC shown in Figure 5.4. Advancing or retarding the injection timing from there increases the burn duration.

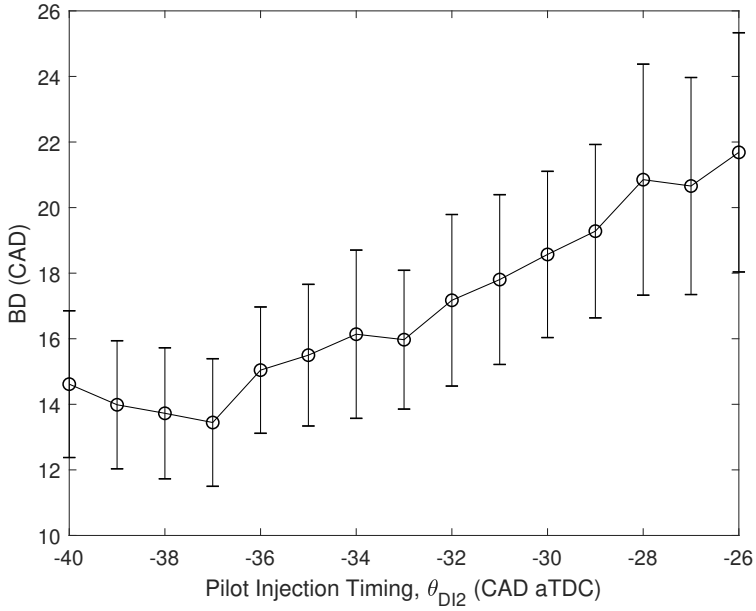

Figure 5.4: Burn Duration versus Pilot Injection Timing θ_{DI2} (CAD bTDC) for R1A, n=1000, λ=1.19

The maximum PRR and HRR are shown in Figure 5.5 and Figure 5.6 respectively and in this case show similar trends as a function of pilot injection timing θ_{DI2}. The higher rates of pressure and heat release are attributed to faster and shorter HTHR. Late injection timings causes the ignition to start late and propagate slower resulting in a longer burn duration.

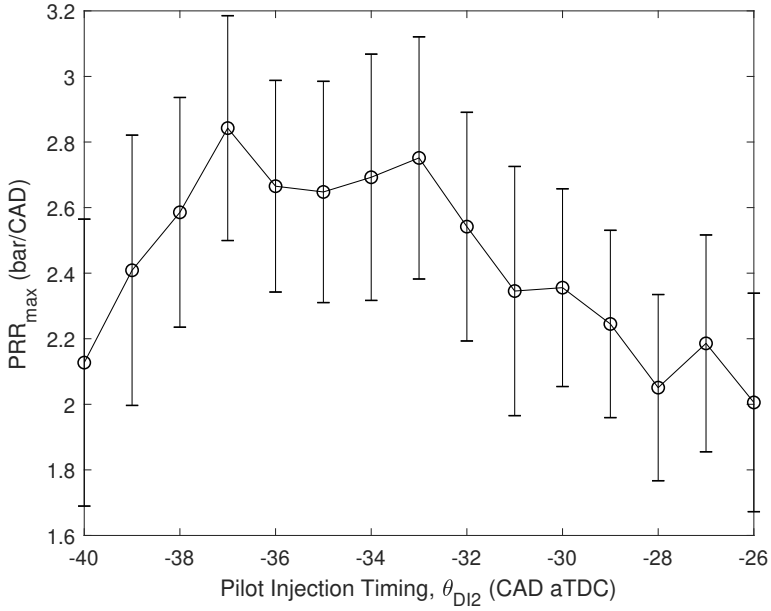

Figure 5.5: PRR versus Pilot Injection Timing θ_{DI2} for R1A, n=1000, λ=1.19

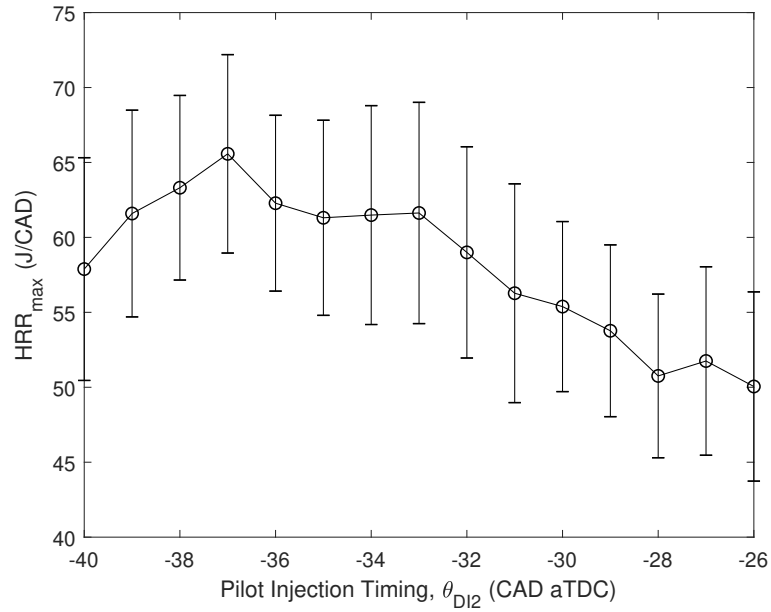

Figure 5.6: Maximum HRR versus Pilot Injection Timing θ_{DI2} for R1A, n=1000, λ=1.19

5.1.4 Effect of the Pilot Injection on the Engine Performance for R1A

The indicated mean effective pressure plotted against pilot injection timing θ_{DI2} is shown in Figure 5.7. The power output is larger with advanced θ_{DI2}. With an advanced CA50 and shorter BD, the HR occurs at crank angles closer to TDC thus producing more power. With a delayed θ_{DI2} the injected n-heptane is mixes less thus causing longer BD with fuel igniting at later and less efficient crank angles of the power stroke. The thermal efficiency η_{th} and combustion efficiency η_{comb} in Figure 5.8 mimics the IMEP as the injected fuel energy for these tests was held constant.

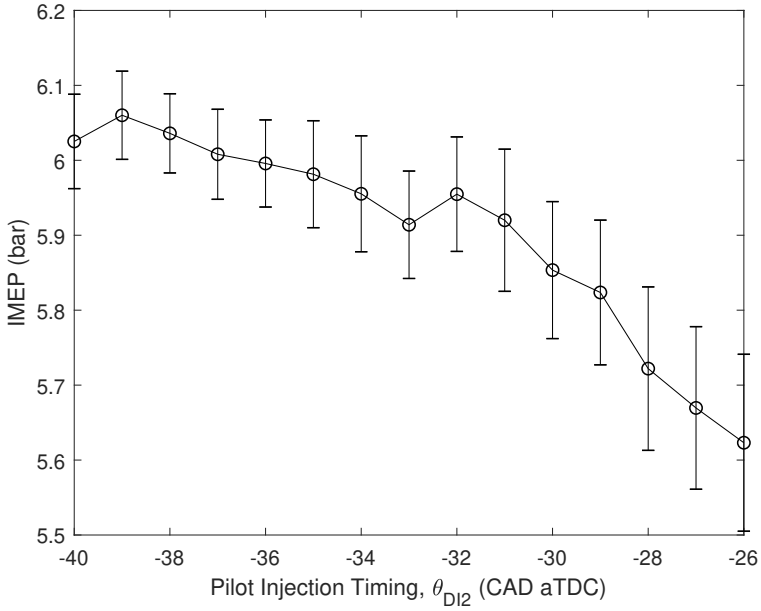

Figure 5.7: Power Output versus Pilot Injection Timing θ_{DI2} for R1A, n=1000, λ=1.19

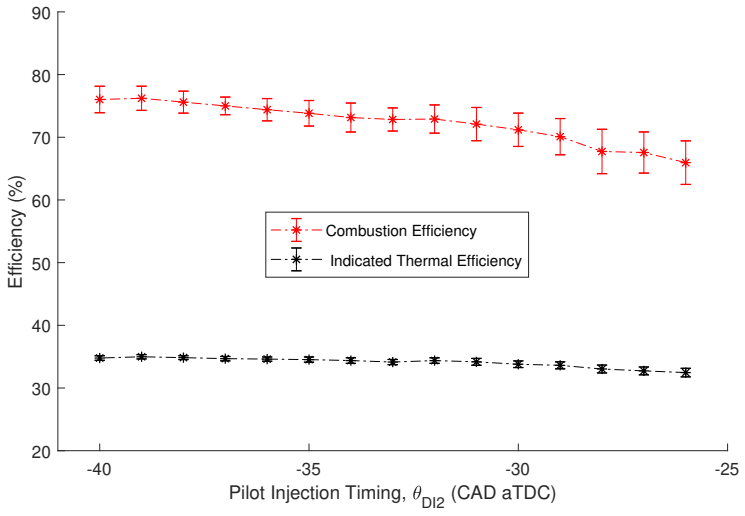

Figure 5.8: Combustion and Indicated Thermal Efficiency versus Pilot Injection Timing θ_{DI2} (CAD bTDC) for R1A, n=1000, λ=1.19

5.1.5 Pilot Injection Timing Effect on R1B

The pilot injection timing θ_{DI2} sweep for operating point R1B was conducted at an engine speed n of 1200 RPM with a richer λ of 1.04 closer to stoichiometric than R1A. The cylinder pressure trace for the R1B cases are shown in Figure 5.9. It important to note that a fixed difference in CAD is a different time increment at different engine speeds. Fuel auto-ignition is a chemically driven process typically depends strongly on time. This entails that the optimal timing for injection in CAD would change for different engine speeds.

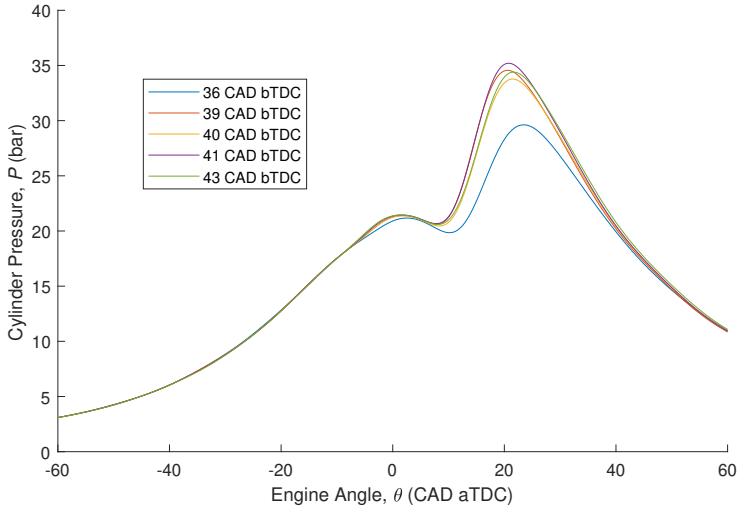

Figure 5.9: Cylinder Pressure varying Pilot Injection Timing θ_{DI2} (CAD bTDC) for R1B, n=1200, λ=1.04

The HRR calculated from the pressure trace is shown in Figure 5.10. Advancing θ_{DI2} from -43 CAD aTDC only 7 degrees to -36 CAD aTDC caused the LTHR and HTHR to be delayed significantly. A pocket of n-heptane fuel may not have had time to disperse and atomize in the cylinder chamber. This may have caused a delay in initiating ignition as shown by the large delay in the LTHR. The combustion timings from Table 5.5 are plotted in Figure 5.11.

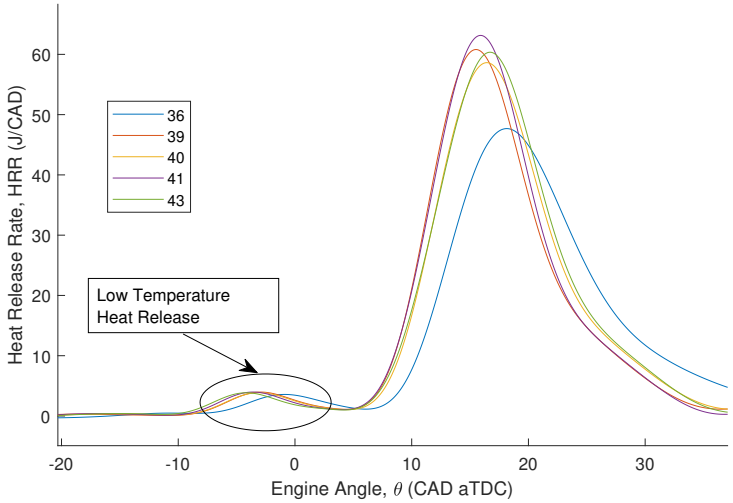

Figure 5.10: Heat Release Rate varying Pilot Injection Timing θ_{DI2} (CAD bTDC) for R1B, n=1200, λ=1.04

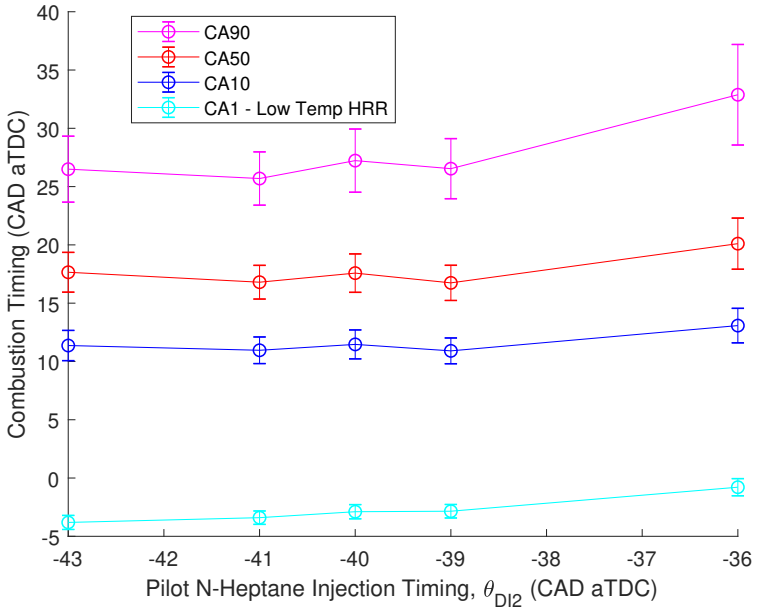

Figure 5.11: Combustion Timing versus Pilot Injection Timing θ_{DI2} (CAD bTDC) for R1B, n=1200, λ=1.04

Operating point R1B shows a similar "U" shaped optimization as R1A for combustion timing CA50. However delaying the θ_{DI2} drastically weakens and delays the combustion almost to the point of misfiring.

The engine output, IMEP, thermal and combustion inefficiencies both decreased as the θ_{DI2} was delayed and similar to the R1A case in Figure 5.8 the combustion strength and consistency declined with increased θ_{DI2} as shown in Figure 5.12.

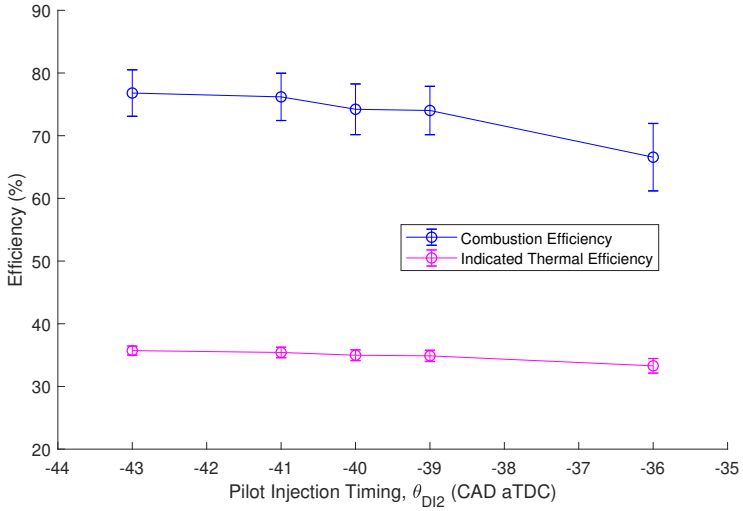

Figure 5.12: Combustion and Indicated Thermal Efficiency versus Pilot Injection Timing θ_{DI2} (CAD bTDC) for R1B, n=1200, λ=1.04

5.2 Case 2: RCCI with NVO

5.2.1 Obtaining RCCI Combustion with NVO

RCCI combustion with NVO was obtained by beginning with RCCI auto-ignition with no NVO at the default position ($\phi_{NVO} = 0$) and slowly adjusting the cam phasing while adjusting fueling rates to maintain stable auto-ignition. An example of the RCCI operating points with increasing amounts of NVO are shown in Figure 5.13 with this case denoted as R2A. The operating parameters for R2A are listed in Table 5.7. These operating points do not have consistent fuel to air ratios thus they may have different λ.

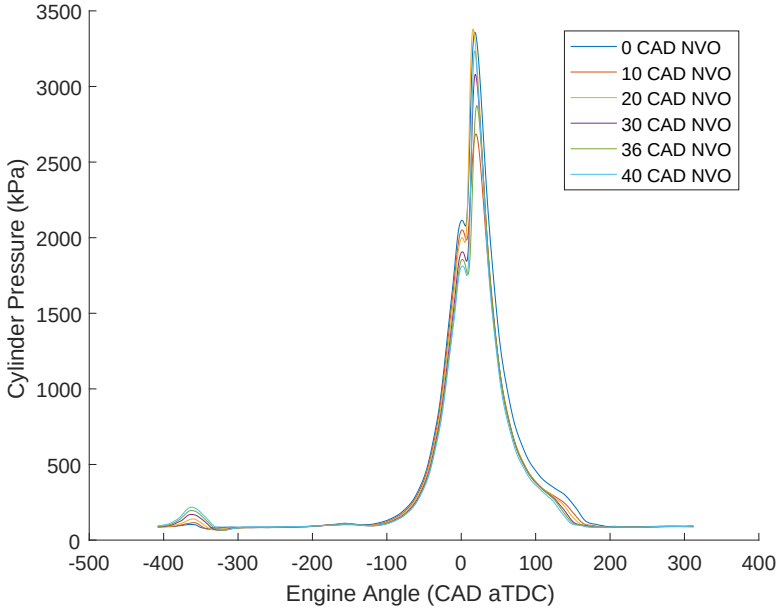

Figure 5.13: Cylinder Pressure of various Auto Ignition Operating points varying the NVO duration

To maintain RCCI auto-ignition with similar peak pressure location and combustion timing CA50 while increasing NVO phasing the injected natural gas amount must be reduced. Increasing the ϕ_{NVO} decreases the fresh air flow into the engine thus delays and weakens the combustion. By decreasing the natural gas amount, the overall fuel reactivity increases and the combustion is advanced. This also reduces the total fuel amount which balances the air reduction so λ stays approximately the same. The combustion for operating point ϕ_{NVO} of 10 CAD is leaner than the other operating points with λ of 1.34 and has a weaker combustion with more cyclic variation.

The intake air heater power must be decreased with larger amounts of NVO due to a lower mass air flow rate into the engine.

5.2.2 Effect of NVO on the engine

The engine performance parameters for R2A are listed in Table 5.8 and Table 5.9. It can be seen from Figure 5.14 that as ϕ_{NVO} increases the motoring pressure decreases

Table 5.7: Operating Parameters for R2A, n=1200

ϕ_{NVO}	n	θ_{DI1}	E_{DI1}	θ_{DI2}	E_{DI2}	θ_{PI1}	E_{PI1}	E_{t}	λ	m_a	T_{in}	T_{exh}
0	1200	360	0.150	39	0.228	310	0.521	0.899	1.19	15.7	80.7	329.1
10	1200	360	0.150	39	0.254	310	0.383	0.786	1.34	14.9	82.6	337.2
20	1200	362	0.150	39	0.293	310	0.331	0.773	1.25	14.3	83.9	329.5
30	1200	370	0.150	39	0.306	310	0.296	0.752	1.20	13.4	85.1	322.7
36	1200	369	0.150	39	0.319	310	0.262	0.730	1.17	12.8	83.5	316.3
40	1200	369	0.150	39	0.332	310	0.227	0.708	1.16	12.5	83.9	311.9

Table 5.8: Combustion Timing Operating Results for R2A varying NVO duration (ϕ_{NVO}), n=1200

ϕ_{NVO} (CAD)	LTHR (CA1) (CAD aTDC)	CA10 (CAD aTDC)	CA50 (CAD aTDC)	CA90 (CAD aTDC)	BD (CAD)
0	-5.0 ± 0.8	9.0 ± 1.0	15.1 ± 1.4	28.9 ± 3.7	19.9 ± 3.5
10	-8.1 ± 1.2	9.6 ± 1.5	17.0 ± 2.4	29.8 ± 3.7	20.2 ± 2.8
20	-9.3 ± 3.2	7.3 ± 0.8	12.3 ± 1.1	21.6 ± 1.4	14.2 ± 1.4
30	-10.5 ± 6.6	9.3 ± 1.0	14.9 ± 1.5	22.6 ± 1.9	13.2 ± 1.5
36	-8.4 ± 1.3	10.9 ± 1.3	17.0 ± 2.0	23.7 ± 2.7	12.8 ± 1.8
40	-6.8 ± 0.5	9.7 ± 0.9	14.3 ± 1.3	19.2 ± 1.5	9.4 ± 1.0

Table 5.9: Combustion Metrics Operating Results for R2A varying NVO duration (ϕ_{NVO}), n=1200

θ_{DI2} (CAD aTDC)	$\mathrm{PRR_{max}}$ (bar/CAD)	$\mathrm{HRR_{max}}$ (J/CAD)	IMEP (bar)	η_{th} (%)	η_{comb} (%)	η_{vol} (%)
0	1.93 ± 0.41	54.7 ± 7.5	6.36 ± 0.13	35.4 ± 0.7	72.4 ± 3.7	79.7
10	1.09 ± 0.36	37.1 ± 6.5	4.93 ± 0.25	31.4 ± 1.6	63.1 ± 4.7	76.1
20	2.49 ± 0.35	63.2 ± 6.5	5.47 ± 0.15	35.4 ± 1.0	76.1 ± 3.3	73.3
30	2.07 ± 0.39	60.0 ± 7.1	5.31 ± 0.11	35.3 ± 0.8	79.2 ± 3.0	68.9
36	1.86 ± 0.47	59.1 ± 9.0	5.22 ± 0.10	35.8 ± 0.7	81.6 ± 3.3	65.5
40	2.80 ± 0.43	76.1 ± 7.6	5.18 ± 0.07	36.6 ± 0.5	84.3 ± 1.6	64.1

since delaying the IVC during the compression stroke decreases the effective compression ratio of the engine. The recompression pressure during the NVO is shown in Figure 5.15. The recompression increases in duration and peak with increasing ϕ_{NVO}. It is noted that the pressure in the cylinder is below ambient as the intake valve opens. Thus it is expected that trapped residual gases would not backflow into the intake manifold.

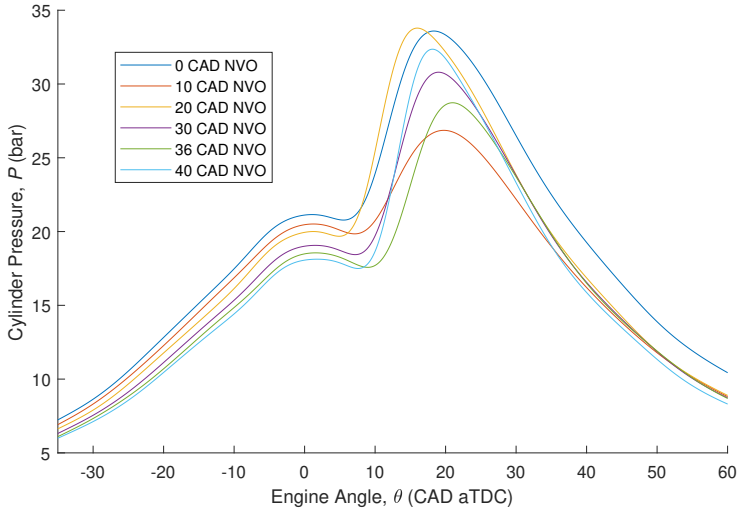

Figure 5.14: Zoomed in Cylinder Pressure of various auto-ignition operating points varying NVO duration ϕ_{NVO} (CAD) for R2A

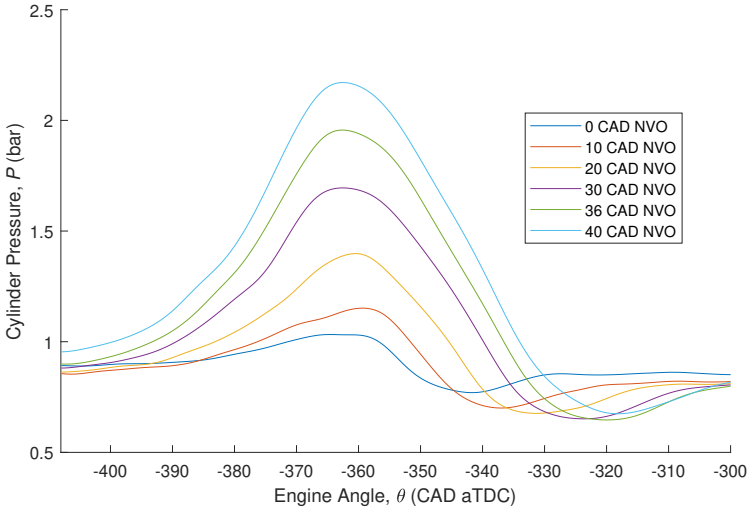

Figure 5.15: Cylinder Pressure in the NVO of various auto-ignition operating points varying NVO duration ϕ_{NVO} (CAD) for R2A

The PV diagram for R2A in Figure 5.16 shows the increase of the pumping loss with larger pumping loops with increased NVO. The increase of the pumping loss is quite insignificant being two orders of magnitude lower than the power produced during the power stroke. More residual gas is trapped in the exhaust stroke with larger NVO durations due to earlier EVC timings. The exhaust is recycled to be used for the next engine cycle in what is called internal EGR. With more exhaust being recirulated and later IVO timings, less fresh air is aspirated into the engine with larger ϕ_{NVO}. This is also represented by the decrease in volumetric efficiency with more NVO. The total in-cylinder temperature is expected to increase with larger NVO since a larger fraction of hot exhaust gas from the previous cycle is present in the cylinder.

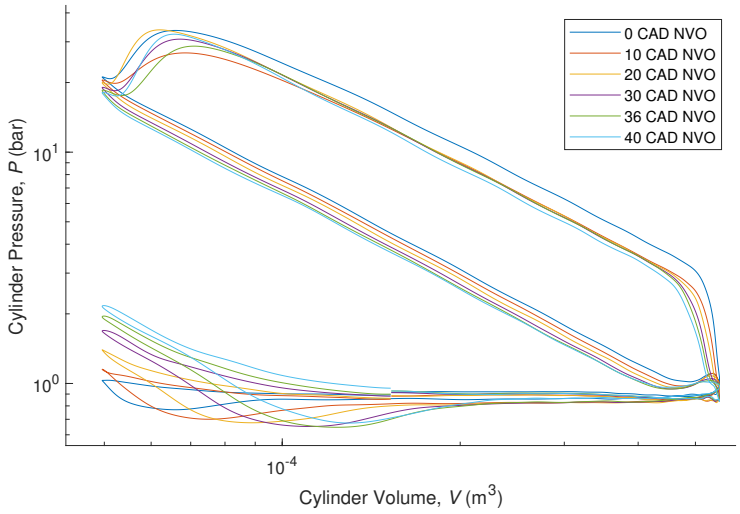

Figure 5.16: PV diagrams of various auto-ignition operating points varying NVO duration ϕ_{NVO} (CAD) for R2A

5.2.3 Effect of NVO on the Heat Release

The heat release plot for R2A is shown in Figure 5.17. Since the operating points in R2A have a wide variety of operating conditions including different injection timings and total injected fuel energy, it is difficult to compare the HTHR to each other. It is noted however that the LTHR (CA1) for all the operating points occur approximately at the same time with the same fuel injection timing. The heat release for the one leaner operating point, ϕ_{NVO} of 10 CAD, is slower than the others and ends later. A trend of lower burn durations with increased NVO duration is observed in Figure 5.18. Shorter burn durations (CA90-CA10) are desirable since the heat release cab be optinmally converted to piston work during the power stroke. This leads to higher efficiencies as shown in Figure 5.19.

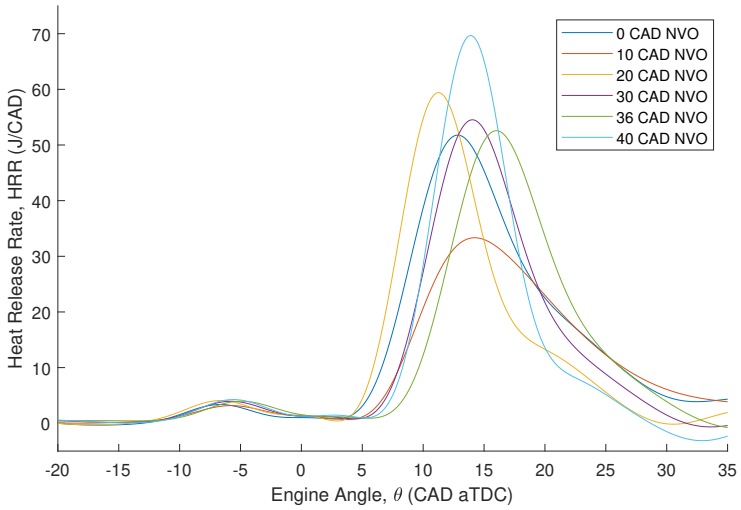

Figure 5.17: Heat Release Rate of various auto-ignition operating points varying NVO duration ϕ_{NVO} (CAD) for R2A

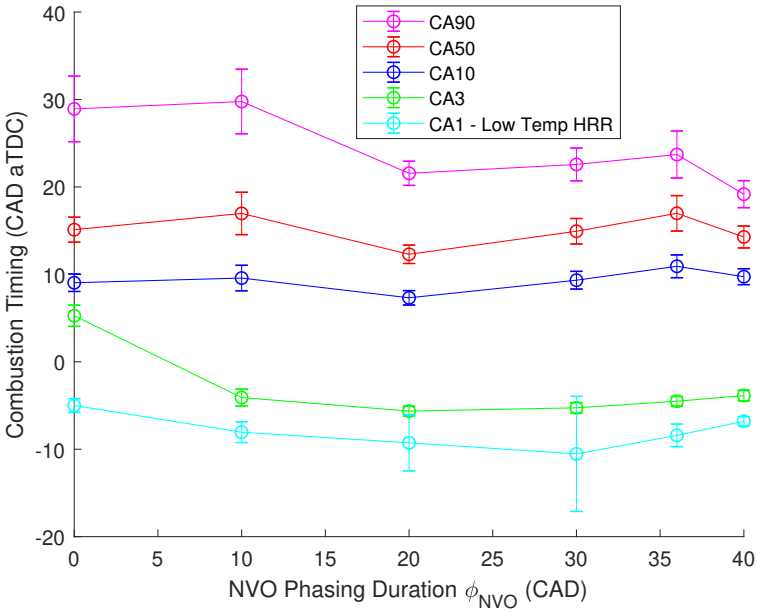

Figure 5.18: Combustion Timing versus NVO duration ϕ_{NVO} (CAD) of various auto-ignition operating points for R2A

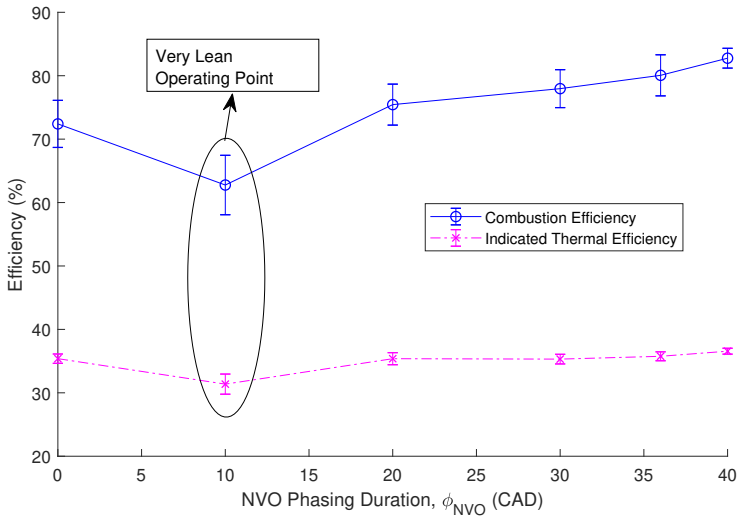

Figure 5.19: Combustion and Indicated Thermal Efficiency versus NVO duration ϕ_{NVO} (CAD) of various auto-ignition operating points for R2A

5.2.4 Effect of NVO Duration Perturbations

Sensitivity tests were conducted for an RCCI operating point with a single n-heptane pilot injection (DI2) and fixed natural gas injection (PI1) with these tests denoted as R2B. Baseline operating parameters for test R2B can be found in Table 5.10. The NVO phasing duration, ϕ_{NVO} was varied slightly while maintaining all parameters constant to observe the sensitivity of the RCCI combustion to varying cam phasing. Next the intake air heating was changed to observe the effect of changing the intake air charge temperature T_{in}. The results for both tests are shown in Table 5.11 and Table 5.12.

Table 5.10: RCCI Engine Operating Conditions for R2B - Base Case

NVO Phasing Duration, ϕ_{NVO} (CAD)	30
Engine Speed, n [RPM]	1200 ± 1
Cycles Collected per OP	200
Intake Air Flow Rate, m_{air} [g/s]	13.0 ± 0.3
Intake Air Temperature, T_{in} [°C]	85.3 ± 0.3
Exhaust Gas Temperature, T_{exh} [°C]	320 ± 5
Engine Coolant Temperature, ECT [°C]	90 ± 5
Air-Fuel Equivalence Ratio, λ	1.24 ± 0.01
N-Heptane Fuel Mass Ratio [%]	56.0
Injected Fuel Energy DI1, E_{DI1} [kJ]	-
Injection Start Angle DI1, θ_{DI1} [CAD bTDC]	-
Injected Fuel Energy DI2, E_{DI2} [kJ]	0.377
Injection Start Angle DI2, θ_{DI2} [CAD bTDC]	39
Injected Fuel Energy PI1, E_{PI1} [kJ]	0.314
Injection Start Angle PI1, θ_{PI1} [CAD bTDC]	310
Total Injected Fuel Energy, E_t [kJ]	0.691

Table 5.11: Combustion Timing Operating Results for R2B with input perturbations (ϕ_{NVO} and T_{in}), n=1200, λ=1.24

NVO Duration					
ϕ_{NVO} (CAD)	LTHR (CA1) (CAD aTDC)	CA10 (CAD aTDC)	CA50 (CAD aTDC)	CA90 (CAD aTDC)	BD (CAD)
26	-3.2 ± 0.7	8.1 ± 0.8	11.7 ± 1.0	17.1 ± 1.8	9.0 ± 1.4
28	-1.6 ± 0.8	9.3 ± 0.9	13.1 ± 1.1	18.9 ± 1.7	9.6 ± 1.3
30 (base)	-0.2 ± 1.2	10.1 ± 0.9	14.1 ± 1.2	20.1 ± 1.7	10.0 ± 1.3
32	2.2 ± 1.4	13.3 ± 1.4	18.6 ± 2.0	26.1 ± 2.9	12.7 ± 1.9
Intake Air Temperature					
T_{in} (°C)	LTHR (CA1) (CAD aTDC)	CA10 (CAD aTDC)	CA50 (CAD aTDC)	CA90 (CAD aTDC)	BD (CAD)
80.3	-2.2 ± 0.6	9.9 ± 0.9	14.1 ± 1.2	19.9 ± 1.7	9.9 ± 1.3
81.1	-0.1 ± 1.0	11.6 ± 1.3	16.3 ± 1.7	22.9 ± 2.4	11.3 ± 1.6
83.0	0.2 ± 1.0	11.7 ± 1.1	16.3 ± 1.5	23.0 ± 2.2	11.3 ± 1.4
84.0	-0.2 ± 1.1	10.3 ± 1.0	14.5 ± 1.2	20.4 ± 2.0	10.1 ± 1.4
85.3 (base)	0.1 ± 1.1	10.3 ± 0.9	14.3 ± 1.2	20.3 ± 1.7	10.0 ± 1.3

Table 5.12: Combustion Metrics Operating Results for R2B with input perturbations (ϕ_{NVO} and T_{in}), n=1200, λ=1.24

NVO Duration					
ϕ_{NVO} (CAD)	PRR_{max} (bar/CAD)	HRR_{max} (J/CAD)	IMEP (bar)	η_{th} (%)	η_{comb} (%)
26	3.30 ± 0.40	79.6 ± 7.5	5.24 ± 0.18	37.9 ± 1.3	82.6 ± 3.3
28	2.91 ± 0.37	74.3 ± 7.0	5.25 ± 0.19	38.0 ± 1.4	83.2 ± 3.9
30 (base)	2.67 ± 0.38	71.1 ± 7.2	5.24 ± 0.16	37.9 ± 1.2	83.7 ± 3.3
32	1.59 ± 0.38	53.6 ± 7.6	5.08 ± 0.17	36.8 ± 1.2	80.0 ± 4.3
Intake Air Temperature					
T_{in} (°C)	PRR_{max} (bar/CAD)	HRR_{max} (J/CAD)	IMEP (bar)	η_{th} (%)	η_{comb} (%)
80.3	2.67 ± 0.37	71.5 ± 6.7	5.27 ± 0.17	38.1 ± 1.2	83.8 ± 3.5
81.1	2.08 ± 0.42	61.7 ± 8.3	5.13 ± 0.19	37.1 ± 1.3	81.9 ± 3.8
83.0	2.07 ± 0.38	61.6 ± 7.4	5.17 ± 0.16	37.4 ± 1.2	82.2 ± 3.4
84.0	2.52 ± 0.40	68.5 ± 7.6	5.20 ± 0.18	37.6 ± 1.3	83.1 ± 3.6
85.3 (base)	2.60 ± 0.36	70.0 ± 6.7	5.22 ± 0.17	37.8 ± 1.2	83.3 ± 3.4

The pressure trace for the NVO duration sweep for R2B shows how the increase of the NVO compression with longer ϕ_{NVO} decreases the power stroke compression as shown in Figure 5.20. The pressure of the auto-ignition advances and reaches higher pressures when the ϕ_{NVO} is reduced while the combustion is delayed and reaches much lower peak pressure as shown in Figure 5.21. These test were conducted with constant fueling rates and timings. With less NVO more air is aspirated into the engine and less air is recycled through internal EGR. The intake air temperature decreases slightly with less NVO since more air is aspirated with the same heater load. With less air being recycled with internal EGR the overall intake charge temperature also decreases. Increasing the NVO duration even by 2 CAD drastically delays the combustion and drops the IMEP while it remained constant for lower durations.

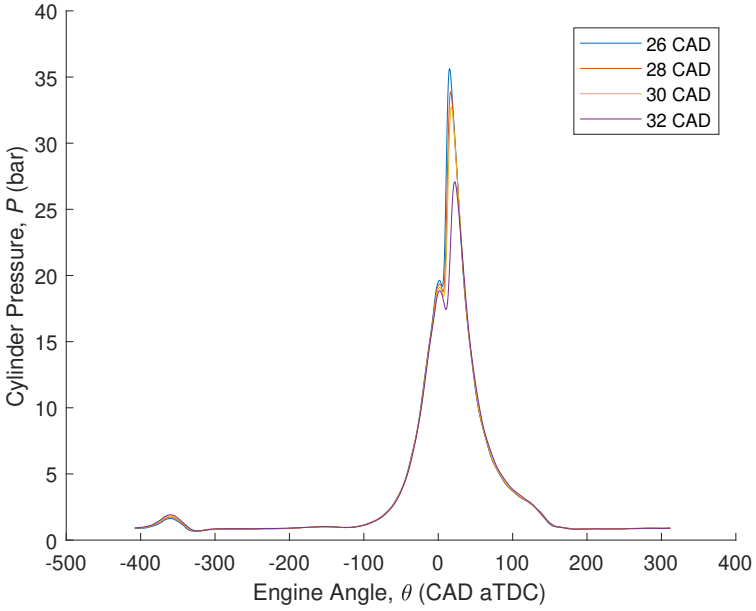

Figure 5.20: Cylinder Pressure varying NVO duration ϕ_{NVO} (CAD) for R2B, n=1200, λ=1.24

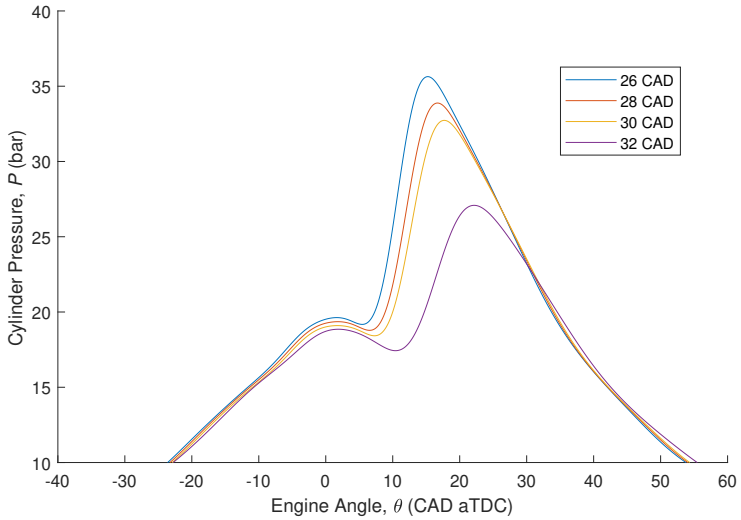

Figure 5.21: Zoomed in Cylinder Pressure varying NVO duration ϕ_{NVO} (CAD) for R2B, n=1200, λ=1.24

The LTHR advances slightly with a decrease of ϕ_{NVO} but is notably delayed when ϕ_{NVO} is increased shown in Figure 5.22. The delay in the HTHR with increased

NVO is quite substantial and leads to a longer burn duration that occurs late in the power stroke shown in Figure 5.23. With delayed combustion higher exhaust gas temperature can be expected and reduced combustion efficiency. Allowing the NVO duration to be shortened increases the maximum PRR and HRR without increasing the engine output power. The PRR_{max} approaches the engine knocking limit of 3.5 bar/CAD discussed in Section 4.3. With increased NVO duration and the delayed combustion phasing, the engine comes closer to misfiring by failing to auto-ignite the fuel.

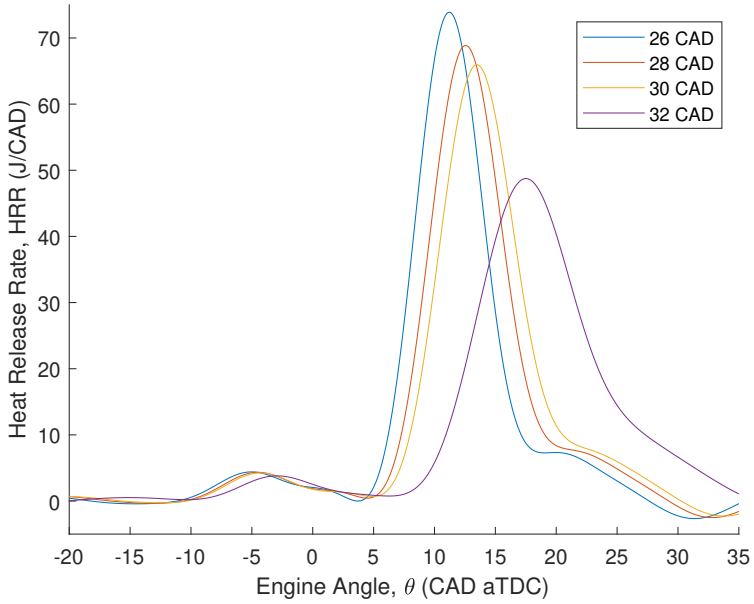

Figure 5.22: Heat Release Rate varying NVO duration ϕ_{NVO} (CAD) for R2B, n=1200, λ=1.24

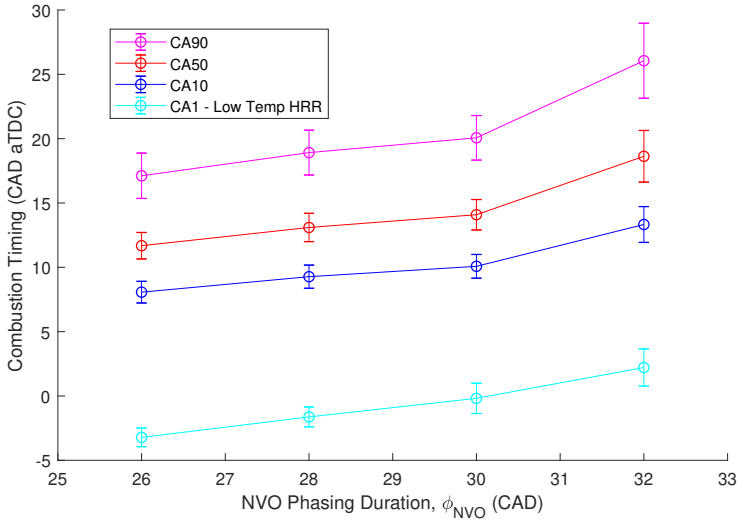

Figure 5.23: Combustion Timing versus NVO duration ϕ_{NVO} (CAD) for R2B, n=1200, λ=1.24

The combustion and thermal efficiency is the highest at the base operating point and decreases slightly with shortened NVO shown in Figure 5.24. When the NVO duration is increased, the combustion was delayed, and the efficiencies decreased.

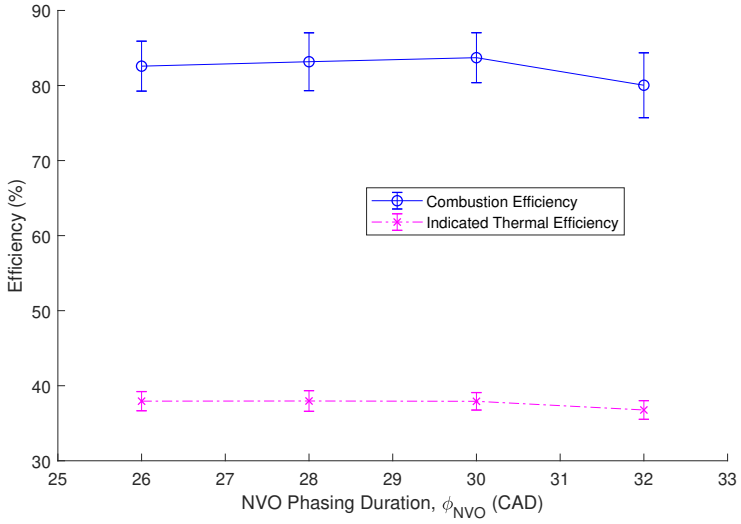

Figure 5.24: Combustion and Indicated Thermal Efficiency versus NVO duration ϕ_{NVO} (CAD) for R2B, n=1200, λ=1.24

5.2.5 Effect of Intake Air Temperature Perturbations

The effect of changing the intake air temperature on the cylinder pressure is shown in Figure 5.25 and Figure 5.26. From the pressure trace there appears to not be a correlation between the intake air temperature and the cylinder pressure. It appears that the data is separated into two groups without any correlation to the intake air temperature. A standard deviation of the peak pressure is shown in Figure 5.26. The cyclic variation is larger than the difference between the operating points.

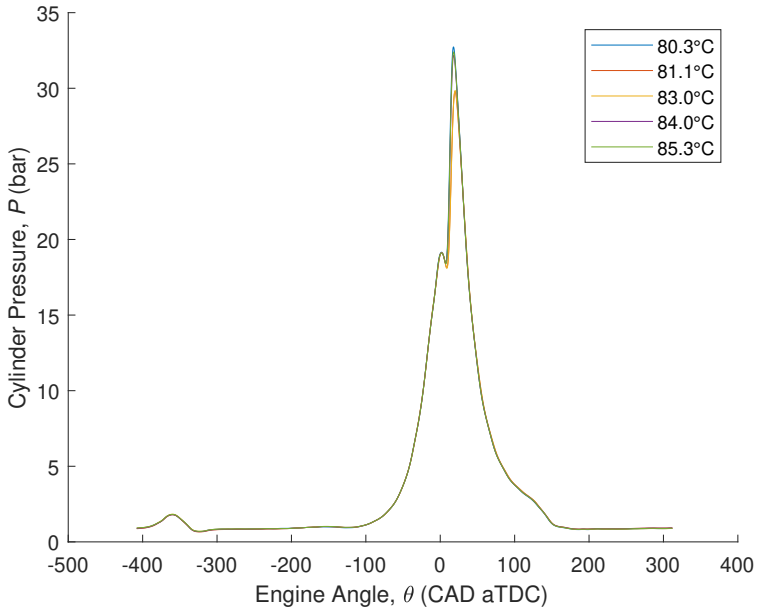

Figure 5.25: Cylinder Pressure varying Intake Air Temperature T_{in} (°C) for R2B, n=1200, λ=1.24

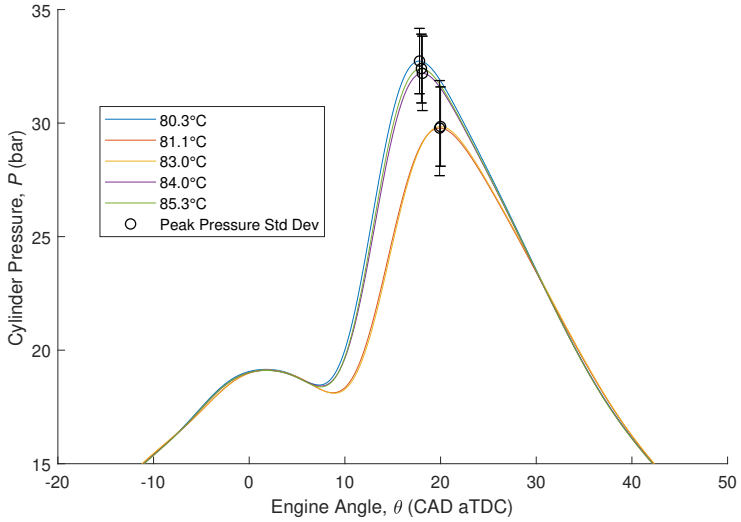

Figure 5.26: Zoomed in Cylinder Pressure varying Intake Air Temperature T_{in} (°C) for R2B, n=1200, λ=1.24

The heat release for the intake air sweep also follows a similar trend shown in Figure 5.27. The combustion timing is shown in Figure 5.28 and the efficiencies in Figure 5.29. The resulting efficiencies are not statistically significant from one another. This is a surprising result since auto-ignition is usually very sensitive to temperature [28].

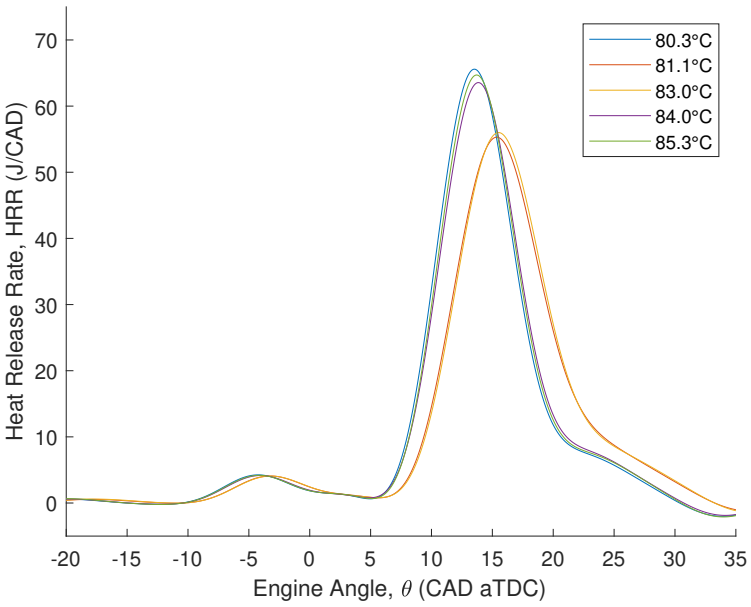

Figure 5.27: Heat Release Rate varying Intake Air Temperature T_{in} (°C) for R2B, n=1200, λ=1.24

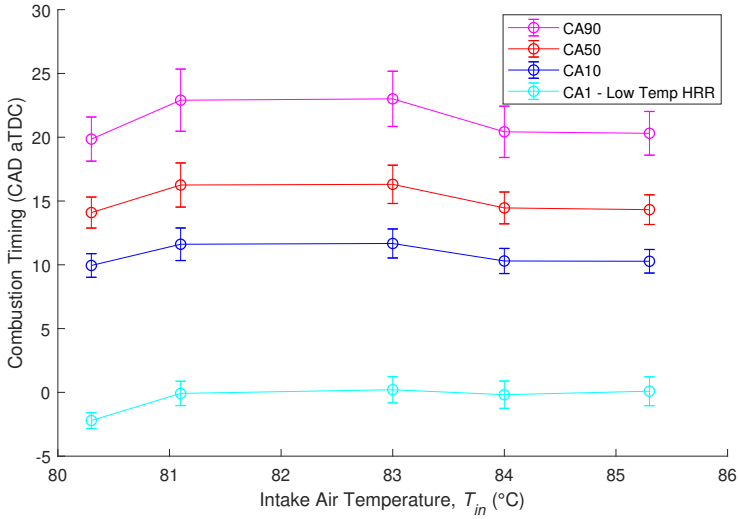

Figure 5.28: Combustion Timing versus Intake Air Temperature T_{in} (°C) for R2B, n=1200, λ=1.24

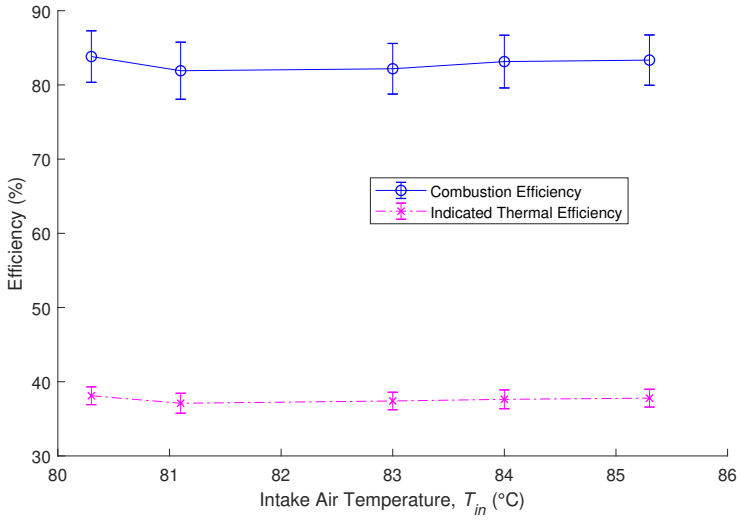

Figure 5.29: Combustion and Indicated Thermal Efficiency versus Intake Air Temperature T_{in} (°C) for R2B, n=1200, λ=1.24

This behavior is attributed to engine coolant temperature fluctuations of ±5°C for test R2B which appear to have a larger effect on the combustion than the intake charge temperature. A subset of the tests may have had higher coolant temperatures which obscures the results of the intake air sensitivity test.

5.3 Case 3: RCCI with NVO using Split Injection

In this section the effects of RCCI using a split injection strategy for n-heptane were examined keeping the natural gas port injection constant. The n-heptane injection was split into two parts, one during the NVO recompression (DI1) and the other during the compression stroke as before (DI2 - see Figure 4.2). The effects of changing the NVO duration, intake air temperation and the NVO injection timing were examined.

5.3.1 Testing Operating Conditions and Results

For the split injection the base operating point used in this section is denoted R3A with details of the base case listed in Table 5.13. From this base operating point the NVO phasing duration ϕ_{NVO} was varied, then the intake air temperature T_{in} followed by the n-heptane NVO injection timing θ_{DI1}. The results of these variations of the base case R3A are summarized in Table 5.14 and Table 5.15

Table 5.13: RCCI Engine Operating Conditions for R3A - Base Case

NVO Phasing Duration, ϕ_{NVO} (CAD)	30
Engine Speed, n [RPM]	1200 ± 1
Cycles Collected per OP	200
Intake Air Flow Rate, m_{air} [g/s]	13.3 ± 0.3
Intake Air Temperature, IAT [°C]	85.3 ± 0.3
Engine Coolant Temperature, ECT [°C]	90 ± 1
Air-Fuel Equivalence Ratio, λ	1.19 ± 0.01
N-Heptane Fuel Mass Ratio [%]	53.3
Injected Fuel Energy DI1, E_{DI1} [kJ]	0.163
Injection Start Angle DI1, θ_{DI1} [CAD bTDC]	360
Injected Fuel Energy DI2, E_{DI2} [kJ]	0.176
Injection Start Angle DI2, θ_{DI2} [CAD bTDC]	39
Injected Fuel Energy PI1, E_{PI1} [kJ]	0.691
Injection Start Angle PI1, θ_{PI1} [CAD bTDC]	310
Total Injected Fuel Energy, E_t [kJ]	0.652

5.3.2 Effect of NVO Duration Perturbations with Split Injection

The NVO phasing duration, ϕ_{NVO}, was varied by increments of 2 CAD from the base of 30 CAD to observe how variations in the valve timings affect the combustion. The effect of varying the NVO duration on the cylinder pressure is shown in Figure 5.30.

Table 5.14: Combustion Timing Operating Results for R3A with input perturbations (ϕ_{NVO}, T_{in} and θ_{DI1}), n=1200, λ=1.19

NVO Duration					
ϕ_{NVO} (CAD)	LTHR (CA1) (CAD aTDC)	CA10 (CAD aTDC)	CA50 (CAD aTDC)	CA90 (CAD aTDC)	BD (CAD)
26	-5.4 ± 0.6	7.5 ± 0.7	11.9 ± 0.9	17.8 ± 1.4	10.4 ± 1.2
28	-4.0 ± 0.8	8.4 ± 0.7	13.0 ± 0.9	19.7 ± 1.7	11.3 ± 1.4
30 (base)	-2.0 ± 1.2	9.7 ± 1.0	14.6 ± 1.2	21.9 ± 1.9	12.3 ± 1.6
32	0.9 ± 1.7	11.3 ± 1.1	16.7 ± 1.5	25.2 ± 2.5	13.9 ± 2.0
34	5.5 ± 2.2	13.6 ± 1.5	20.0 ± 2.1	29.7 ± 3.5	16.0 ± 2.7
Intake Air Temperature					
T_{in} (°C)	LTHR (CA1) (CAD aTDC)	CA10 (CAD aTDC)	CA50 (CAD aTDC)	CA90 (CAD aTDC)	BD (CAD)
81.6	-1.7 ± 1.3	11.2 ± 1.0	16.8 ± 1.4	25.7 ± 3.0	14.5 ± 2.6
83.3	-0.8 ± 1.3	11.4 ± 1.1	17.1 ± 1.5	26.0 ± 2.5	14.6 ± 2.1
85.3 (base)	-2.1 ± 1.1	9.8 ± 0.8	14.8 ± 1.1	22.3 ± 2.0	12.6 ± 1.7
87.5	-1.7 ± 1.2	9.3 ± 0.8	14.0 ± 0.9	20.9 ± 1.8	11.6 ± 1.6
NVO Injection Timing					
θ_{DI1} (CAD bTDC)	LTHR (CA3) (CAD aTDC)	CA10 (CAD aTDC)	CA50 (CAD aTDC)	CA90 (CAD aTDC)	BD (CAD)
345	-6.1 ± 0.5	9.1 ± 0.8	14.8 ± 1.1	22.4 ± 1.8	13.2 ± 1.6
350	-6.1 ± 0.5	9.0 ± 0.8	14.6 ± 1.0	22.2 ± 1.8	13.2 ± 1.7
355	-6.2 ± 0.5	8.8 ± 0.8	14.3 ± 1.0	21.7 ± 1.7	12.9 ± 1.5
360 (base)	-6.2 ± 0.5	8.7 ± 1.0	14.2 ± 1.2	21.5 ± 1.8	12.8 ± 1.5
365	-6.2 ± 0.5	8.9 ± 0.8	14.4 ± 1.1	21.9 ± 1.8	13.0 ± 1.5
370	-6.0 ± 0.5	8.9 ± 0.8	14.5 ± 1.0	22.1 ± 1.8	13.1 ± 1.6
375	-6.2 ± 0.5	8.9 ± 0.9	14.5 ± 1.0	21.9 ± 1.7	13.0 ± 1.5

Table 5.15: Combustion Metrics Operating Results for R3A with input perturbations (ϕ_{NVO}, T_{in} and θ_{DI1}), n=1200, λ=1.19

NVO Duration					
ϕ_{NVO} (CAD)	$\mathrm{PRR_{max}}$ (bar/CAD)	$\mathrm{HRR_{max}}$ (J/CAD)	IMEP (bar)	η_{th} (%)	η_{comb} (%)
26	2.83 ± 0.31	69.4 ± 6.6	5.70 ± 0.05	43.7 ± 0.4	97.3 ± 1.2
28	2.57 ± 0.29	65.8 ± 6.2	5.65 ± 0.05	43.4 ± 0.4	97.4 ± 1.1
30 (base)	2.21 ± 0.33	61.3 ± 6.3	5.60 ± 0.06	42.9 ± 0.4	97.0 ± 1.8
32	1.76 ± 0.34	54.3 ± 6.6	5.50 ± 0.08	42.2 ± 0.6	93.9 ± 3.5
34	1.24 ± 0.31	46.3 ± 6.2	5.34 ± 0.11	41.0 ± 0.8	87.2 ± 6.1
Intake Air Temperature					
T_{in} (°C)	$\mathrm{PRR_{max}}$ (bar/CAD)	$\mathrm{HRR_{max}}$ (J/CAD)	IMEP (bar)	η_{th} (%)	η_{comb} (%)
81.6	1.76 ± 0.37	54.4 ± 7.5	5.53 ± 0.11	42.4 ± 0.8	93.6 ± 4.9
83.3	1.66 ± 0.33	52.5 ± 6.5	5.51 ± 0.08	42.2 ± 0.6	93.1 ± 4.1
85.3 (base)	2.18 ± 0.32	60.9 ± 6.8	5.59 ± 0.06	42.8 ± 0.5	96.7 ± 2.2
87.5	2.37 ± 0.31	63.9 ± 7.0	5.60 ± 0.06	43.0 ± 0.5	97.2 ± 1.6
NVO Injection Timing					
θ_{DI1} (CAD bTDC)	$\mathrm{PRR_{max}}$ (bar/CAD)	$\mathrm{HRR_{max}}$ (J/CAD)	IMEP (bar)	η_{th} (%)	η_{comb} (%)
345	2.13 ± 0.31	61.4 ± 6.3	5.59 ± 0.07	42.8 ± 0.5	98.1 ± 2.3
350	2.14 ± 0.31	61.3 ± 6.5	5.58 ± 0.06	42.8 ± 0.5	98.0 ± 2.1
355	2.23 ± 0.29	62.6 ± 6.0	5.59 ± 0.06	42.9 ± 0.5	98.3 ± 1.9
360 (base)	2.23 ± 0.31	62.6 ± 6.2	5.60 ± 0.06	42.9 ± 0.4	98.4 ± 1.5
365	2.20 ± 0.30	62.2 ± 6.0	5.60 ± 0.05	43.0 ± 0.4	98.5 ± 1.7
370	2.16 ± 0.33	61.4 ± 6.5	5.60 ± 0.07	43.0 ± 0.5	98.4 ± 2.1
375	2.20 ± 0.29	62.2 ± 6.2	5.60 ± 0.06	42.9 ± 0.4	98.4 ± 1.9

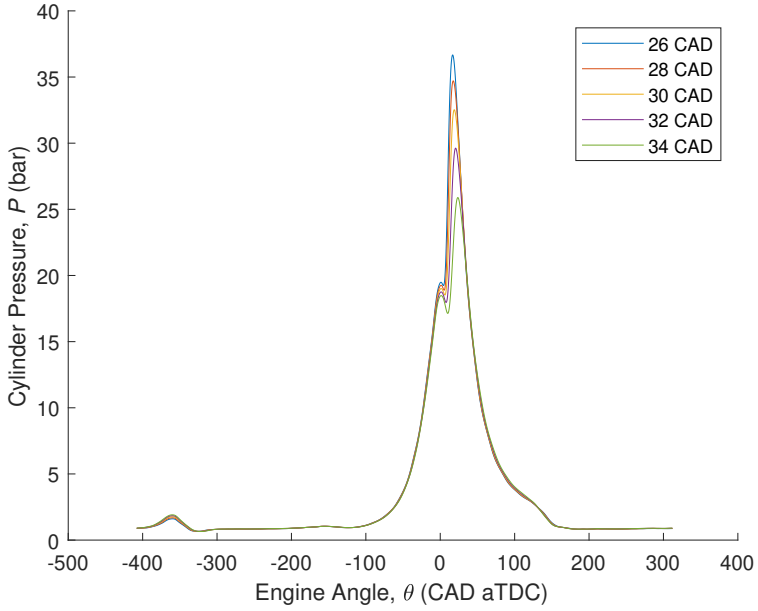

Figure 5.30: Cylinder Pressure varying NVO duration ϕ_{NVO} (CAD) for R3A, n=1200, λ=1.19

As in the R2B case, a smaller ϕ_{NVO} increases the peak pressure and advances its location while longer NVO durations reduces the peak pressure while also delaying it as shown in Figure 5.31. Likewise, longer ϕ_{NVO} leads to higher recompression pressure as shown in the NVO in Figure 5.32. The LTHR does not change position with the variations in cam phasing however the HTHR has longer delays with longer NVO durations and the burn duration is longer as shown in Figure 5.33. The combustion timing parameters are plotted in Figure 5.34.

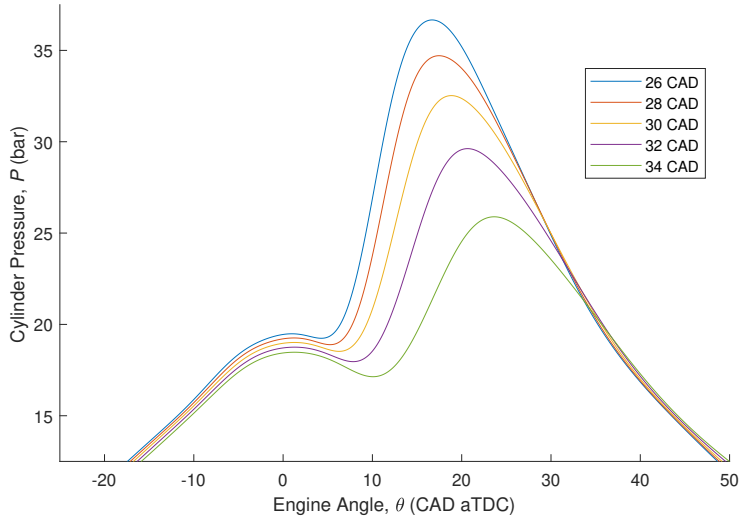

Figure 5.31: Zoomed in Cylinder Pressure varying NVO duration ϕ_{NVO} (CAD) for R3A, n=1200, λ=1.19

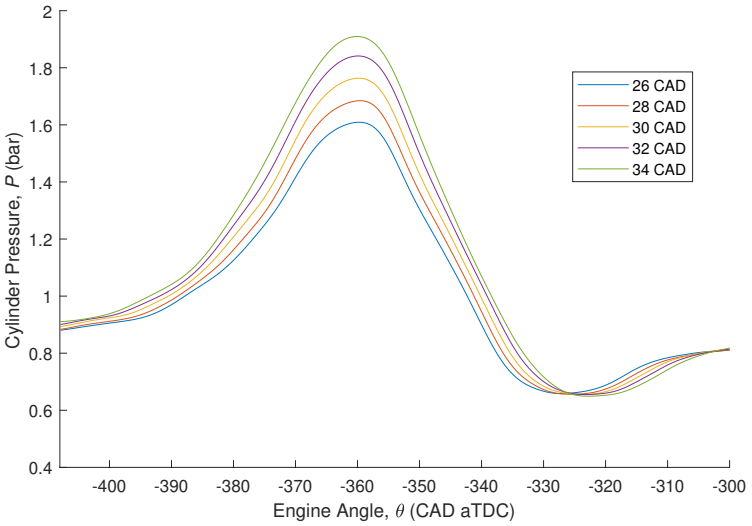

Figure 5.32: Cylinder Pressure in the NVO varying NVO duration ϕ_{NVO} (CAD) for R3A, n=1200, λ=1.19

The pressure rise rates and heat release rates are strongly affected by the NVO amount. With less ϕ_{NVO} more air is aspirated in the engine thus the heat release occurs earlier and faster. Pressure rises need to be limited in order to avoid engine knocking conditions. Here the pressure rise rate is well below the limit of 3.5 bar/CAD.

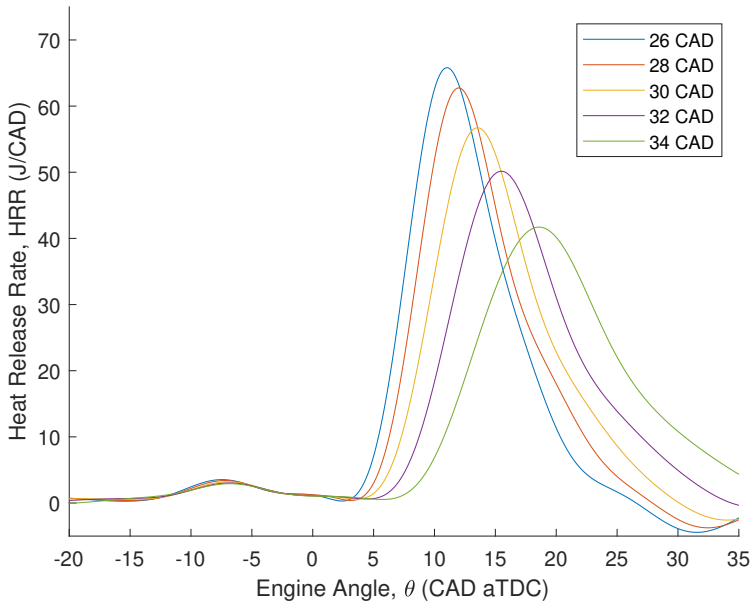

Figure 5.33: Heat Release Rate varying NVO duration ϕ_{NVO} (CAD) for R3A, n=1200, λ=1.19

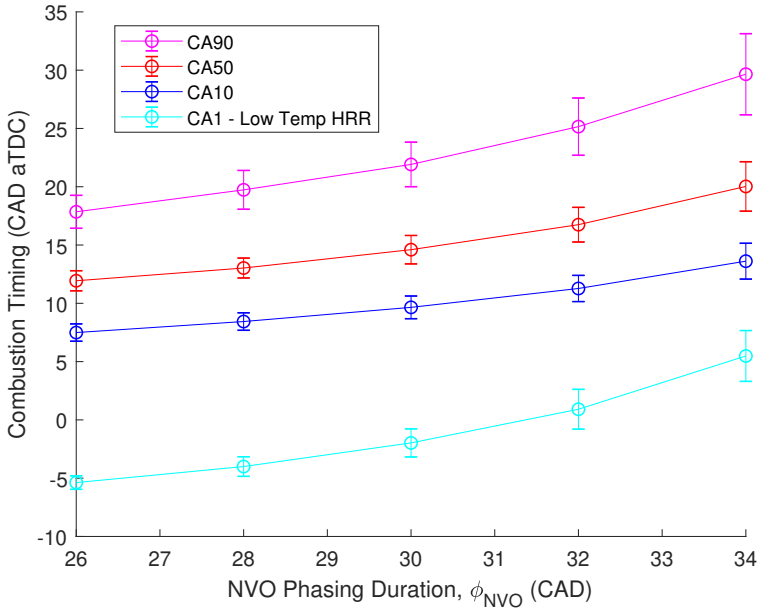

Figure 5.34: Combustion Timing versus NVO duration ϕ_{NVO} (CAD) for R3A, n=1200, λ=1.19

The engine indicated thermal efficiency and combustion efficiency does not de-

crease with when ϕ_{NVO} is decreased from 30 CAD however the efficiencies decrease and are more variable when the NVO duration is increased as shown in Figure 5.35.

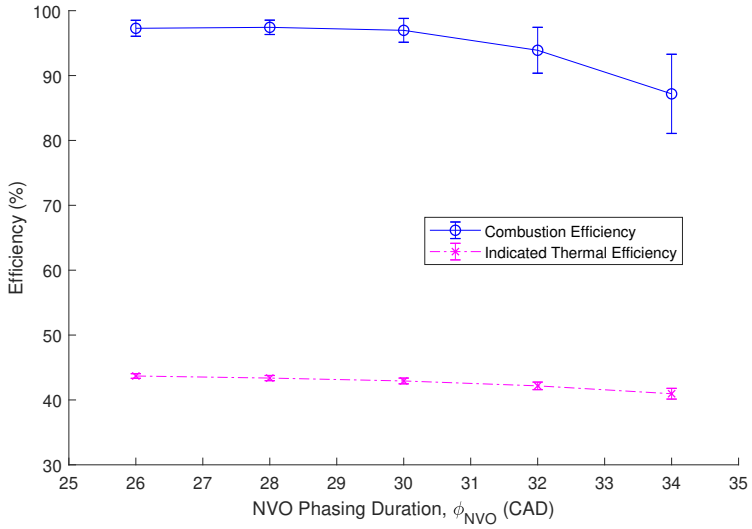

Figure 5.35: Combustion and Indicated Thermal Efficiency versus NVO duration ϕ_{NVO} (CAD) for R3A, n=1200, λ=1.19

5.3.3 Effect of Intake Air Temperature Perturbations with Split Injection

The intake air heating was varied from the base case at T_{in} = 85.3°C to observe the effect of fresh air intake temperature on the split injection auto-ignition. In this case the engine coolant temperature fluctuations were minimized to ±1°C compared to ±5°C of the R2B case. The cylinder pressure trace with varying T_{in} is shown in Figure 5.36. When the T_{in} increases the peak pressure increases while decreasing the temperature had little effect on the cylinder pressure as shown in Figure 5.37.

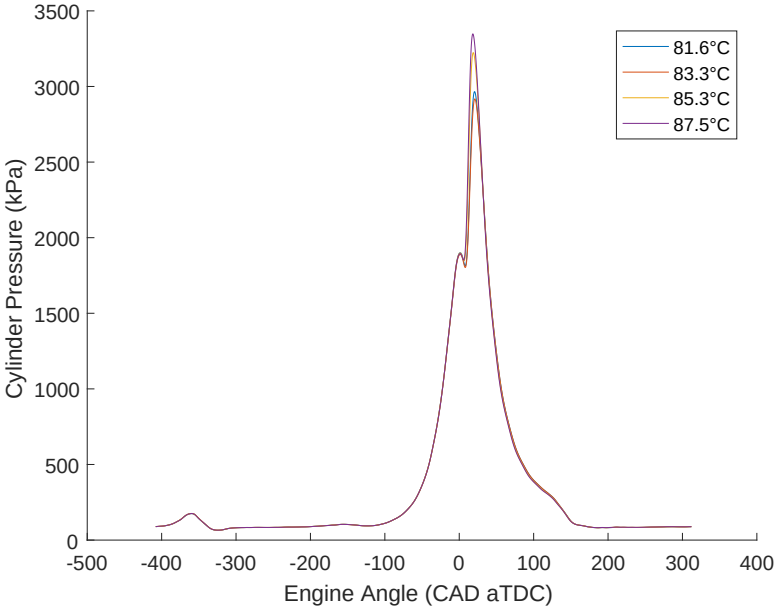

Figure 5.36: Cylinder Pressure varying Intake Air Temperature T_{in} (°C) for R3A, n=1200, λ=1.19

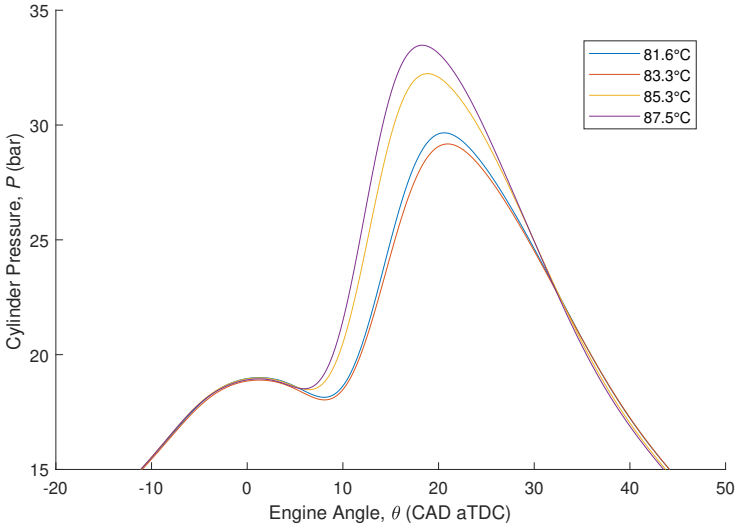

Figure 5.37: Zoomed in Cylinder Pressure varying Intake Air Temperature T_{in} (°C) for R3A, n=1200, λ=1.19

The heat release occurs earlier and quicker when T_{in} is increased while there is no significant change when the temperature was decreased shown in Figure 5.38.

The shorter burn durations and slightly advanced combustion timing are shown in Figure 5.39. This has similar trends to other published RCCI research [11] where T_{in} affects the auto-ignition combustion phasing.

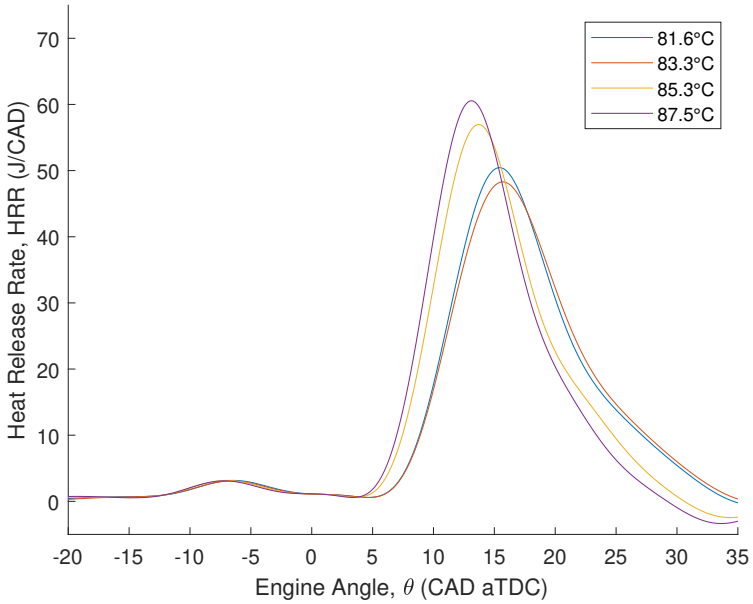

Figure 5.38: Heat Release Rate varying Intake Air Temperature T_{in} (°C) for R3A, n=1200, λ=1.19

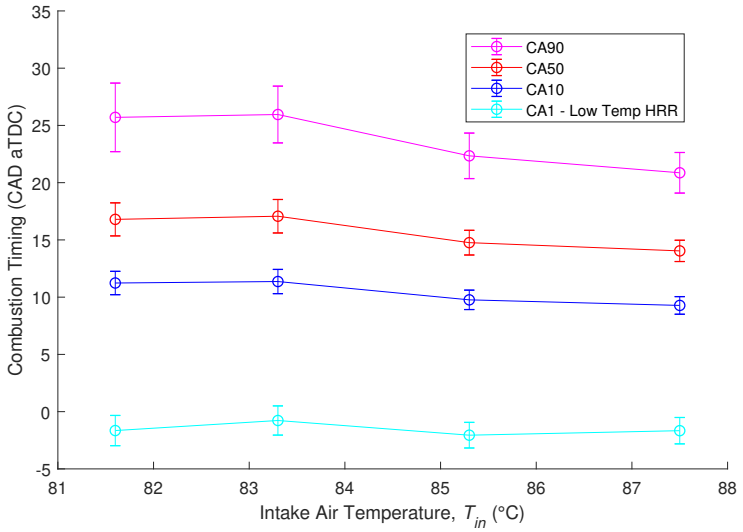

Figure 5.39: Combustion Timing versus Intake Air Temperature T_{in} (°C) for R3A, n=1200, λ=1.19

With lower intake air temperature the CA50 is delayed, the IMEP drops and the combustion becomes less consistent with the variability doubling to ±0.11 bar compared to ±0.06 bar of the base case. When T_{in} is increased the maximum PRR and HRR increases. The temperature T_{in} needs to be limited to ensure the maximum PRR does not rise to the limit of 3.5 bar/CAD. Although T_{in} is higher than a typical SI engine, the temperatures are still below the underhood engine component design limit of roughly 150°C.

The combustion and indicated thermal efficiencies are shown in Figure 5.40. When T_{in} increases the combustion efficiency improves slightly and less variance occurs. There is a slight increase in the thermal efficiency with higher intake temperatures.

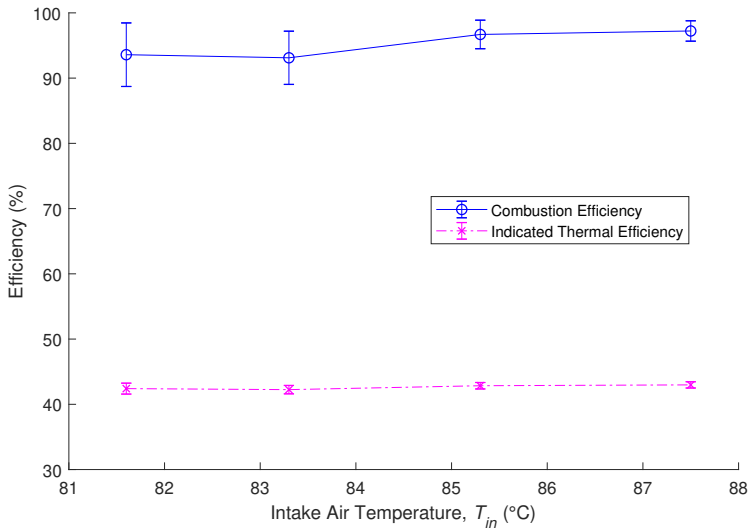

Figure 5.40: Combustion and Indicated Thermal Efficiency versus Intake Air Temperature T_{in} (°C) for R3A, n=1200, λ=1.19

5.3.4 Effect of NVO Injection timing

Changing the NVO injection timing, θ_{DI1}, did not significantly change the main ignition pressure trace. A pressure drop is noted in the NVO shortly after the direct n-heptane injection occurs shown in Figure 5.41. This pressure drop moves when the

θ_{DI1} changes. A pressure drop is expected when fuel is injected in the cylinder because the liquid fuel is much colder than the exhaust gases trapped in the cylinder. The n-heptane, with an enthalpy of vaporization of 36 kJ/mol [29], takes heat from the the in-cylinder gases as it vaporizes thus reducing the in-cylinder temperature and pressure.

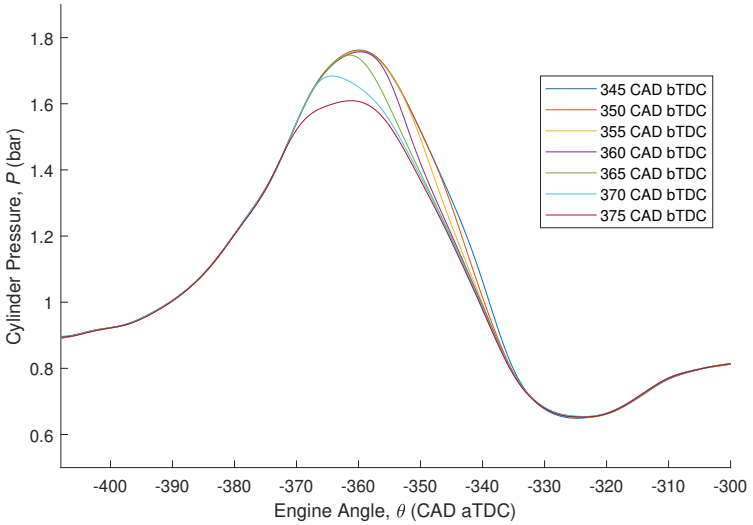

Figure 5.41: Cylinder Pressure in the NVO varying NVO Injection Timing θ_{DI1} (CAD bTDC) for R3A, n=1200, λ=1.19

Changing the θ_{DI1} has no measurable effect on the LTHR or the HTHR of the main injection. This would imply that the mixing and molecular composition of the fuel-air mixture within the NVO does not change or does not have an effect on the combustion.

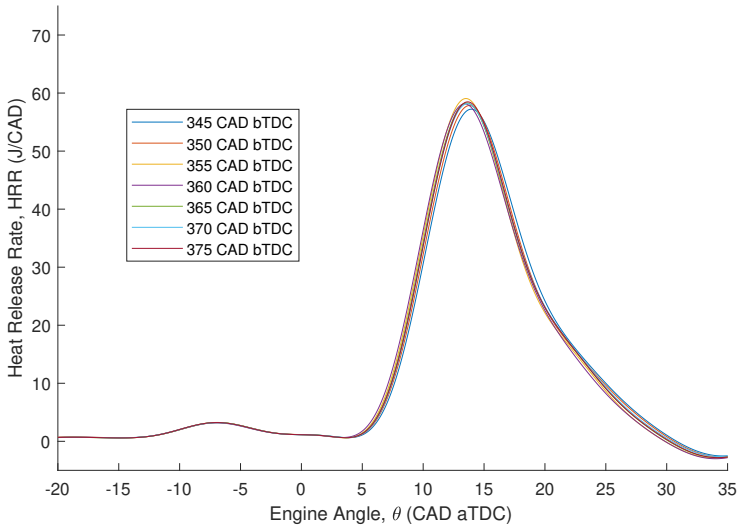

Figure 5.42: Heat Release Rate varying NVO Injection Timing θ_{DI1} (CAD bTDC) for R3A, n=1200, λ=1.19

There is a drop in the HRR during the NVO shown in Figure 5.43 shortly after the start angle θ_{DI1} when the n-heptane is injected. This pressure drop is from the cooling of the exhaust gasses in the cylinder when cool liquid n-heptane is injected. Apart from the dip in the HRR from the injected fuel which occurs roughly 2 CAD after the injection start angle θ_{DI1} there is no other significant heat generated within the NVO.

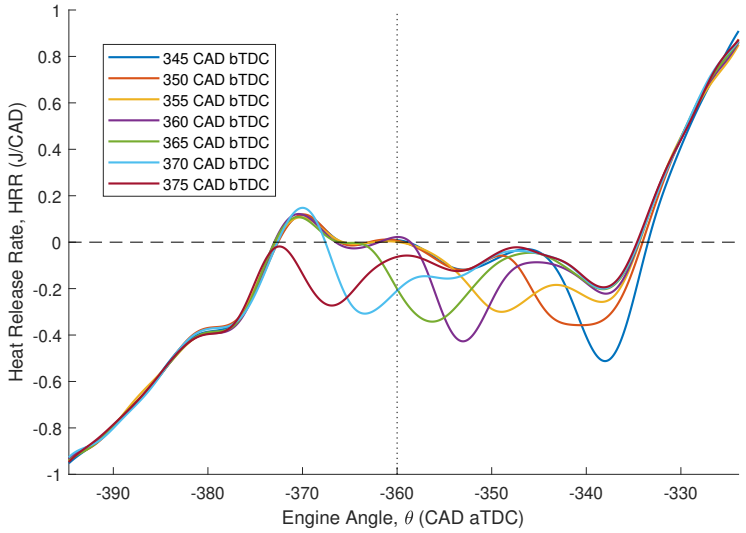

Figure 5.43: Heat Release Rate in the NVO varying NVO Injection Timing θ_{DI1} (CAD bTDC) for R3A, n=1200, λ=1.19

The NVO injection timing for the range tested has no effect on the combustion timing shown in Figure 5.44 or the efficiencies shown in Figure 5.45 for this operating point.

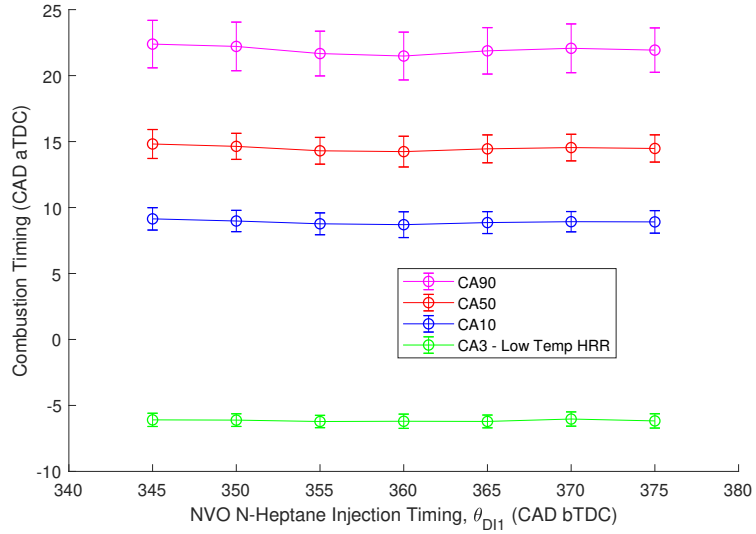

Figure 5.44: Combustion Timing versus NVO Injection Timing θ_{DI1} (CAD bTDC) for R3A, n=1200, λ=1.19

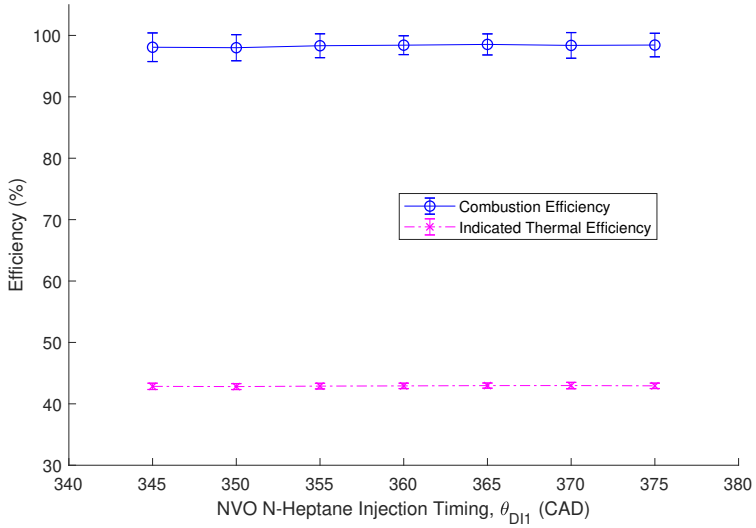

Figure 5.45: Combustion and Indicated Thermal Efficiency versus NVO Injection Timing θ_{DI1} (CAD bTDC) for R3A, n=1200, λ=1.19

5.4 Case 4: RCCI emisisons

In this section emissions data was collected with the FTIR (see Figure 3.15) gas analyzer for various engine operating conditions. Operating point R4A is spark ignited operating point using only natural gas shown in Table 5.16. This set of data provides a baseline of conventional natural gas spark combustion to compare to RCCI at similar loads. Two spark operating points were taken for R4A, one with similar combustion timing as RCCI test in the study (around CA50 of 14 using a spark timing of θ_{IG} = 15.5 CAD bTDC) and another with a CA50 more typical in conventional SI engine operation (CA50 around 9 CAD aTDC using a spark timing of θ_{IG} = 20.5 CAD bTDC). Base operating point R4B shown in Table 5.17 is a single n-heptane injection RCCI strategy similar to operating point R2B. Two additional operating points with lower amounts of NVO for R4B were recorded to observe the effect of ϕ_{NVO} on the engine emission output. Operating point R4B with ϕ_{NVO} of 30 CAD was also repeated without the safety spark to observe if the spark had any significant

effect on the engine combustion. Lastly a split n-heptane injection operating point R4C shown in Table 5.18 similar to R3A was recorded. The NVO n-heptane injection θ_{DI1} was advanced from the base condition of 360 to 390 CAD bTDC to observe any effects of recompressing the n-heptane fuel in the NVO.

Table 5.16: Engine Operating Conditions for R4A - Natural Gas SI

NVO Phasing Duration, ϕ_{NVO} [CAD]	0
Engine Speed, n [RPM]	1200 ± 1
Cycles Collected	200
Intake Air Flow Rate, m_{air} [g/s]	15.5 ± 0.3
Intake Air Temperature, IAT [°C]	45.5 ± 0.3
Engine Coolant Temperature, ECT [°C]	90 ± 1
Air-Fuel Equivalence Ratio, λ	1.01 ± 0.01
N-Heptane Fuel Mass Ratio [%]	0
Injected Fuel Energy P-Inj1, E_{PI1} [kJ]	0.799
Injection Start Angle P-Inj1, θ_{PI1} [CAD bTDC]	310
Total Injected Fuel Energy, E_t [kJ]	0.799
Spark Timing, θ_{IG} [CAD bTDC]	15.5 and 20.5

Table 5.17: Engine Operating Conditions for R4B - RCCI Single Injection varying ϕ_{NVO}

NVO Phasing Duration, ϕ_{NVO} [CAD]	0	20	30
Engine Speed, n [RPM]	1200 ± 1	1200 ± 1	1200 ± 1
Cycles Collected	200	200	200
Intake Air Flow Rate, m_{air} [g/s]	15.8 ± 0.3	14.4 ± 0.3	13.3 ± 0.3
Intake Air Temperature, IAT [°C]	81.5 ± 0.3	83.8 ± 0.3	85.8 ± 0.3
Engine Coolant Temperature, ECT [°C]	90 ± 1	90 ± 1	90 ± 1
Air-Fuel Equivalence Ratio, λ	1.22 ± 0.03	1.24 ± 0.03	1.24 ± 0.03
N-Heptane Fuel Mass Ratio [%]	40.2	49.7	59.3
Injected Fuel Energy DI1, E_{DI1} [kJ]	–	–	–
Injection Start Angle DI1, θ_{DI1} [CAD bTDC]	–	–	–
Injected Fuel Energy DI2, E_{DI2} [kJ]	0.332	0.358	0.384
Injection Start Angle DI2, θ_{DI2} [CAD bTDC]	39	39	39
Injected Fuel Energy PI1, E_{PI1} [kJ]	0.522	0.383	0.279
Injection Start Angle PI1, θ_{PI1} [CAD bTDC]	310	310	310
Total Injected Fuel Energy, E_t [kJ]	0.853	0.741	0.663

Table 5.18: Engine Operating Conditions for R4C - RCCI Split Injection varying θ_{DI1}

NVO Phasing Duration, ϕ_{NVO} [CAD]	30
Engine Speed, n [RPM]	1200 ± 1
Cycles Collected	200
Intake Air Flow Rate, m_{air} [g/s]	13.5 ± 0.3
Intake Air Temperature, IAT [°C]	86.9 ± 0.3
Engine Coolant Temperature, ECT [°C]	90 ± 1
Air-Fuel Equivalence Ratio, λ	1.24 ± 0.03
N-Heptane Fuel Mass Ratio [%]	54.7
Injected Fuel Energy DI1, E_{DI1} [kJ]	0.169
Injection Start Angle DI1, θ_{DI1} [CAD bTDC]	360
Injected Fuel Energy DI2, E_{DI2} [kJ]	0.169
Injection Start Angle DI2, θ_{DI2} [CAD bTDC]	39
Injected Fuel Energy PI1, E_{PI1} [kJ]	0.296
Injection Start Angle PI1, θ_{PI1} [CAD bTDC]	310
Total Injected Fuel Energy, E_t [kJ]	0.635

The engine performance parameters calculated from the cylinder pressure are shown in Table 5.19 and Table 5.20. The relevant FTIR emissions data are summarized in Table 5.21. The measured water content in the exhaust for this test is not accurate. It is believed that some of the water vapor condensed in the the metal tube port line before the heated Flexotherm line. Thus the water content recorded is lower. As such the measured gas components were measured on a dry basis if possible. It should be noted that no element for gaseous n-heptane exists currently on the FTIR gas recipes, thus it could not be measured.

5.4.1 Spark Ignited Natural Gas

The cylinder pressure trace for the SI natural gas operating mode is shown in Figure 5.46. Compared to RCCI operating points the SI mode pressure trace does not have the large pressure rise after TDC but instead steadily rises starting just before TDC. The PV diagram for the SI mode operation is shown in Figure 5.47. Without any NVO phasing there is no recompression during the exhaust stroke. It is also

Table 5.19: Combustion Timing Operating Results for R4A, R4B and R4C

R4A: Spark Ignited Natural Gas					
CA50 (CAD aTDC)	LTHR (CA1) (CAD aTDC)	CA10 (CAD aTDC)	CA50 (CAD aTDC)	CA90 (CAD aTDC)	BD (CAD)
9	N/A	-1.5 ± 1.1	9.0 ± 1.5	17.8 ± 2.2	19.4 ± 1.7
14	N/A	2.8 ± 1.3	14.0 ± 1.7	23.4 ± 2.5	20.6 ± 1.8
R4B: Single Injection RCCI					
ϕ_{NVO} (CAD)	LTHR (CA1) (CAD aTDC)	CA10 (CAD aTDC)	CA50 (CAD aTDC)	CA90 (CAD aTDC)	BD (CAD)
0	-2.6 ± 0.7	9.2 ± 1.1	14.8 ± 1.6	23.4 ± 2.4	14.2 ± 1.7
20	-3.3 ± 0.5	10.8 ± 1.2	16.7 ± 1.6	23.8 ± 2.4	13.0 ± 1.7
30	-4.7 ± 0.4	9.0 ± 0.9	14.0 ± 1.2	18.8 ± 1.8	9.8 ± 1.2
30 (no spark)	-4.9 ± 0.5	8.5 ± 1.0	13.3 ± 1.3	17.9 ± 1.7	9.4 ± 1.2
R4B: Split Injection RCCI					
θ_{DI1} (CAD bTDC)	LTHR (CA3) (CAD aTDC)	CA10 (CAD aTDC)	CA50 (CAD aTDC)	CA90 (CAD aTDC)	BD (CAD)
360	-8.1 ± 0.6	8.5 ± 0.9	14.5 ± 1.2	22.7 ± 2.2	14.2 ± 1.8
390	-7.7 ± 0.6	8.8 ± 1.0	14.9 ± 1.3	23.1 ± 2.1	14.3 ± 1.8
390 (no spark)	-7.2 ± 0.5	9.4 ± 1.1	15.8 ± 1.7	24.5 ± 2.4	15.1 ± 2.0

Table 5.20: Combustion Metrics Operating Results for R4A, R4B and R4C

R4A: Spark Ignited Natural Gas					
CA50 (CAD aTDC)	$\mathrm{PRR_{max}}$ (bar/CAD)	$\mathrm{HRR_{max}}$ (J/CAD)	IMEP (bar)	η_{th} (%)	η_{comb} (%)
9	1.27 ± 0.18	36.5 ± 3.3	5.46 ± 0.09	34.2 ± 0.6	76.1 ± 1.4
14	0.86 ± 0.16	32.3 ± 2.8	5.35 ± 0.11	33.5 ± 0.7	75.5 ± 2.5
R4B: Single Injection RCCI					
ϕ_{NVO} (CAD)	$\mathrm{PRR_{max}}$ (bar/CAD)	$\mathrm{HRR_{max}}$ (J/CAD)	IMEP (bar)	η_{th} (%)	η_{comb} (%)
0	2.06 ± 0.45	59.8 ± 9.0	5.83 ± 0.25	34.2 ± 1.5	72.3 ± 3.8
20	1.80 ± 0.37	57.7 ± 8.1	5.31 ± 0.26	35.9 ± 1.8	78.8 ± 5.0
30	2.68 ± 0.41	73.5 ± 8.1	5.07 ± 0.16	38.3 ± 1.2	86.5 ± 3.5
30 (no spark)	2.85 ± 0.40	75.7 ± 7.8	5.07 ± 0.15	38.2 ± 1.1	86.1 ± 3.2
R4C: Split Injection RCCI					
θ_{DI1} (CAD bTDC)	$\mathrm{PRR_{max}}$ (bar/CAD)	$\mathrm{HRR_{max}}$ (J/CAD)	IMEP (bar)	η_{th} (%)	η_{comb} (%)
360	2.01 ± 0.32	57.5 ± 6.4	5.36 ± 0.07	42.2 ± 0.6	96.4 ± 2.9
390	1.93 ± 0.35	56.8 ± 7.0	5.35 ± 0.08	42.1 ± 0.6	95.8 ± 3.3
390 (no spark)	1.73 ± 0.36	53.2 ± 6.8	5.31 ± 0.08	41.8 ± 0.7	94.2 ± 4.0

Table 5.21: Emissions Results for R4A, R4B and R4C

R4A: Sprak Ignited Natural Gas					
CA50 (CAD aTDC)	H_2O (%)	CO_2 (% dry)	CO (ppm dry)	NO_x (ppm dry)	CH_4 (ppm)
9	14.0 ± 0.1	11.1 ± 0.1	1770 ± 90	3260 ± 30	1050 ± 40
14	13.7 ± 0.2	11.2 ± 0.1	1650 ± 70	2510 ± 30	800 ± 20
R4B: Single Injection RCCI					
ϕ_{NVO} (CAD)	H_2O (%)	CO_2 (% dry)	CO (ppm dry)	NO_x (ppm dry)	CH_4 (ppm)
0	11.7 ± 0.1	9.1 ± 0.1	4420 ± 50	1060 ± 10	2660 ± 30
20	11.2 ± 0.2	9.5 ± 0.1	3590 ± 100	930 ± 10	1980 ± 40
30	11.1 ± 0.1	9.6 ± 0.1	2680 ± 30	1080 ± 10	1230 ± 20
30 (no spark)	10.8 ± 0.1	9.5 ± 0.1	2700 ± 40	1110 ± 10	1220 ± 10
R4C: Split Injection RCCI					
θ_{DI1} (CAD bTDC)	H_2O (%)	CO_2 (% dry)	CO (ppm dry)	NO_x (ppm dry)	CH_4 (ppm)
360	20.2 ± 0.2	9.9 ± 0.1	1410 ± 10	1170 ± 5	740 ± 5
390	11.5 ± 0.4	9.8 ± 0.1	1300 ± 30	1210 ± 20	710 ± 30
390 (no spark)	12.2 ± 0.3	9.9 ± 0.1	1310 ± 40	1230 ± 40	650 ± 20

noted that the intake pressure is lower for these operating points since the intake was throttled to achieve a similar engine load as the RCCI operating points.

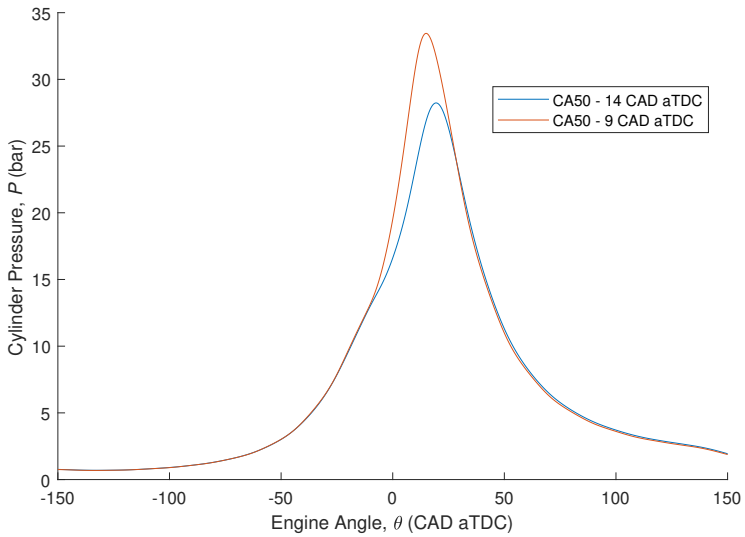

Figure 5.46: Cylinder Pressure for both SI natural gas operating points for R4A, n=1200, λ=1.01

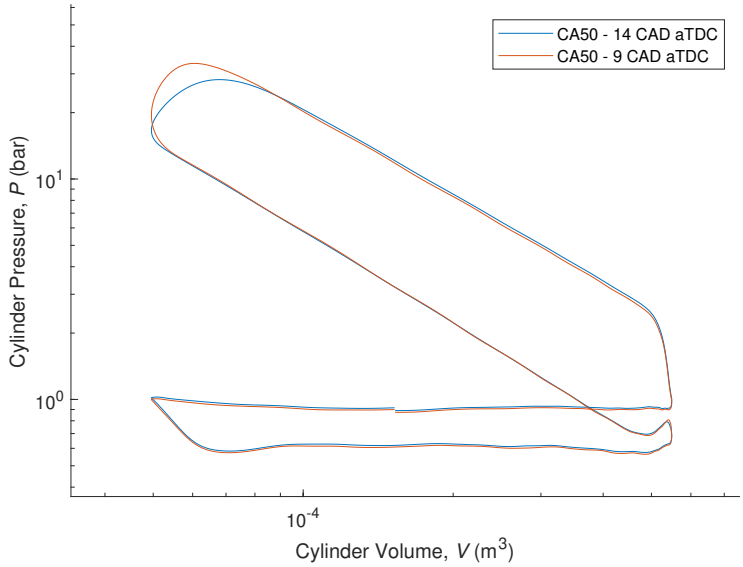

Figure 5.47: PV diagram for both SI natural gas operating points for R4A, n=1200, λ=1.01

The heat release for the SI operating mode is shown in Figure 5.48. It is noted that there is no LTHR for spark ignition and the heat release is much more gradual since the fuel is ignited through flame propagation initiated by the spark.

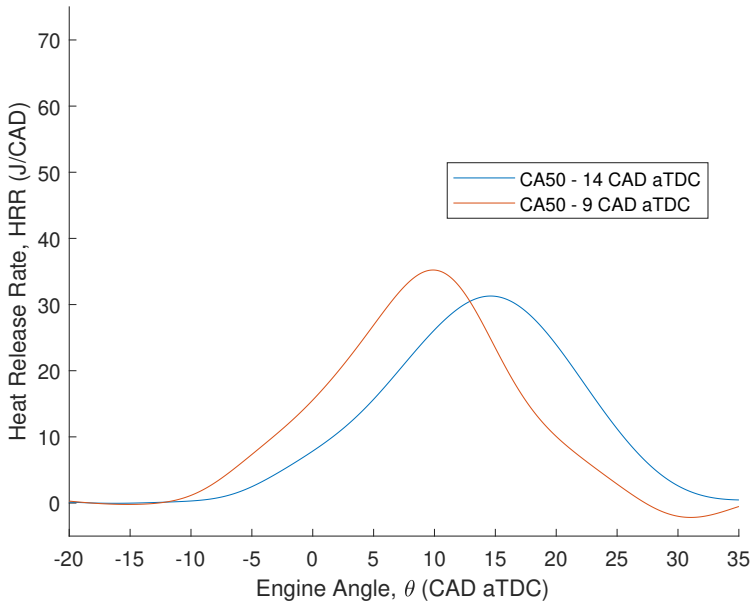

Figure 5.48: Heat Release Rate for both SI natural gas operating points for R4A, n=1200, λ=1.01

It is noted that the NO_x emissions are quite high with 3260 ppm and 2510 ppm for the CA50 of 9 CAD aTDC and the 14 CAD aTDC operating points respectively. This is not unexpected as the natural gas in the crevice does not usually burn well in an SI engine [30]. The calculated combustion efficiency η_{comb} of 76.1% and 75.5% are not consistent with the measured exhausted methane of 1050 and 800 ppm. The low combustion efficiency would presume that roughly a quarter of the injected natural gas is not burned which is not what was measured.

5.4.2 Emissions for Single Pilot Injected RCCI

The cylinder pressure traces for the single injection RCCI operating point R4B are shown in Figure 5.49 with their respective PV diagrams shown in Figure 5.50

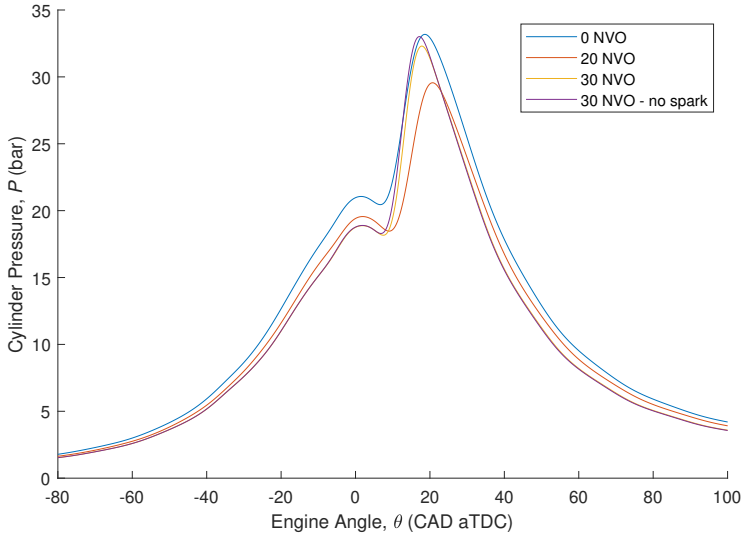

Figure 5.49: Cylinder Pressure of Single Injection RCCI operating points for R4B, n=1200

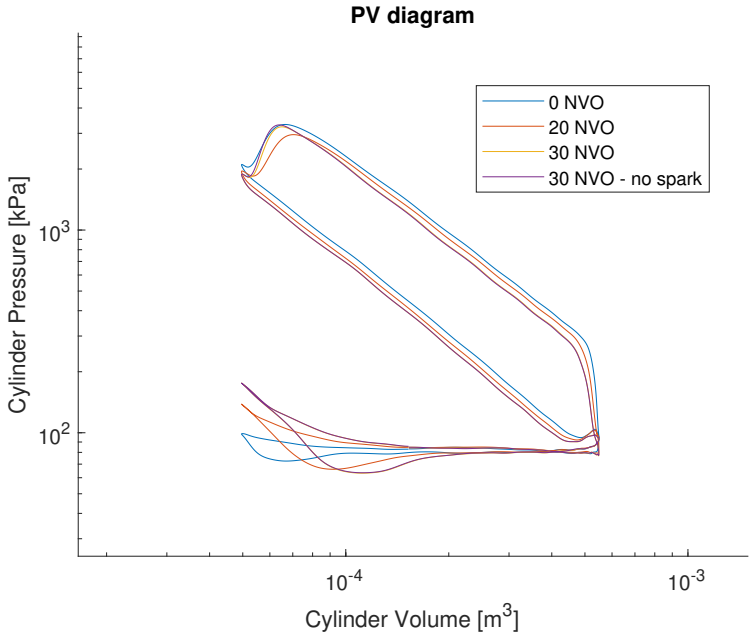

Figure 5.50: PV diagram of Single Injection RCCI operating points for R4B, n=1200

The heat release for the single injection RCCI operating points are shown in Figure 5.51. It is noted that the ϕ_{NVO} of 30 CAD has a much faster heat release rate that dies down very quickly. Eliminating the safety spark has no effect on the

combustion or the emissions for the RCCI combustion. From Table 5.21, it is noted that the CO emissions are 2 to 3 times higher than the SI operating points R4A. The amount of CO decreases with operating points with more NVO. The NO_x emissions are also lower, around 1000 ppm, than in SI mode while the amount of methane is higher but decreases with operating points using more NVO. A more detailed discussion of the combustion and emission results is included in Section 6.4.

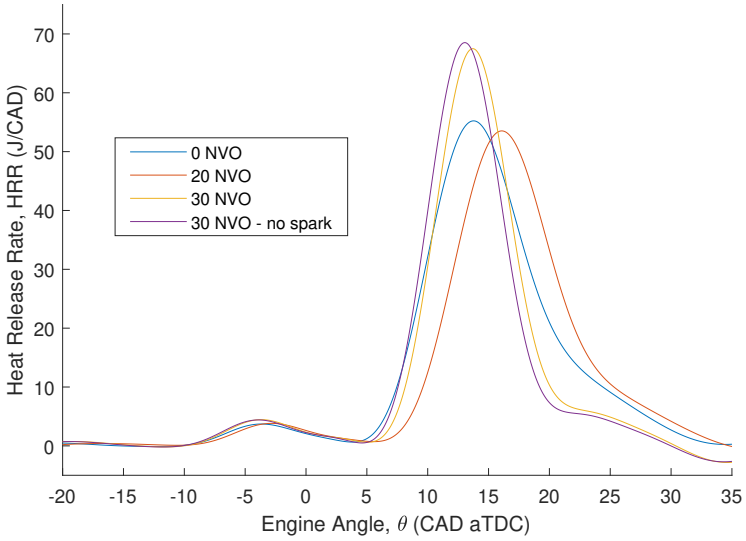

Figure 5.51: Heat Release Rate of Single Injection RCCI operating points for R4B, n=1200

5.4.3 Emissions for Split Injected RCCI

The pressure trace for split injection RCCI operating point R4C with NVO phasing of 30 CAD is shown in Figure 5.52. Very little deviation is noted in the operating points. The same drop in pressure in the NVO as in R3A is observed in Figure 5.53 due to the injection of liquid n-heptane.

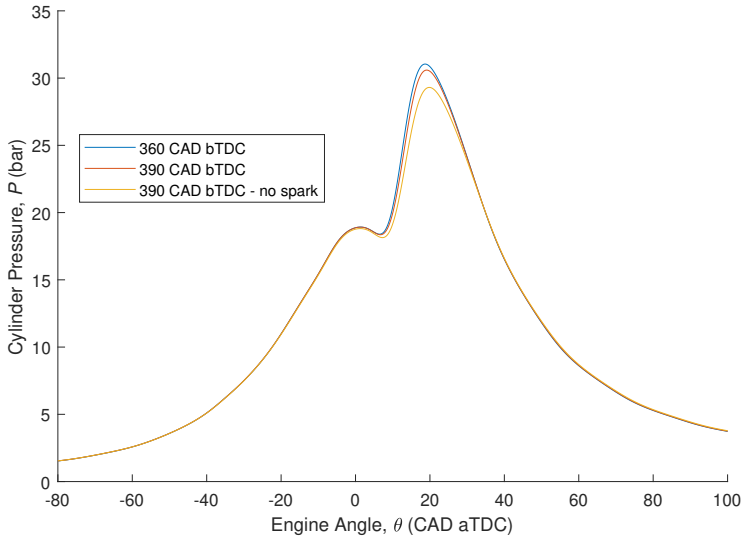

Figure 5.52: Cylinder Pressure of Split Injection RCCI operating points for R4C, n=1200, λ=1.24

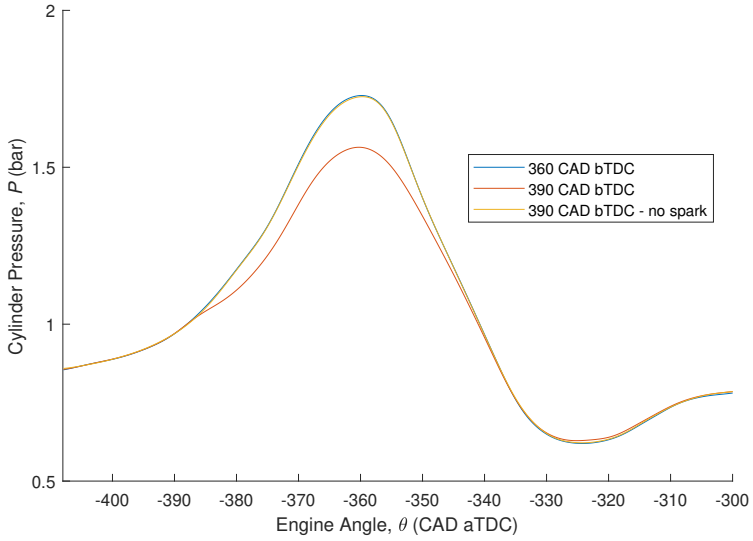

Figure 5.53: Cylinder Pressure in the NVO of Split Injection RCCI operating points for R4C, n=1200, λ=1.24

The heat release rate for R4C is plotted in Figure 5.54. It appears that when the safety spark is switched off the combustion timing is delayed only slightly.

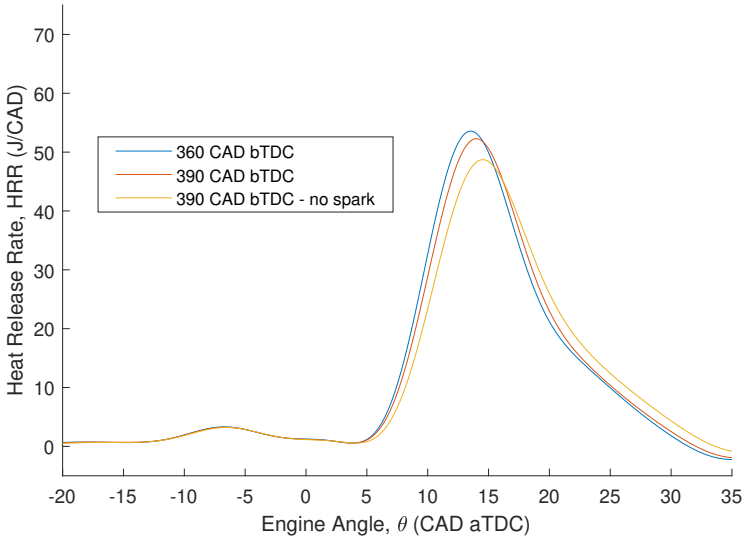

Figure 5.54: Heat Release Rate of Split Injection RCCI operating points for R4C, n=1200, λ=1.24

The CO levels for split injection RCCI are much lower than that of the single injection strategy R4B and even slightly below the SI mode. The NO_x levels are less than half of the SI mode but slightly higher than the single injection strategy. Unlike single injection RCCI, the split injection strategy has less unburnt methane in the exhaust. The emission results are discussed in more detail in Section 6.4.

Chapter 6

Discussion

6.1 RCCI compared to SI

The combustion in a spark ignition engine occurs relatively gradually as the flame generated by the spark expands to the fuel dispersed in the cylinder chamber. In contrast, the heat release of RCCI combustion can occur quickly due to the high-reactivity fuel mixture being close to auto-igniting with the flame propagating quickly. The heat release for spark ignition (R4A), single injection RCCI with ϕ_{NVO} of 30 CAD (R4B) and split injection (R4C) for similar load, IMEP and CA50 were compared in Figure 6.1. Differences between single and split injection strategies are also discussed in [31].

The concentrated heat release of RCCI combustion allows for the majority of the combustion to occur at the optimal timing just after TDC. The gradual heat release of SI is not optimally converted to power thus has lower efficiencies (η_{th} of 33.5% and η_{comb} of 75.5% from Table 5.15) than RCCI. The heat release of split injection does not reach as high of peaks as the single injection strategy, but has a more gradual decline and longer burn duration (14.2 CAD as oppose to 9.8 CAD from Table 5.14). The quick combustion of the single injection strategy leads to higher maximum PRR, 2.68 bar/CAD compared to 1.93 for the split injection case.

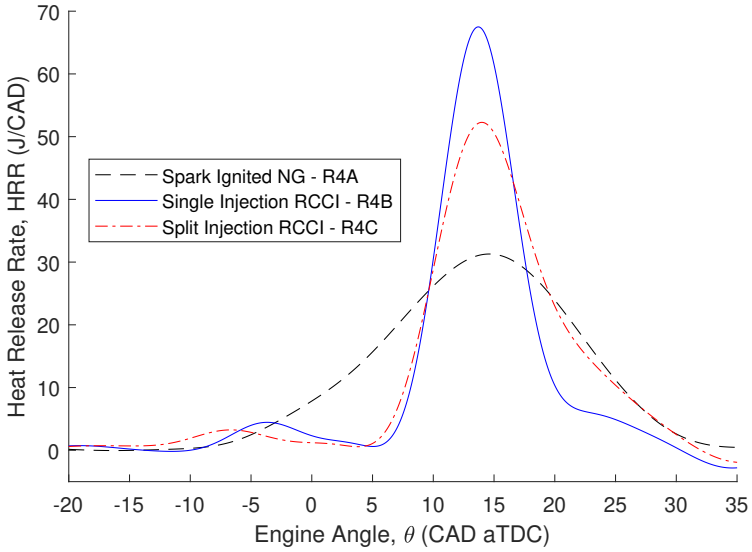

Figure 6.1: Heat Release Comparison of Different Combustion Configurations on the LNF Engine

Although the split injection case has a concentrated shorter combustion, which more closely mirrors the instantaneous pressure rise for the ideal Otto cycle, the single injection combustion with efficiencies of η_{th} of 38.3% and η_{comb} of 86.5% is less efficient than the split injection case with η_{th} of 42.2% and η_{comb} of 96.4%.

The average in-cylinder gas temperature calculated as part of the heat release analysis for the three combustion methods above are shown in Figure 6.2. The single injection temperature raises faster than the SI and the split injection strategy but quickly begins declining. The split injection method has a quick temperature rise after TDC that mirrors the SI temperature profile after roughly 15 CAD aTDC. This steady decline in temperature and in HRR indicates that after the initial auto-ignition of the fuel, the system behaves more similarly to SI combustion with a flame propagation to the rest of the cylinder.

The significant increase in combustion efficiency for the split injection case can be attributed to the partially incomplete combustion that occurs in the split injection case. The amount of unburnt methane and the amount of CO are almost doubled for

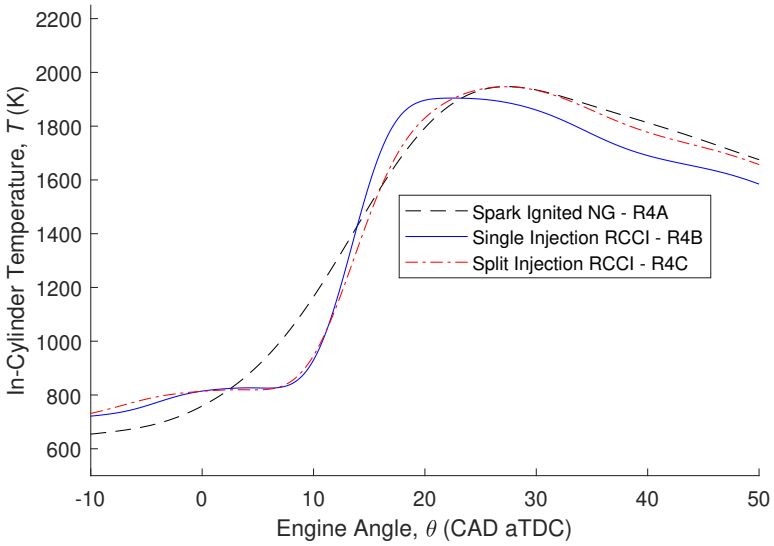

Figure 6.2: Calculated Average Cylinder Gas Temperatures of Different Combustion Configurations on the LNF Engine

the single injection strategy compared to the split injection shown in Table 5.21. The high pressure rise rates of the single injection strategy also limits its operating region. Advancing the RCCI combustion or increasing the engine load more will raise the PRR even higher which could cause the engine to reach knocking conditions. Thus the split injection strategy has a wider operating region than the split injection case in which more power and more optimally advanced combustion is possible.

6.2 Control Parameters for RCCI

The combustion timing, CA50 and the engine load IMEP are the important parameters to control for RCCI combustion. Several engine inputs could be considered as outputs for a feedback controller.

6.2.1 NVO duration

Using the NVO duration, ϕ_{NVO}, as an engine input allows for the residual exhaust gas amount through internal EGR to be varied. With larger NVO more exhaust

is recycled thereby increasing the overall intake charge temperature which should help increase the engine efficiency and helps achieve auto-ignition conditions in the cylinder. Due to the fixed cam profiles of the LNF engine, increasing the NVO decreases the effective compression ratio of the cycle by delaying the IVC timing during the compression stroke and advancing the EVO timing during the power stroke as shown in Figure 5.13.

Decreasing the NVO duration even slightly increases the intake manifold back pressure causing less air to be aspirated in the engine shown in Figure 5.30. With less air the engine operating point moves towards misfire region as CA50 is delayed. With increased air the CA50 advances and increases the PRR and HRR towards knocking conditions as shown in Table 5.15. The effect of restricted intake air flow could be mitigated by boosting (via turbocharging or supercharging) the engine intake pressure.

The cam phaser control designed and implemented in the MAB is much slower than the proprietary GM cam phaser controller. A step change in the cam phaser position takes seconds to stabilize and can cause the cam position to hover around the new set point before settling.

Although varying the amount of ϕ_{NVO} can effect the the combustion timing, it is accomplished by changes to the cam position resulting in changes to the intake air flow rate. When the air flow rate is increased (or restricted) it influences the combustion towards high PRR knocking conditions and towards delayed combustion and possible misfires. The current response speed of changing the cam position using the MAB is too slow for an effective cycle-by-cycle controller. Thus it is not recommended to use the ϕ_{NVO} as an actuator for a cycle-by-cycle controller.

6.2.2 Intake Air Heating

The auto-ignition of n-heptane is dependent on the in-cylinder temperature and pressure conditions. Typically higher temperatures and pressures help achieve auto-ignition conditions. As observed in test R3A when the intake air temperature T_{in} was varied in Figure 5.33 increasing the T_{in} advances the combustion and causes higher HRR and PRR while lower the intake temperature slightly had little noticeable effect perhaps due to coolant temperature fluctuations. For too high intake air temperatures, knocking conditions may occur while too low intake air temperatures can cause the fuel to not ignite or misfire.

With internal EGR from NVO a portion of the in-cylinder charge is recycled exhaust gas. This means that the overall gas temperature is dependent on the fresh intake air charge temperature T_{in} and the recycled exhaust gas heat. The in-cylinder gas temperature at IVC is difficult to maintain constant since a portion of the heat is recycled in the cylinder, some of the heat is transferred from the exhaust gases to the fresh intake air in the turbocharger and then the fresh air is heated using the inline air heater.

The Omegalux inline air heater is located in between the turbocharger and the intake air manifold and heats the fresh intake air to attain the in-cylinder temperatures required for RCCI. The heater is controlled using the Variac Autotransformer by varying the output voltage to the Omegalux heater manually. To incorporate the intake air heater for control purposes in future work a thermocouple and controller need to be installed so that the heater can be incorporated and controlled directly from the MAB system.

The intake charge temperature could be used as a control parameter if the Omegalux was incorporated into the MAB along with an estimate of the exhaust gas fraction and temperature based on the amount of NVO used. This calculation

and control would be difficult to do on a cycle-by-cycle basis since there are multiple parameters and dynamics that affect the heat in the system and the response speed is too slow for cycle-by-cycle control.

6.2.3 N-heptane NVO Injection Timing

The effect of the early NVO injection timing θ_{DI1} for the split injection RCCI strategy was investigated in Section 5.3.4. Earlier injection timings can create radicals (from fuel reforming) to form which could advance the CA50 of the main ignition. As shown in Figure 5.44 neither the LTHR or the HTHR was affected by the timing of the NVO injection. The engine load IMEP does not vary either with changes in θ_{DI1}. This would suggest that the n-heptane disperses fully but does not generate any radicals that affect auto-ignition. Likewise in test R4C when θ_{DI1} was advanced from 360 to 390 CAD bTDC no meaningful variation occurred in the engines combustion timing load or load. Since the θ_{DI1} is inside the NVO and is early enough to uniformly mix in the cylinder, the injection timing within the NVO does not have an effect on the RCCI combustion as no fuel reforming takes place at the engine conditions tested.

6.2.4 N-heptane Pilot Injection Timing

The n-heptane pilot injection (DI2) is quite critical to maintaining stable RCCI combustion as shown in Section 3.3.3. The effect of the pilot injection timing θ_{DI2} was investigated in Section 5.1. The pilot injection timing appears to have a "U" shaped effect on the combustion timing where there is an optimally advanced injection timing with maximum engine output IMEP. Even with split n-heptane injections, the pilot injection timing has a large effect of the combustion timing and optimal engine output.

6.2.5 Fueling Rates

RCCI operating methods require on using two fuels with different reactivities. This allows for control over the total fuel mixture reactivity within the engine cylinder. It has been demonstrated that the air to fuel ratio λ can have a large effect on the quality of combustion as shown in Figure 5.19 where operating point R2A with ϕ_{NVO} of 10 CAD had a λ of 1.34 and had a much lower efficiency compared to RCCI operating points of λ of 1.04 to 1.26.

The RCCI split injection strategy uses two n-heptane injections and a port injection for natural gas. Increasing the amount of n-heptane that is injected early changes the premixed air-fuel mixture reactivity and fuel equivalence ratio. With higher premixed reactivities the ignition from the pilot injection can spread more easily and burns more of the natural gas in the cylinder shown in Table 5.21. Also with less pilot injected fuel, the pilot auto-ignition is less locally rich which prevents incomplete combustion and reduced engine efficiency as shown by the single injection test in Table 5.20

By adjusting the fueling rates between the two n-heptane injections in the split injection RCCI operating mode and the natural gas port injection, the local and global equivalence ratio and fuel mixture reactivity can be controlled. Injecting more fuel allows for higher loads to be achieved, changing the amount of pilot injected n-heptane can change the SOI by creating a locally more reactive fuel mixture. Increasing the reactivity of the premixed fuel composition in the outskirts of the cylinder facilitates the flame propagation to distant regions in the cylinder thus increasing engine efficiency.

Table 6.1: Combustion Timing Sensitivity to Input Parameters

Parameter X	Case	Base Value X_b	$CA50_b$ (CAD aTDC)	$\frac{\delta CA50}{\delta X}$	S_X
T_{in} (°C)	R3A	85.3	14.8	-0.74 ± 0.57	4.25
ϕ_{NVO} (CAD)	R3A	30	14.6	0.93 ± 0.60	1.90
θ_{DI2} (CAD bTDC)	R1A	33	9.8	-0.40 ± 0.80	1.35

6.2.6 Combustion Timing Sensitivity

The sensitivity of the combustion timing was determined around the base point of R3A for T_{in}, ϕ_{NVO} and around R1A for θ_{DI2}. The sensitivity was calculated as the slope between the points before and after the base operating parameter. A normalized sensitivity is calculated and shown in Table 6.1 as ($S_X = |\frac{\delta CA50}{\delta X}| \times \frac{X_b}{CA50_b}$) where S_X is the normalized sensitivity of CA50 to parameter X with index b indicating the base parameter value and $CA50_b$ being the combustion timing at the base operating point.

There is a large uncertainty in the calculated sensitivities ($\frac{\delta CA50}{\delta X}$) since they are calculated using only two parameters with sizable standard deviations. The combustion phasing appears to be most sensitive to changes in intake temperature with the highest normalized sensitivity where an increase in 1°C leads to an advance in combustion phasing of 0.74 CAD. Increasing ϕ_{NVO} by 1 CAD delays the CA50 by approximately 0.93 CAD. The intake temperature T_{in} and ϕ_{NVO} greatly influence the combustion timing but are too unreliable to adjust during engine operation to control the combustion timing. Thus it is important to maintain T_{in} and ϕ_{NVO} constant during engine operation.

It is noted that θ_{DI2} is not very sensitive at the optimal base operating point since the combustion timing is close to the optimally advanced position as shown in Figure 5.3. Although θ_{DI2} may not be able to advance the combustion beyond a certain point, it is important to control the pilot injection timing to obtain maximum efficiency.

6.2.7 Proposed Feedback Control Scheme

The control of LTC auto-ignition strategies is discussed in [8]. The main advantage of using two-fuels in RCCI is the ability to control the overall fuel reactivity to control the combustion phasing. An example of an RCCI controller that was developed and tested is shown in [32]. A proposed feedback control scheme for this experimental setup is shown in Figure 6.3 to control split injection RCCI on the LNF engine. For the proposed setup the engine would run at near steady-state conditions with constant engine speed n maintained by the dynamometer with a fixed amount of NVO phasing ϕ_{NVO} and constant intake air heating T_{in}. The RCCI combustion can be optimized for the desired engine load and combustion timing while also maintaining the fuel equivalence ratio at globally lean conditions.

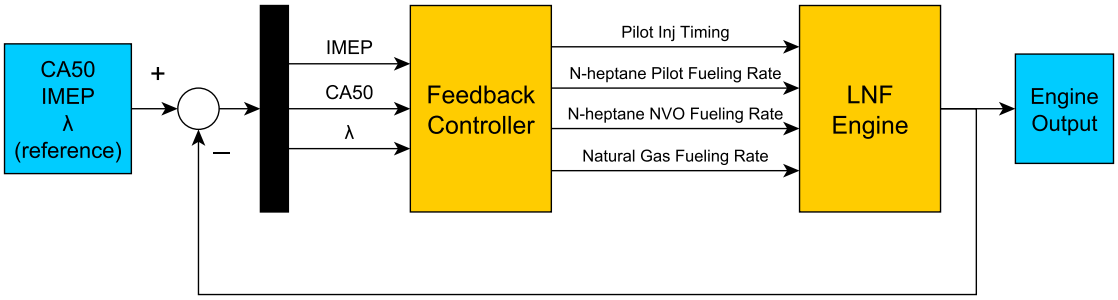

Figure 6.3: Proposed Feedback Control Methodology for RCCI with NVO on the LNF engine

Set points are combustion timing CA50 and IMEP would be able to be set by the user which the controller would try to target by adjusting the fueling rates of the fuels and the pilot injection timing. Further work would be necessary to determine a model for the engine through model order reduction [12] or system identification [33] to develop a controller. Physics based models are difficult to use for control purposes without extensive knowledge of the specific combustion and physical phenomena occurring within the engine cylinder.

Constraints on the engine outputs and actuator constraints need to be determined based on engine knocking and engine misfires are avoided. Determining these constraints may be difficult since the engine must be operated near the instabilities (such as knock) which could damage the engine.

6.3 Fuel Reforming

In addition to attaining better fuel mixing as motivation of injecting n-heptane during the NVO, the possibility of n-heptane fuel reforming was desired. Fuel reforming creates some of the chemical radicals for combustion before the main ignition. N-heptane reforming in the NVO is typically an endothermic process [14] therefore it takes energy from its surroundings. The heat release inside the NVO for the single injection case R4B with ϕ_{NVO} of 30 CAD and the split injection cases R4C with θ_{DI1} of -360 and -390 CAD aTDC is shown in Figure 6.4.

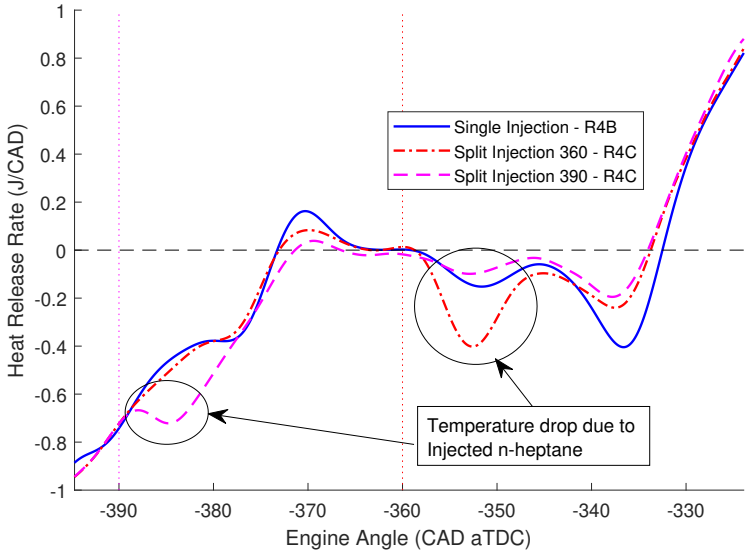

Figure 6.4: Heat Release in the NVO during different RCCI injection strategies

The dip in pressure shortly after the injection of n-heptane occurs due to the temperature drop of the in-cylinder gases when cool liquid fuel is injected and evap-

orates. The cumulative heat release during the NVO from -390 to -330 CAD aTDC was calculated for each operating point. The single injection case has a cumulative HR of -9.7 J while the -360 CAD aTDC split injection strategy has a HR of -10.5 J and -10.2 J with the -390 CAD aTDC injection. By comparing the heat loss between the case with and without n-heptane injections, it is calculated that 0.7 J and 0.5 J were transferred to the n-heptane fuel.

Based on the latent heat of evaporation of n-heptane, the energy required to vaporize the amount of fuel injected in NVO is 1.36 J. Thus the amount of energy transferred to the n-heptane fuel is on the same order of magnitude but slightly less than the energy required to vaporize the n-heptane. Thus it can be concluded for split injection, a portion of the fuel does vaporize which assists in fuel mixing causing a more homogeneous mixture. This helps contribute to lower particulate matter formation in theory, since localized rich regions in the main ignition is the main contributor to particulate formation for this type of engine combustion [4]. No endothermic heat transfer for fuel reforming beyond the portion to vaporize the n-heptane liquid was measured even with the early injection of -390 CAD aTDC before the NVO recompression. Longer NVO durations thus larger recompression pressures would be needed to achieve fuel reforming for this engine setup. However, the NVO durations on the engine are limited due delayed IVC timings restricting the fresh intake air flow rate so this was not performed.

6.4 RCCI combustion analysis using emissions

The NOx levels for the SI operating mode R4A were 2 to 3 times higher than the RCCI operating points R4B and R4C shown in Table 5.21. NOx is produced at high-temperatures in the engine cylinder that SI mode achieves. The split injection strategies produced slightly more NOx (10 to 20% more) than the single pilot injection

strategy. This increase in NOx is most likely due to slightly higher instantaneous temperatures in the cylinder for the split injection operating mode [4]. The RCCI NOx levels are still quite elevated compared to ultra-low NOx emissions of 5 ppm from the fully homogenous and very lean dual-fuel HCCI [7].

The unburnt methane in the exhaust was significantly higher for the single injection strategy R4B with ϕ_{NVO} of 0 and 20 CAD. The unburnt methane is almost 3 times higher than that of the engine running in SI mode. Two factors contribute to the large amount of unburnt methane. The lower NVO operating points had more natural gas, E_{PI1} , and thus has more methane dispersed in the cylinder and is collected in the cylinder crevasse. Secondly without the first NVO injection of n-heptane like in R4B the port injected natural gas is dispersed without n-heptane and is lean and forms a low-reactivity mixture. The flame from the pilot injection auto-ignition quenches more quickly at the walls and in the crevasses, thus more fuel is left unburnt. Using a split injection strategy allows for more of the n-heptane fuel to be dispersed in the cylinder allowing less n-heptane in the pilot to initiate the auto-ignition. Since the dispersed fuel is a mixture of both n-heptane and natural gas is both locally more reactive and less lean compared to the single injection method. This allows for better propagation of the flame in the entire cylinder which leads to higher combustion efficiencies, longer burn durations and lower peak PRR and HRR.

The production of CO is roughly twice as high for the single injection RCCI , R4B, compared to conventional spark method R4A while it is roughly 20% less for the split injection RCCI R4C. Carbon monoxide is typically produced when there is incomplete rich combustion. The large amounts of carbon monoxide are attributed to the large locally rich concentrations of n-heptane from the pilot injection E_{DI2} of the single injection strategy.

Both methane and CO emissions increase with a larger pilot injection DI2 because the local regions are richer. Thus it is desirable to have as small of a pilot injection as

possible. The split injection strategy has slightly increased NOx emissions compared to the single injection case due to higher combustion temperatures. The slight increase in NOx emissions is a tradeoff between the reduced CO and unburnt methane emissions.

6.5 Combustion Stability

The stability of RCCI combustion on the LNF engine is difficult to characterize since the cyclic variability on the engine is quite significant operating in conventional spark methods (standard deviations as high as ±2.2 CAD for CA50, ±1.6 bar for P_{max} and ±0.08 bar for IMEP operating at n=1250 RPM) [15]. RCCI testing is conducted on only one cylinder on a 4-cylinder engine with a shared intake air manifold.

When the NVO phasing duration was manipulated in test R3A, it was noted that the standard deviation of both the CA50 and IMEP increase with longer ϕ_{NVO} as shown in Table 5.13. A probability density was generated to visualize the distribution of both the IMEP, in Figure 6.5, and the CA50 in Figure 6.6 for the 200 cycle tests for R3A (using the Matlab function *ksdensity*).

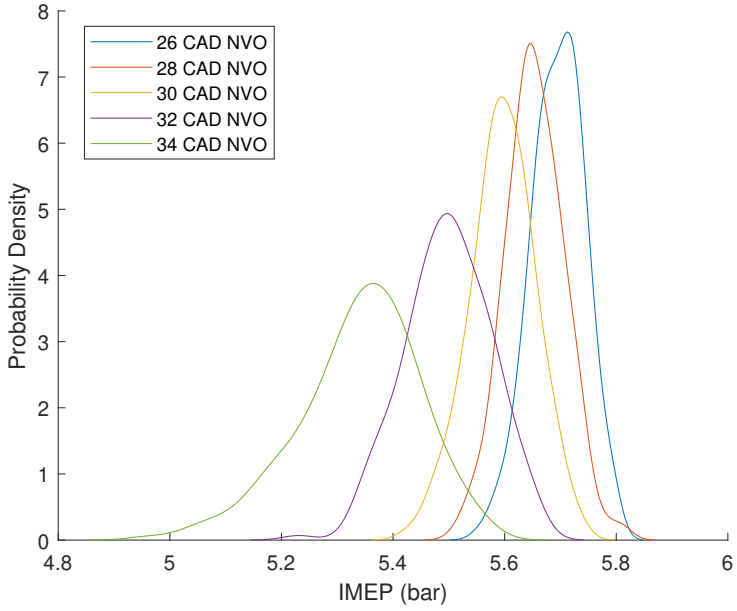

Figure 6.5: Probability Distribution of IMEP of point R3A with varying NVO Phasing Duration

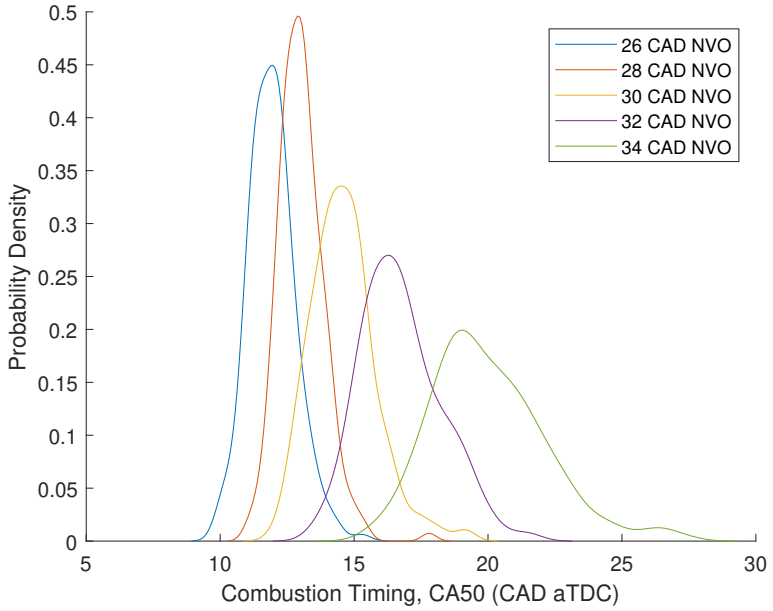

Figure 6.6: Probability Distribution of CA50 of point R3A with varying NVO Phasing Duration

The narrower probability density curves indicate that less variation in the com-

bustion power output and combustion timing when the ϕ_{NVO} is shortened. When the combustion is delayed with slightly longer NVO durations, there is a significant amount more variation in the IMEP and CA50. A smaller second peak is observed for all 5 operating points implying a late combustion with weak power output close to misfiring occurs periodically. The frequency of this delayed combustion increases when the combustion phasing is delayed and as the variability increases.

Tests with 1000 cycles were collected for operating points R4A, R4B and R4C, compared in Section 6.1, with similar engine load and combustion timing were used to help compare the combustion stability between the natural gas SI, single injection RCCI with NVO and the split injection RCCI with NVO operating modes. The probability density for the engine load IMEP and the combustion timing CA50 are shown in Figure 6.7 and Figure 6.8 respectively. This matches [34] where operating points with late CA50 tend to have higher cyclic variation.

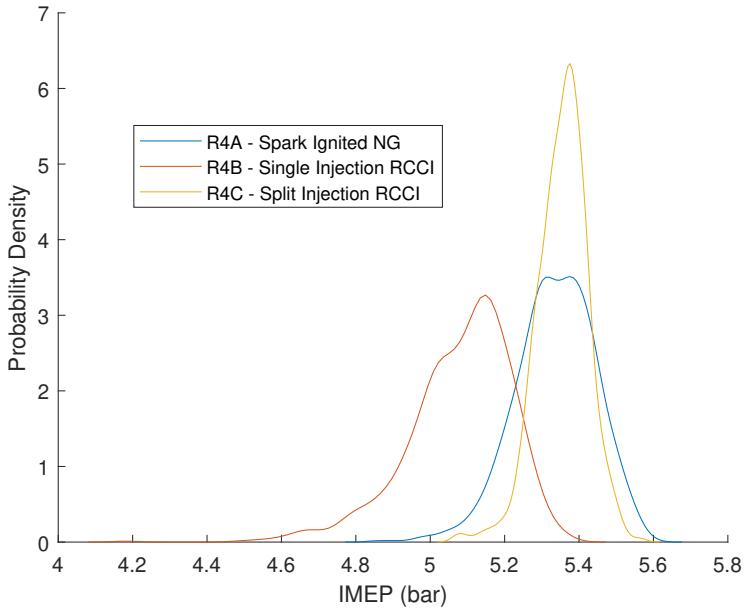

Figure 6.7: Probability Distribution of IMEP of various Combustion Methods

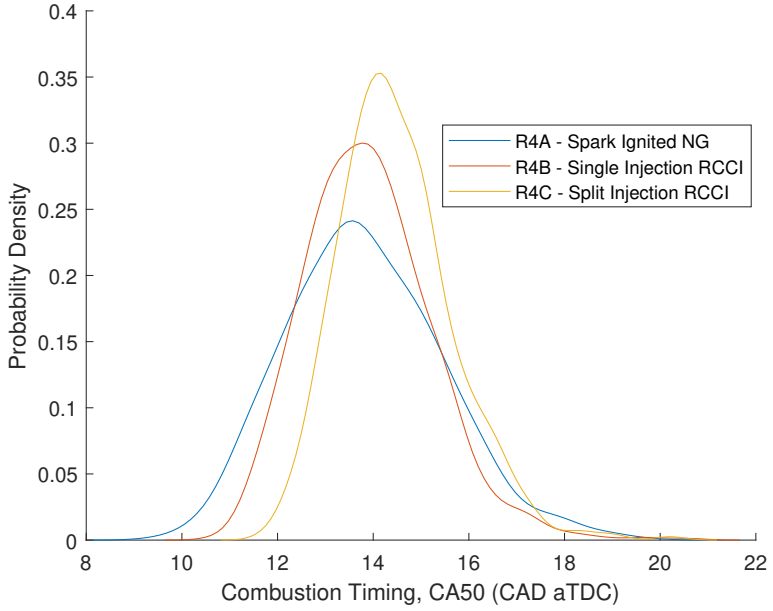

Figure 6.8: Probability Distribution of CA50 of various Combustion Methods

The single injection RCCI operating method has a noticeable tail with low engine load and has more near misfire low power cycles than both the split injection RCCI and the natural gas RCCI operating methods. This could be due to the low efficiency and incomplete combustion observed with the single injection strategy. The split injection RCCI operating mode has a narrower probability density than the natural gas SI baseline mode. Therefore the split injection RCCI operating mode has less variability than the engine operating with conventional SI with natural gas. The CA50 for the three operating methods have similar amount of variability compared to the IMEP variability. The RCCI combustion timing is slightly more consistent than that of the spark ignition. This is expected as properly timed auto-ignition is typically more stable than SI.

Chapter 7

Conclusions

This chapter contains the conclusions and recommendations for future work.

7.1 Conclusions

The goal of this study was to explore the use of dual-fuel RCCI on a production 4-cylinder SI engine. Modifications were required to achieve auto-ignition of n-heptane and natural gas fuel mixtures. The stock engine pistons were replaced with custom Wiseco pistons to raise the engine compression ratio to 11.1. An intake air heater was added to help achieve fuel auto-ignition conditions. The n-heptane direct injection pressure was raised so an n-heptane pilot injection could be used during the compression stroke to help control combustion timing.

Case 1 tests are conducted with a single n-heptane pilot injection strategy where n-heptane is injected during the compression stroke while natural gas is injected in the port during the air intake. The effect of the n-heptane pilot injection timing on the combustion timing and heat release was investigated. Case 2 investigated the use of NVO with RCCI auto-ignition. A split injection strategy for the n-heptane where half the n-heptane was injected during the NVO recompression and the rest as the pilot injection during the compression stroke was investigated in Case 3. Engine exhaust emissions were measured using an FTIR for the single and split injection

RCCI cases and are compared to spark ignited natural gas at similar engine loads in Case 4.

RCCI combustion occurs more quickly compared to spark ignition flame propagation. The RCCI auto-ignition has a concentrated heat release which allows for the majority of the combustion to occur at the optimal timing for the largest power output. The single injection strategy has a much larger heat release peak as the majority of the fuel is concentrated in one area. However, in this strategy the reactions have difficulty spreading to the outer regions of the cylinder thus has increased unburnt methane emissions. The split injection strategy has lower pressure rise rate peaks and smaller maximum heat releases but has longer burn durations. The mixture of n-heptane and natural gas in the outer regions of the engine cylinder facilitates the flame propagation thus resulting in more fuel being burned and faster burn durations than spark ignition strategies. Smaller pressure rise rates allow for the split injection engine load to be extended without reaching the knocking conditions.

Various parameters that influence the RCCI combustion were investigated to determine their viability for engine load and combustion timing control. Although parameters such as the NVO phasing duration and the intake air heating amount can heavily influence the combustion strength, the parameters can not be actuated fast enough for an effective cycle-by-cycle controller. The NVO n-heptane injection timing did not have an observable effect on the combustion. The n-heptane pilot injection was chosen as a desirable control parameter since it has observable controllability over the combustion timing of the engine with a "U" shaped trend with an optimally advanced combustion timing at a certain operating point. The fueling rates for the n-heptane NVO injection, n-heptane pilot injection and the natural gas port injection were also parameters for a controller since changing these fueling rates affects the fuel reactivity and fuel equivalence ratio amounts and stratification in the cylinder.

The possibility of fuel reforming of n-heptane inside the NVO is investigated. It

is determined that the injected n-heptane fuel only vaporizes and that no preliminary endothermic combustion reactions occur that changes the chemical composition of the n-heptane.

The amount of NOx produced by single and split injection RCCI is 2 to 3 times lower than traditional spark operating mode due to lower combustion temperatures. The amount of carbon monoxide emissions and unburnt methane for the split injection RCCI operating mode are slightly better than the engine operating on spark mode with natural gas. The single injection method produced more carbon monoxide and unburnt methane than the other operating methods due to a more locally rich pilot injection region with a poorer flame propagation to outer regions of the cylinder. The RCCI operating methods have improved combustion stability compared to the spark operating mode.

7.2 Future Work

- Implement a temperature controller for the intake air heating system
- Explore optimal operating conditions for RCCI combustion at higher operating speeds
- Determine actuator constraints for controller parameters to avoid unstable operating conditions
- Implement the proposed feedback controller to control and optimize RCCI engine load and combustion timing
- Add intake air boosting to allow for larger NVO durations
- Investigate n-heptane fuel reforming for larger NVO durations

References

[1] P. Najt and D. Foster. Compression-ignited homogeneous charge combustion. *SAE Technical Paper 830264*, 1983.

[2] EPA. EPA and NHTSA Set Standards to Reduce Greenhouse Gases and Improve Fuel Economy for Model Years 2017-2025 Cars and Light Trucks. *Energy Procedia*, EPA-420-F-051, 2012.

[3] Iida M., Hayashi M., Foster D.E., and Martin J.K. Characteristics of Homogeneous Charge Compression Ignition (HCCI) Engine Operation for Variations in Compression Ratio, Speed, and Intake Temperature While Using n-Butane as a Fuel. *Journal of Engineering for Gas Turbines and Power*, 125(2):472478.

[4] T. Kamimoto and M Bae. High combustion temperature for the reduction of particulate in diesel engines. *SAE Technical Paper 880423*, 1983.

[5] Aaron Oakley, Hua Zhao, Nicos Ladommatos, and Tom Ma. Experimental Studies on Controlled Auto-ignition (CAI) Combustion of Gasoline in a 4-Stroke Engine. In *SAE 2001 World Congress*, volume SAE 2001-01-1030. SAE International, mar 2001.

[6] R. Stone. *Introduction to Internal Combustion Engines*. Macmillan Education UK, 2012. ISBN 9780230576636.

[7] Rudolf H. Stanglmaier, Thomas W. Ryan, and Jason S. Souder. HCCI Operation

of a Dual-Fuel Natural Gas Engine for Improved Fuel Efficiency and Ultra-Low NOx Emissions at Low to Moderate Engine Loads. SAE 2001-01-1897, may 2001.

[8] Adam B. Dempsey, N. Ryan Walker, Eric Gingrich, and Rolf D. Reitz. Comparison of low temperature combustion strategies for advanced compression ignition engines with a focus on controllability. *Combustion Science and Technology*, 186 (2):210–241, 2014.

[9] Christof Noehre, Magnus Andersson, Bengt Johansson, and Anders Hultqvist. Characterization of Partially Premixed Combustion. SAE 2006-01-3412, oct 2006.

[10] Mazda Motor Corporation. SKYACTIV-X Next-Generation Gasoline Engine: Our Contribution to the Earth, People, and Society, 2017. URL `http://www.mazda.com/globalassets/en/assets/csr/download/2017/2017_p007.pdf`. Mazda Sustainability Report 2017.

[11] Rolf D. Reitz and Ganesh Duraisamy. Review of high efficiency and clean reactivity controlled compression ignition (RCCI) combustion in internal combustion engines. *Progress in Energy and Combustion Science*, 46:12 – 71, 2015. ISSN 0360-1285.

[12] K Ebrahimi. *Model Based Control of Combustion Timing and Load in HCCI Engines*. PhD thesis, University of Alberta, 2016.

[13] Yong Qian, Xiaole Wang, Lifeng Zhu, and Xingcai Lu. Experimental studies on combustion and emissions of RCCI (reactivity controlled compression ignition) with gasoline/n-heptane and ethanol/n-heptane as fuels. *Energy*, 88:584 – 594, 2015. ISSN 0360-5442.

[14] Jacek Hunicz, Alejandro Medina, Grzegorz Litak, Pedro L. Curto-Risso, and Lev Guzmn-Vargas. Effects of direct fuel injection strategies on cycle-by-cycle variability in a gasoline homogeneous charge compression ignition engine: Sample entropy analysis. *Entropy*, 17(2):539–559, 2015. ISSN 1099-4300.

[15] D. Stang. Characterization and Control of Cyclic Variability in a Gasoline/Natural Gas Dual-Injection Spark Ignition Engine. M.Sc. thesis, University of Alberta, 2016.

[16] D. I. Handford and M. D. Checkel. Extending the Load Range of a Natural Gas HCCI Engine using Direct Injected Pilot Charge and External EGR. In *Powertrains, Fuels and Lubricants Meeting*. SAE International, jun 2009. doi: https://doi.org/10.4271/2009-01-1884. URL `https://doi.org/10.4271/2009-01-1884`.

[17] MKS Instuments Inc. MultiGas 2030 data sheet, 2017. URL `https://www.mksinst.com/docs/UR/onlinemultigas2030ds.pdf`.

[18] David G. Goodwin, Harry K. Moffat, and Raymond L. Speth. Cantera: An object-oriented software toolkit for chemical kinetics, thermodynamics, and transport processes, 2017. URL `http://www.cantera.org`. Version 2.3.0.

[19] S.P. Chincholkar and J.G. Suryawanshi. Gasoline direct injection: An efficient technology. *Energy Procedia*, 90:666 – 672, 2016. 5th International Conference on Advances in Energy Research (ICAER) 2015.

[20] Mohammad Taghi Shervani-Tabar, Meysam Sheykhvazayefi, and Morteza Ghorbani. Numerical study on the effect of the injection pressure on spray penetration length. *Applied Mathematical Modelling*, 37(14):7778 – 7788, 2013.

[21] John B Heywood. *Internal combustion engine fundamentals*. Mcgraw-hill New York, 1988.

[22] Magnus Christensen and Bengt Johansson. *Homogeneous Charge Compression Ignition with Water Injection*, volume SAE 1999-01-0182. Society of Automotive Engineers, 1999.

[23] Rudolf H. Stanglmaier and Charles E. Roberts. Homogeneous Charge Compression Ignition (HCCI): Benefits, Compromises, and Future Engine Applications. SAE 1999-01-3682, oct 1999.

[24] Koch C. Mashkournia M., Audet A. Knock Detection and Control in an HCCI Engine Using DWT. *Internal Combustion Engine Division Fall Technical Conference*, pages 391–399, 2011. ASME 2011 Internal Combustion Engine Division Fall Technical Conference.

[25] J. A. Eng. Characterization of Pressure Waves in HCCI Combustion. *SAE Technical Paper*, SAE 2002-01-2859, oct 2002. ISSN 0148-7191. doi: https://doi.org/10.4271/2002-01-2859. URL `https://doi.org/10.4271/2002-01-2859`.

[26] John Dec, Yi Yang, and Nicolas Dronniou. Improving Efficiency and Load Range of Boosted HCCI using Partial Fuel Stratification with Conventional Gasoline, 2011. URL `https://www.energy.gov/sites/prod/files/2014/03/f8/deer11_dec.pdf`. Directions in Engine-Efficiency and EmissionsResearch Conference.

[27] R. M. Wagner, J. A. Drallmeier, and C. S. Daw. Origins of cyclic dispersion patterns in spark ignition engines, 1998. Proceedings of the 1998 Technical Meeting of the Central States Section of the Combustion Institute.

[28] Mahdi Shahbakhti, Robert Lupul, and Charles Robert Koch. Sensitivity analysis & modeling of HCCI auto-ignition timing. *IFAC Proceedings Volumes*, 40(10):303 – 310, 2007. ISSN 1474-6670. 5th IFAC Symposium on Advances in Automotive Control.

[29] NIST. NIST Chemistry WebBook, SRD 69, Heptane, 2017. URL `https://webbook.nist.gov/cgi/cbook.cgi?ID=C142825&Mask=4`. National Institue of Standards and Technology.

[30] Haeng Muk Cho and Bang-Quan He. Spark ignition natural gas engines - A review. *Energy Conversion and Management*, 48(2):608 – 618, 2007. ISSN 0196-8904.

[31] R.V. Klikach, K. Ebrahimi, and C.R. Koch. Experimental Investigation and Analysis of Natural Gas RCCI on a Modified GDI Engine using NVO. *Proceedings of Combustion Institute - Canadian Section*, 2018.

[32] Nithinteja Kondipati, Jayant Kumar Arora, Mehran Bidarvatan, and Mahdi Shahbakhti. Modeling, design and implementation of a closed-loop combustion controller for an rcci engine. pages 4747–4752, 05 2017.

[33] Lennart Ljung. *System Identification: Theory for the User*. Prentice-Hall, Inc., Upper Saddle River, NJ, USA, 1986.

[34] M. Shahbahkti. *Modeling and Experimental Study of an HCCI Engine for Combustion Timing Control*. PhD thesis, University of Alberta, 2009.

[35] Keyvan Bahlouli, Ugur Atikol, R. Khoshbakhti Saray, and Vahid Mohammadi. A reduced mechanism for predicting the ignition timing of a fuel blend of natural-gas and n-heptane in HCCI engine. *Energy Conversion and Management*, 79: 85 – 96, 2014. ISSN 0196-8904. doi: https://doi.org/10.1016/j.enconman.

2013.12.005. URL http://www.sciencedirect.com/science/article/pii/S0196890413007814.

Appendix A: Wiseco Piston Order Specifications

Custom Order Piston Kit Specifications

Made exclusively for:
Wiseco Piston Canada
948 Keyes Dr
PO Box 1513
Woodstock, ON N4S0A7

Date: 07/20/2016

Part #: WD-02980
Cust #: W0002

General Information

Forging #: F6636XA0
Comp Height: 1.215
Bore Size: 3.3860 **Suggested Clearance:** 0.0040

(Measured at lowest point of piston skirt, or 1.300" from bottom of oil ring, as shown in sketch.)

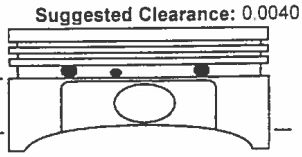

Shape:
Weight @ Inspection 403.0-403.7 g

Piston Pins / Retainer Clips

Piston Pin #:	S752
Diameter:	.905
Length:	2.362
Retainer Clip #:	W5860
Width or Wire Dia:	.0720

Rings

Oil Rail Support #:
Ring Type:

	Land Thick	Grv Width	Grv Root Dia
Top Ring	.2500	.0410	3.082
Second Ring	.1900	.0490	3.0580
Third Ring	.0800	.1113	3.0900

Dome and Valve Pockets

Dome Rise: .2600 **Dome Volume:** 16.6
Deck Thickness: .300

	Intake	Exhaust
Valve Dia		
Pocket Dia	1.5500	1.3000
Angle	18.00	16.00
Rotation		
Depth from TE	-.0900	-.0900

Specifications and Installation Instructions for Wiseco Automotive Pistons

Piston to Cylinder Wall Clearance - Wiseco pistons are machined with a special cam and barrel design. When measuring for piston to wall clearance, measure at widest point of piston skirt 1.300" from bottom of oil ring groove, 90 degrees from piston pin hole.

Valve to Piston Clearance - Most Wiseco pistons are machined with valve pockets that are deeper and larger than stock. These pockets provide adequate valve clearance under most conditions. It is very important that valve to piston clearance be checked upon piston installation. This is necessary due to many variations in cams, how much a block has been decked or if the heads have been cut or angle milled.

CAUTION: Use only Wiseco Spiro Lox retainer clips in pistons manufactured for Spiro Lox clips and round wire retainer clips for pistons manufactured for round wire clips. Use only Wiseco part number retainer clips in Wiseco pistons. Substitution can result in severe engine damage. Wiseco also recommends that retainer clips are not reused.

WISECO *7201 Industrial Park Blvd. Mentor, OH 44060-5396*
(440) 951-6600 Fax (440)951-6606

FC-7.5.1-36Rev. A1

Appendix B

Cantera Combustion Simulations

In order to determine whether auto-ignition can occur on the LNF engine, combustion simulations were conducted using the engine mechanical specifications. These simulations were conducted using the detailed physical model from [12] with the reduced reaction mechanism for n-heptane and natural gas (41 species and 109 reactions) [35]. The detailed physical model does a step by step calculation of the in-cylinder environment conditions and the chemical reactions of the cylinder contents. These test assume a fully homogeneous mixture (for HCCI) thus are only used to simulate if auto-ignition can occur with the given conditions.

The initial conditions for the simulations are shown in Table B.1. The intake air pressure is assumed to be wide open throttle with no additional boost using 35% n-heptane by mass at n = 1000 RPM. An initial simulation was conducted with unheated intake air $T_{in} = 30°C$ to replicate the test conducted in Figure 3.21.

Table B.1: Cantera Simulation Operating Parameters

Intake Air Temperature, T_{in}	30°C	100°C
Intake Air Pressure, P	1 bar	1 bar
Engine Compression Ratio	11.1:1	11.1:1
N-heptane Pilot Injection Timing, θ_{DI2}	30 CAD bTDC	30 CAD bTDC
N-heptane Fuel Mass Ratio	35%	35%
Engine Speed, n	1000 RPM	1000 RPM

The simulation cylinder pressure and temperature results for intake air temperature of $T_{in} = 30°C$ are shown in Figure B.1 and Figure B.2 respectively. The simulation plots shown no chemical reactions that change the cylinder pressure or temperature thus it can be concluded that auto-ignition does not occur for this test condition. This agrees with the result found in Figure 3.21.

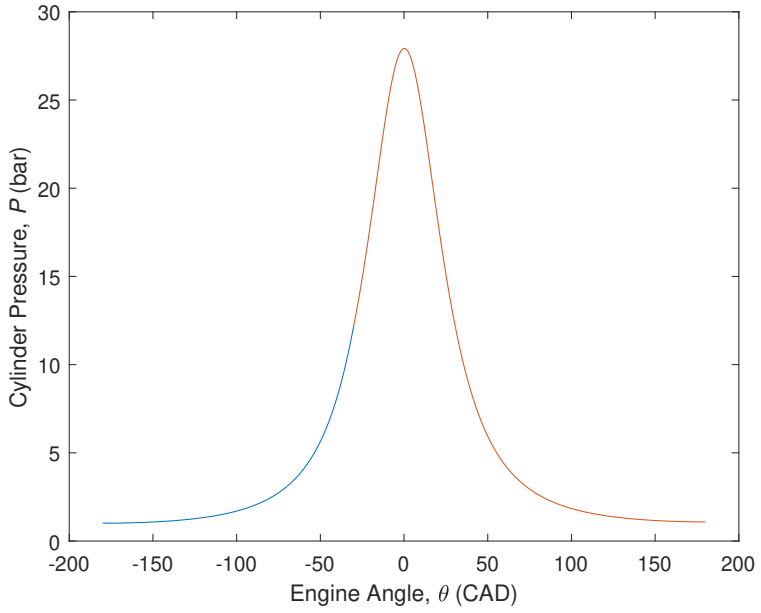

Figure B.1: Cylinder Pressure simulation, $T_{in} = 30°C$, no auto-ignition

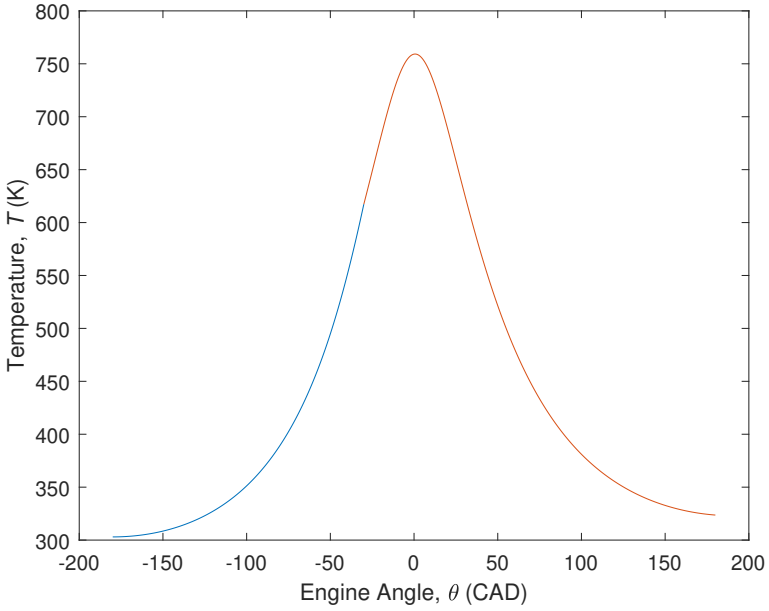

Figure B.2: Cylinder Temperature simulation, $T_{in} = 30°C$, no auto-ignition

The simulation cylinder pressure and temperature results for intake air temperature of $T_{in} = 100°C$ are shown in Figure B.3 and Figure B.4 respectively. A large pressure and temperature rise is noted slightly after TDC for this simulation. This shows that the fuel mixture auto-ignites with a ceratin delay after the pilot injection at 30 CAD bTDC. The pressure and temperature rises very quickly. This rapid rise is due to the simplicity of the model simulation which assumes fully homogeneous conditions in the cylinder in one zone. This sort of pressure rise is not to be expected in a real cylinder but is ignored here as the simulation is used to determine if auto-ignition occurs.

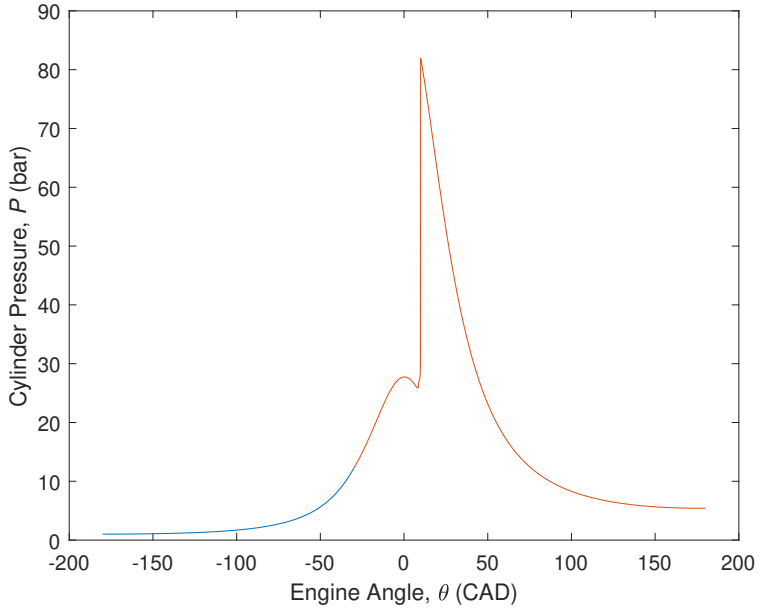

Figure B.3: Cylinder Pressure simulation, $T_{in} = 100°C$, auto-ignition occurs

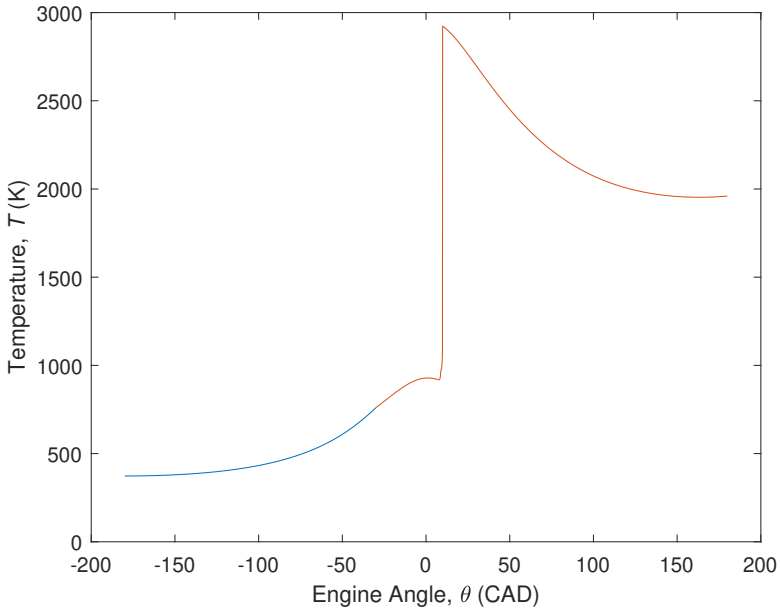

Figure B.4: Cylinder Temperature simulation, $T_{in} = 100°C$, auto-ignition occurs

From these simulation results, it is expected with intake air of $T_{in} = 100°C$ auto-ignition conditions of n-heptane and natural gas mixtures may occur.